Dissecting and Targeting the PUMA and OLIG2 Control Points of Tumors of Neuroectodermal Origin with Stapled Peptides

Dissecting and Targeting the PUMA and OLIG2 Control Points of Tumors of Neuroectodermal Origin with Stapled Peptides

A dissertation presented

by

Amanda Lee Edwards

to

The Division of Medical Sciences

in partial fulfillment of the requirements

for the degree of

Doctor of Philosophy

in the subject of

Biological Chemistry and Molecular Pharmacology

Harvard University

Cambridge, Massachusetts

April 2013

Dissertation Advisor: Dr. Loren Walensky Amanda Lee Edwards

Dissecting and Targeting the PUMA and OLIG2 Control Points of Tumors of Neuroectodermal Origin with Stapled Peptides

Tumors of neuroectodermal origin are among the most aggressive and treatment-refractory forms of human cancer. While such tumors arise from a variety of defects, two key targets are the transcription factors p53 and OLIG2. We have developed stabilized peptides to study and target deregulated p53 and OLIG2 pathways in neuroectodermal cancers.

PUMA (p53-upregulated modulator of apoptosis) is a BH3-only member of the BCL-2 protein family that regulates apoptosis in response to p53-dependent and p53-independent stress signals. The specific interactions that mediate the pro-apoptotic activity of PUMA remain controversial. We generated stabilized alpha-helices of BCL-2 domains (SAHB) peptides modeled after the BH3 effector domain of PUMA. Structural analyses determined that PUMA SAHB contacts BAX at both the N-terminal α1/α6 trigger site and the canonical BH3 binding pocket, binding events that functionally activate BAX. Notably, both PUMA SAHB and PUMA protein pull-downs identified anti- and pro-apoptotic binding partners in a cellular context. As PUMA has been implicated in driving apoptosis in multiple neural cell types, we further demonstrated that treatment of neuroblastoma cell lines with a cell-permeable PUMA SAHB analog triggered dose-dependent apoptosis. Together, we find that the PUMA BH3 domain activates apoptosis through multimodal interactions with BCL-2 family proteins, and its mimetics may serve as prototype therapeutics in tumors of neural origin.

Whereas suppression of p53 signaling and apoptosis are features of diverse tumor types, the basic helix-loop-helix (bHLH) transcription factor OLIG2 is selectively overexpressed in gliomas. Early in development, OLIG2 is responsible for maintaining progenitor cells in a

replication-competent state. Tumor stem cells are believed to co-opt this OLIG2 functionality to continually repopulate glial tumors. To achieve its transcriptional function, OLIG2 must dimerize via its bHLH domain. Stabilized alpha-helices of OLIG2 (SAH-OLIG2) peptides of the OLIG2 bHLH domain were generated in an effort to disrupt this pathologic dimerization. While helical stabilization of several SAH-OLIG2 peptides was achieved, specific engagement and disruption of the native bHLH dimer did not occur, informing alternative design strategies for future targeting efforts. These studies underscored the importance of interrogating the OLIG2 dimeric structure and catalyzed the discovery of candidate OLIG2 interaction partners for therapeutic targeting.

Table of Contents

Title Page i

Abstract iii

Table of Contents v

Lists of Figures and Tables viii

Acknowledgements x

Chapter 1: Introduction 1
Protein-protein interactions 2
Protein structure and function 2
Probing and targeting protein-protein interactions 3
Small molecules 4
Antibodies 6
Alpha-helical peptide mimetics 6
Summary 11
Apoptosis and the BCL-2 family 11
Apoptosis 11
The BCL-2 family of proteins 14
p53 upregulated modulator of apoptosis (PUMA) 16
PUMA and neuroblastoma 18
Structural interaction of multidomain pro-apoptotics and BH3-only proteins 18
Summary 21
Transcription factor targeting 21
Overview of transcription factor targeting 21
Basic helix-loop-helix proteins 24
The bHLH protein OLIG2 26
OLIG2 and glioma 27
Summary 28
References 30

Chapter 2: Multimodal Interaction with BCL-2 Family Proteins Underlies the Pro-Apoptotic Activity of PUMA BH3 43
Abstract 44
Introduction 45
Results 47
Design, synthesis, and anti-apoptotic binding activity of hydrocarbon-stapled PUMA BH3 helices 47
Biophysical and anti-apoptotic binding characterizations of PUMA SAHB$_{A1}$ and its negative control point mutant 51
PUMA SAHB directly binds to BAX by initial interaction at the α1/α6 trigger site . . . 51
PUMA SAHB directly activates BAX-mediated pore formation 57
Generation of a cell permeable PUMA SAHB 60
PUMA SAHB induces caspase 3/7 activation and cell death by engagement of anti- and pro-apoptotic targets 64

Specificity and physiologic relevance of PUMA SAHB activity . . . 68
Discussion . . . 71
Methods . . . 75
Attributions . . . 83
References . . . 83

Chapter 3: Targeting of OLIG2 Using Stapled Alpha-Helical Peptides . . . 88
Abstract . . . 89
Introduction . . . 90
Results . . . 93
Design, synthesis, and biophysical characterization of SAH-OLIG2 peptides . . . 93
Functional evaluation of SAH-OLIG2 peptides using electrophoretic mobility shift assays . . . 97
Yeast two-hybrid binding assay for Olig2 subdomains . . . 101
Design, synthesis, and biophysical characterization of doubly-stapled SAH-OLIG2 peptides . . . 104
Functional evaluation of dSAH-Olig2 peptides using electrophoretic mobility shift assays . . . 104
Generation of recombinant OLIG2 protein . . . 107
Improved EMSA assay allows for separation of DNA/peptide binding from potential protein/peptide disruption effect . . . 110
Discovery of putative novel interactors of OLIG2 using a whole genome yeast Two-hybrid screen . . . 111
Discussion . . . 116
Methods . . . 118
Attributions . . . 121
References . . . 122

Chapter 4: Ongoing and Future Work . . . 126
Identification of novel binding partners of PUMA . . . 127
Full-length PUMA protein pulldowns identify a variety of novel interaction partners . . . 127
Stapled PUMA peptides identify direct PUMA BH3-binding proteins . . . 129
Initial validation of nuclear exportins as PUMA-interacting proteins . . . 131
Future directions . . . 134
Structural and interaction analyses of OLIG2 . . . 135
Structural and biochemical studies using recombinant OLIG2 protein . . . 135
Evaluation of putative interacting proteins of oLIG2 identified by yeast two-hybrid . . . 137
Summary . . . 138
Methods . . . 140
Attributions . . . 143
References . . . 143

Chapter 5: Conclusions . . . 146
Discussion of results . . . 147
Mechanistic dissection of PUMA BH3 domain's role in promoting apoptosis . . . 147
Targeting pathogenic OLIG2 transcription using stabilized α-helical peptides . . . 148
Considerations . . . 150

Structured peptide versus whole protein biology 150
Future generations of stapled peptide 151

List of Figures and Tables

Chapter 1

Figures

1-1: Schematic of chemical stapling technique . . . 9
1-2: The BCL-2 family of apoptotic regulators can be separated into three families . . . 15
1-3: BIM SAHB directly binds BAX in a site directly opposite the canonical BH3 binding groove . . . 20
1-4: *Olig2* is required for the formation of gliomas in a mouse tumor model . . . 29

Tables

1-1: Published stapled alpha-helical peptides . . . 10

Chapter 2

Figures

2-1: Circular dichroism analysis of PUMA BH3 . . . 48
2-2: Sequence composition and anti-apoptotic binding activity of a panel of hydrocarbon-stapled PUMA BH3 peptides . . . 50
2-3: Helicity and anti-apoptotic binding activity of PUMA $SAHB_{A1}$ and its negative control point mutant . . . 52
2-4: NMR analysis of ^{15}N-BAX upon PUMA $SAHB_{A1}$ titration . . . 54
2-5: Photoreactive PUMA SAHBs localize the BH3 interaction site on BFL-1/A1DC with high fidelity . . . 56
2-6: BAX interaction site analysis by PUMA SAHB photoaffinity labeling and mass spectrometry . . . 58
2-7: Deletion of the C-terminal α9 helix of BAX increases PUMA SAHB photoaffinity labeling to the canonical BH3 binding pocket . . . 59
2-8: PUMA $SAHB_{A1}$ triggers BAX-mediated liposomal and cytochrome *c* release . . . 61
2-9: Characterization of cell permeable PUMA $SAHB_{A2}$ . . . 62
2-10: Cell permeable PUMA $SAHB_{A2}$ engages a diversity of BCL-2 family targets, activates caspase 3/7, and decreases the viability of neuroblastoma cells . . . 65
2-11: A biotinylated version of PUMA SAHB co-precipitates native anti- and pro-apoptotic BCL-2 family proteins . . . 67
2-12: PUMA $SAHB_{A2}$ activity is BAX/BAK-dependent . . . 69
2-13: Full-length PUMA protein, expressed in HEK 293T cells, targets native anti- and pro-apoptotic BCL-2 family proteins . . . 70
2-14: Sequence homology of BIM, BAX, and PUMA BH3 domains . . . 72
2-15: A model for multimodal activation of BCL-2 family proteins by PUMA . . . 74

Tables

2-1: Published stapled alpha-helical peptides . . . 82

Chapter 3

Figures

3-1: Schematic of bHLH dimerization disruption using stapled peptides . . . 92
3-2: A panel of SAH-OLIG2 and -E12 peptides with varying lengths and staple positions show a range of α-helical stabilization . . . 94
3-3: Evaluation of SAH-OLIG2 and -E12 peptides by electrophoretic mobility shift assays (EMSA) . . . 98
3-4: Specificity testing identifies charge, not sequence, as the driving force behind the observed SAH-OLIG2 activity . . . 100

3-5: Yeast two-hybrid analysis of full-length OLIG2 and its subdomains 102
3-6: Double stapled, two helix SAH-OLIG2 peptides demonstrate enhanced α-helical character 105
3-7: dSAH-OLIG2 peptides compete non-specifically for DNA as assessed by EMSA 106
3-8: Production and purification of functional, recombinant GB1-OLIG2 108
3-9: Evaluation of SAH-OLIG2, -E12, and dSAH-OLIG2 peptides by a refined EMSA . . . 112
3-10: Whole human genome yeast two-hybrid analysis of full-length OLIG2 and its subdomains identifies novel candidate OLIG2 interaction partners 115

Chapter 4

Figures

4-1: Schematic of proteomics screen to identify novel PUMA interaction partners 128
4-2: Full-length PUMA protein and biotinylated PUMA pSAHB both pull down native XPO5 from mammalian cells 132
4-3: Full-length PUMA protein pulls down native XPO1, whereas BIM does not 133
4-4: OLIG2 has a predicted helix-loop-helix domain 136
4-5: OLIG2 binds to DVL3 in mouse neurospheres 139

Tables

4-1: Top four identified biological pathways of full-length PUMA interaction partners 130
4-2: Top four identified biological pathways of direct PUMA BH3 interaction partners . . . 130

Acknowledgements

Completion of this thesis would not have been possible without the help of several people.

I would like to thank Drs. Bruce Zetter, James DeCaprio, Nika Danial, and Matthew Shoulders for agreeing to serve on my thesis defense committee. I would also like to thank Drs. Bruce Zetter, Charles Stiles, and Jarrod Marto for their years of advice and guidance as my dissertation advisory committee. Dr. Stiles has also been an essential collaborator for the OLIG2 work in this thesis, and his mentorship has been invaluable. The entire Stiles lab has been wonderful and welcoming, allowing me to be an honorary Stiles lab member. In particular, Pat Nakatani and John Alberta offered frequent technical help. Dimphna Meijer has been the best collaborator I could imagine, teaching me about OLIG2 biology and keeping me sane through the ups and downs of our project.

In addition to the Stiles lab, several labs have been welcoming when I needed help with a new technique or system. Dr. Marc Vidal permitted me to perform yeast two-hybrid screens in his lab, aided by Drs. David Hill, Amelie Dricot and Nidhi Sahni. Drs. David Andrews (McMaster University) and Riccardo Dalla-Favera (Columbia University) allowed me to come to their labs to learn various techniques. All of these collaborations, whether a week or several years, have greatly aided my work, and I'm deeply appreciative.

I would also like to thank my advisor, Dr. Loren Walensky, and all of the members, past and present, of the Walensky lab. Loren's optimism and enthusiasm for our work and for science in general is incredibly motivating, and his attention to detail and high standards have made me a better scientist. Craig Braun was a terrific bay mate and a good friend who was always willing to brainstorm with me when things weren't working. James LaBelle, Greg Bird, Liza Leshchiner, Marina Godes, Kojo Opoku-Nsiah, and Michelle Stewart provided me with

encouragement and support, scientific and otherwise, throughout my time in graduate school. The Walensky lab as a whole is a great family, and it makes it so much nicer to go to work every day.

Most importantly, I would like to thank my friends and family. Maija Garnaas, Chelsea He, Tim Curran, and Jim Abshire are fellow graduate students across Boston who have been instrumental in my scientific development as well as in the maintenance of my sanity through ski trips, spin classes, Sunday night dinners, and friendly faces. My sister Katherine served as my vent when things got difficult – those five minute phone calls got me through some tough days. I would like to thank my parents, Doug and Nancy, for their unfailing support and for instilling in me the values of hard work and persistence. Finally, to my husband Matt: you push me harder than anyone else because you think I can do it. Thanks for believing in me.

Chapter 1

Introduction

I. Protein-protein interactions

Since their discovery in the mid-19th century[1], proteins have long proven critical to the inner workings of cells. The vast majority of cellular functions are carried out by proteins, leading one early scientist to ask "[w]ould it be far from the truth, therefore, to look upon the enzyme as the chemical basis of life?"[2] A protein's regulatory function is carried out by its physical interactions with cellular metabolites, lipids, nucleic acids, and other proteins. The nature of these protein-protein interactions (PPIs) and the ability to selectively activate or disrupt them continues to be the subject of intense exploration and is the basis for this thesis.

Protein structure and function

Protein structure and function are intimately intertwined, and thus in order to understand how proteins work, one must delve into their structure. Protein structure can be organized into four tiers: primary, secondary, tertiary, and quaternary structure. A protein's primary structure consists of its amino acid sequence, as determined by its DNA coding sequence, subsequent RNA processing, and translation. The secondary structure of a protein is defined by a series of local substructures, including α helices, β sheets, and turns. Stretches of unstructured and structured sections of the protein are strung together into an extended three dimensional structure, termed the tertiary structure. An array of forces holds these chains together, including hydrophobic interactions, hydrogen bonding, salt bridges, and disulfide bonding. These substructures frequently have local consequences on function, generating pockets of activity and interaction. Finally, the quaternary structure is comprised of complexes of proteins, which interact with one another in numerous ways to further diversify cellular functions.

Protein-protein interactions, or PPIs, are as variable as the proteins that comprise them. However, overarching principles have been determined. Given their importance in the functional output of proteins, PPI sites display stronger evolutionary conservation than non-binding sites in

the protein sequence[3,4]. The average size of a PPI site is 1600 ± 400 Å^2 [5], although this range can vary widely from approximately 350 – 4750 Å^2 [6]. Importantly, the entirety of the interaction surface is not required for binding. Mutational analyses have identified a number of "hot spot" residues that contribute disproportionately to the interaction's binding affinity[3,4]. These hot spots tend to cluster near the center of the PPI surface and are surrounded by a ring of residues of more flexible content. These surrounding residues frequently occlude the local solvent from the core interaction[7].

Hot spot residues have diverse character. Hydrophobic patches often create greasy binding surfaces for interaction[8], with an increase in aromatic (histidine, tyrosine, phenylalanine, and tryptophan) and aliphatic residues (leucine, isoleucine, valine, and methionine) observed at the interface[5]. Amino acids with hydrogen bonding capacity are frequently critical residues, with 67% of hot spot residues participating in hydrogen bonding with the partnering protein (as opposed to 30% of non-hot spot residues)[4]. While most charged residues are less prominent on the interaction face, electrostatic interactions can contribute to binding affinity, albeit less frequently[5,9]. Finally, all of the hot spot residues are more tightly packed than those not involved in interaction[3,5], indicating the narrow margin for error on the PPI surface.

Probing and targeting protein-protein interactions

Prior to the completion of the Human Genome Project, the total number of predicted human genes climbed to greater than 100,000. This number has since been amended to 20,000-25,000 genes[10], with the human proteome numbering around 20,000 proteins[11]. Of these 20,000 proteins, there are an estimated 3,000 that are deemed "druggable" with conventional therapeutics, based upon similarity to targets already drugged successfully[12]. This accounts for about one-quarter of known disease-driving drug targets[12], leaving several thousand desirable targets "undruggable." Given the importance of PPIs in both normal and

diseased cellular settings, this number would decrease significantly if protein-protein interactions were tractable targets. However, such targeting has proven difficult for the larger, more featureless nature of PPI surfaces. Nevertheless, a variety of modalities have been investigated for targeting PPIs, including small molecules, antibodies, and peptide mimetics.

Small molecules

It has historically been difficult to target protein interaction surfaces with small molecules, primarily because PPIs are much larger than typical small molecule-protein interaction surfaces (1600Å^2 as compared to 300-1000Å^2)[5,13]. Given their size, small molecules are frequently more adept at binding deep grooves or pockets, features which are atypical of PPIs. In addition, existing small molecules serve as ineffective screening libraries for PPI targeting. In general, these libraries are biased for low molecular weight compounds that target common enzymatic binding clefts, such as protein kinase active sites[1]. Despite these limitations, several molecules have been developed which can selectively perturb PPIs.

- p53, the "guardian of the genome"[14], is the most frequently mutated or deleted gene in human cancers[15]. However, wildtype p53 can also be thwarted by upregulation of the proteins MDM2 and MDMX, which bind to p53 and prevent its transcriptional functions and target it for degradation[16]. Structural analyses of this interaction identified a short 15-amino acid domain of p53 which bound to a deep hydrophobic pocket on MDM2. Three hot spot residues (F19, W23, and L26) were shown to be particularly important for the interaction[17]. This finding suggested that it might be feasible to find a small molecule which could target this subset of residues in a well-defined groove. Screening of a library of synthetic chemicals led to the discovery of a family of molecules that could disrupt the p53-MDM2 interaction with IC_{50} values between 100 and 300 nM[16]. Further optimization identified one molecule, Nutlin-3a (IC_{50}, 90nM), a potent analog that restores p53

function and displays efficacy in a mouse model of sarcoma. Nutlin-3 molecules have provided a blueprint for next-generation designs of MDM2 and MDMX inhibitors.

- Human papillomavirus (HPV) is responsible for an array of disease manifestations, spanning harmless warts to malignant tumors[18]. The small genome of this virus encodes two proteins, E1 and E2, whose interactions enable the continued replication of viral DNA. High throughput screening identified a lead molecule with an IC_{50} of 350 nM in an *in vitro* disruption assay[18]. Additional optimization enhanced the potency nearly 40-fold[19]. In this case, no structural information was available to direct optimization.
- Interleukin-2 (IL-2) receptors reside on the cell surface of T cells, signaling the cells to grow and divide upon engagement by the IL-2 ligand[20,21]. Recombinant IL-2 has been used to restore immune system function in a variety of disease states[21], and antibodies used to disrupt the IL-2/IL-2R interaction are clinically effective as immunosuppressive therapy[21]. Structural studies led to the development of small molecule antagonists of the IL-2/IL-2R interaction with an IC_{50} of 3 μM[22]. Additional fragment-based medicinal chemistry efforts resulted in a 50-fold improvement in efficacy *in vitro* and modest effects in short-term cellular assays[23].
- The BCL-2 family of proteins regulates the intrinsic pathway of apoptosis, and members of the anti-apoptotic class of this family are frequently upregulated in cancer[24,25]. In 2005, Abbott Laboratories performed a fragment-based NMR screen against the canonical interaction pocket of BCL-X_L, an anti-apoptotic member of the BCL-2 family[26]. The lead compound, ABT-737, binds three anti-apoptotic proteins BCL-2, BCL-w, and BCL-X_L with high affinity (Ki ≤1 nM) and displays potent single agent efficacy in a series of cancer cell lines. Treatment with the molecule led to complete regression of tumors in a xenograft model of small cell lung cancer. In addition, ABT-737 also shows strong synergistic effects with clinical chemotherapeutic agents in a variety of cancer models. This

molecule has since been further optimized for reduced serum binding and is in Phase I/II clinical trials for small cell lung cancer and hematologic malignancies[27].

Antibodies

The use of antibodies for targeting proteins or PPIs is an attractive strategy, since they are nature's solution to the challenge of binding large and flat surfaces. While antibodies have the therapeutic benefit of being highly specific for their intended target, they have proven difficult to use due to their poor oral bioavailability and immunogenic side effects[21]. Additionally, antibodies fail to penetrate the cellular membrane, and thus their targets are limited to those on the exterior or surface of the cell. Nevertheless, early technical challenges have been overcome (e.g. humanized monoclonal antibodies), and antibodies now represent one of the most rapidly growing classes of novel drugs, with 17 antibodies approved for clinical use to date[28].

Perhaps the most famous example of a therapeutic antibody is Herceptin, which is used for the treatment of HER2-positive metastatic breast cancer. HER2 is a transmembrane receptor tyrosine kinase which, upon dimerization, promotes cellular proliferation and survival through the RAS-MAP kinase pathway[29]. Aberrant dimerization can result from receptor overexpression or mutagenesis, as is often observed in metastatic breast cancer, leading to abnormally high levels of cellular growth[30]. Herceptin blocks HER2 dimerization and the resultant signaling cascade, leading to tumor regression[29]. Since its introduction into the clinic almost 20 years ago, it has become one of the standards of care for HER2-positive breast cancer.

Alpha-helical peptide mimetics

Alpha helices commonly mediate PPIs, participating in 40% of homodimeric interfaces and 26% of heterodimeric interfaces[31]. The prevalence of this interaction makes α-helical peptides an attractive option as dominant negative regulators of PPIs. As such, one could

generate peptides consisting of the relevant amino acid sequence to serve such a purpose; however, outside the constraints of the protein infrastructure, short peptides do not typically maintain their native α-helical shape. In addition, the loss of secondary structure renders such peptides susceptible to proteolytic degradation. This combined with the cell impermeability of most peptides have limited their therapeutic use. A variety of methods have been developed to synthesize modified peptides that recreate the natural structure or binding surface of the interacting α-helix.

One approach is to produce molecules that differ in the naturally observed chemical backbone of a protein. Peptoids are one example of this, in which the R group of each amino acid is shifted from the α-carbon to the backbone nitrogen[32]. While these molecules do not necessarily form α-helices (in fact, the loss of CO • • • HN intrapeptide bonds may discourage it), they are more proteolytically stable due to the protected nitrogen in the backbone[32]. Other alterations have been attempted in the peptide backbone, including urea peptidomimetics and peptidosulfonamides[33]. Some success has been observed by substituting β-amino acids in place of the more common α-amino acids, generating β-peptides. These amino acids have more inherent α-helical character and are more proteolytically stable due to a more rigid backbone.[34]

More directed attempts to restore α-helical character have involved changes at the α-carbon or R groups of the amino acids. The insertion of glutamate/lysine pairs one α-helical turn apart (*i,i+4*) can form stabilizing salt bridges in short peptides[35], and the insertion of two histidines at the *i,i+4* positions can similarly stabilize α-helical structure[36]. The formation of covalent bonds through lactams[37] or disulfide interactions[38] between residues one or two α-helical turns apart (*i,i+3*; *i,i+4*; *i,i+7*) can nucleate α-helicity. Finally, α, α-disubstitution at the α-carbon has also been found to induce α-helicity[39].

To date, the most advanced method of generating stabilized α-helical peptides is the formation of "stapled" peptides. In 1998, Grubbs and colleagues developed a system in which non-natural amino acids with terminal olefins (L-serine and L-homoserine O-allyl ethers) were inserted into a peptide sequence at *i,i+4* positions[40]. These olefins were methathesized using a ruthenium catalyst, generating a closed ring holding the residues together. At this stage, there was little evidence that this crosslinking strategy enhanced the α-helicity of the peptide.

Two years later, Schafmeister et al. further developed this technique by screening a variety of all-hydrocarbon non-natural amino acids, sampling alternative sites of insertion, stereochemistry (R vs. S), and crosslinker length[41]. An α-methyl group was installed on the α-carbon along with the non-natural R group to further nucleate helicity. The α-helicities of these peptides were evaluated using circular dichroism, demonstrating significantly enhanced α-helical character (35-85% α-helical). Improved proteolytic stability of the peptides, evaluated by trypsin cleavage, was observed, likely due to both the increased structure of the peptide and the lack of labile atoms in the closed ring or "staple" (**Figure 1-1**). An α-helical domain of the BCL-2 family member protein BID was the first functional stapled peptide. This domain, known as the BH3 domain, regulates interactions between BID and other members of the BCL-2 family, which together mediate the intrinsic pathway of apoptosis[42]. The BID stapled peptide, termed BID SAHB for stabilized alpha-helix of BCL-2 domains, showed restored α-helical structure, protease resistance, and cell permeability. BID SAHB recapitulated the biological activity of BID protein, including the induction of cytochrome *c* release from intact mitochondria and activation of apoptosis in a number of cancer cell lines. In addition, BID SAHB suppressed tumor growth in a mouse xenograft model of human leukemia. Today, multiple iterations of stapled peptides have been used for a variety of purposes, including mechanistic studies and therapeutic applications (**Table 1-1**).

Figure 1-1

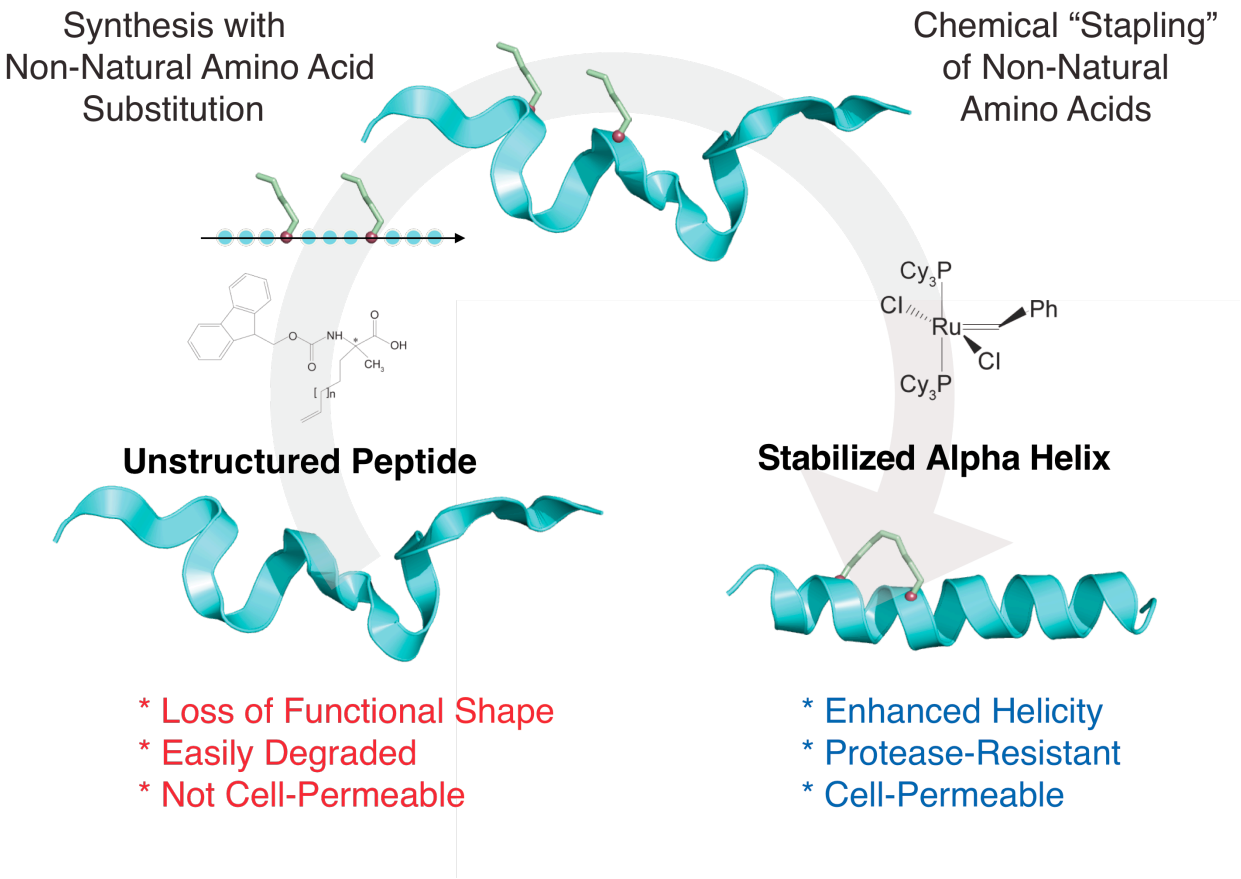

Schematic of chemical stapling technique. Unstructured short peptides typically have little intrinsic shape, are proteolytically unstable, and are not cell-permeable. Introduction of two non-natural amino acids with olefinic side chains allows for chemical crosslinking of spatially adjacent residues using a ruthenium-based catalyst. Such "stapling" can restore α-helical shape and confer protease resistance and cell permeability.

Table 1-1: Published stapled alpha-helical peptides

Stapled Peptide	Function	Reference
BAD SAHB	Mechanistic studies of BAD's role in apoptosis and the regulation of glucose metabolism	Walensky, *Mol Cell*, 2006[43] Danial, *Nature Med*, 2008[44]
BAX SAHB	Dissection of BAX propagation mechanism	Gavathiotis, *Mol Cell*, 2010[45]
BID SAHB	Targeting of anti-apoptotic BCL-2 family proteins; *in vivo* efficacy in human leukemia mouse xenografts	Walensky, *Science*, 2004[46] Walensky, *Mol Cell*, 2006[43]
fStAx-35	Blocks TCF binding to β-catenin, interfering with canonical Wnt transcriptional activity	Grossmann, *PNAS*, 2012[47]
MCL1 SAHB	Selective inhibitor of MCL1	Stewart, *Nature Chem Bio*, 2010[48]
NPY-S1, -S2	Anticonvulsant neuropeptides that agonize neuroreceptors in the brain; suppress seizures in mouse model of epilepsy	Green, *Bioorg Med Chem*, 2013[49]
NYAD1	Inhibits capsid particle assembly of HIV	Zhang, *J Mol Bio*, 2008[50]
S1A10, S2A10	Apolipoportein mimetics that cause cholesterol efflux from cells by targeting ABCA1 transporter	Sviridov, *Biochem Biophys Res Commun*, 2011[51]
SAH-BCL-9	Disrupts β-catenin/BCL-9 interaction and resulting downstream Wnt transcriptional activity; *in vivo* efficacy in human colorectal carcinoma and myeloma mouse xenografts	Takada, *Sci Trans Med*, 2012[52]
SAH-gp-41	Inhibits fusion of HIV with extracellular membrane; double stapled and orally bioavailable	Bird, *PNAS*, 2010[53]
SAH-p53-8	Disrupts inhibitory p53-MDM2 and –MDMX interactions and restores the p53 transcriptional program	Bernal, *J Am Chem Soc*, 2007[54] Bernal, *Cancer Cell*, 2010[55]
SAHM1	Mastermind peptide that disrupts Notch transcriptional complex; *in vivo* efficacy in T-ALL mouse xenograft	Moellering, *Nature*, 2009[56]
SP1-6	Bind at the co-activator protein binding site of the estrogen receptor	Phillips, *J Am Chem Soc*, 2011[57]

Summary

A protein's function is intimately related to its structure, often dictating its protein interactions, localization, enzymatic activity, and susceptibility to degradation. Few proteins act entirely alone, and a protein's structure also dictates the library of molecules (nucleic acids, carbohydrates, other proteins) with which it can interact. The study of protein-protein interactions has advanced both a mechanistic understanding of cellular biology and approaches for therapeutic intervention. While traditional methods for targeting protein-protein interactions exist (e.g. small molecules and biologics), such approaches are limited due to the larger, flatter surfaces of protein-protein interactions and their intracellular location. Small peptide α-helical mimetics, representative of a common interaction motif at protein-protein interfaces, may serve as dominant negative agents for such interactions. Stapled α-helical peptides, developed in 2000 by Schafmeister et al.[41], have proven to be valuable tools for both dissecting molecular pathways and developing prototype therapeutics.

II. Apoptosis and the BCL-2 family

Cells are perpetually presented with three life choices: proliferation, maintenance, or death. The delicate balance between these three choices ensures a healthy organism, allowing for a steady supply of new cells or disposal of excess or injured cells, as the needs arise. The first identified form of programmed cell death, called apoptosis, is the cell's primary mechanism for "controlled cell deletion"[58]. It is conserved through all multicellular eukaryotes[59], and gain-or loss-of-function in this pathway leads to disease.

Apoptosis

The loss of cells in living organisms was documented in the late 1960s[60-62], but it wasn't until 1972 that the term "apoptosis" was coined[58]. This form of programmed cell death occurs

throughout normal embryonic development and in healthy adult tissues, clearing away unnecessary or damaged cells. In disease states, this process is often deregulated. Too much apoptosis results in degenerative diseases, immunodeficiency, and infertility, while too little apoptosis leads to cancer or autoimmunity[59]. Apoptosis can be induced by a variety of stimuli, including developmental signals[63], DNA damage[64], growth factor deprivation[65,66], anoikis[67], and oncogene activation[68,69]. Morphologically, apoptosing cells undergo nuclear condensation, DNA fragmentation, membrane blebbing, and cell shrinkage[70], producing distinct diagnostic cellular phenotypes for experimental study.

Some of the earliest and most elegant studies to understand the biological basis for apoptosis came from the *C. elegans* research community in the 1980s. The fate of all cells in the nematode was meticulously traced from the beginning of development, and it was noted that a subset of cells always died at predictable times. Robert Horvitz and colleagues decided to mutagenize the worms to elucidate the relevant genes, and what emerged were the earliest known apoptotic genes. *Ced-3* and *ced-4* were shown to be pro-apoptotic factors required for cell death, while *ced-9* had an anti-apoptotic, protective phenotype[71,72]. These genes have since been shown to have homologues throughout all metazoans and are thus fundamental cellular regulators.

Apoptosis proceeds through the activity of enzymes called caspases. Caspases are produced as an inactive pro-caspase, which following proteolytic processing, associates into dimers to form the active enzyme[41,73]. The active enzyme is a cysteine protease that cleaves conserved amino acid sequences following an aspartic acid residue. Caspases can be sorted into two categories: initiator and effector caspases. Initiator caspases, usually capable of self-cleavage and activation, recognize and expand the initial apoptotic signal. Effector caspases, which require initiator caspases for activation, carry out the apoptotic events[59] by cleaving proteins necessary for cell life and disassembling cellular substructures. For example, caspase-

3 cleaves I^{CAD}, which is an inhibitor of the nuclease responsible for DNA fragmentation[74], and caspase-6 cuts nuclear lamins[75]. Together these cleavage reactions produce the observed chromatin condensation characteristic of apoptotic cell death.

Apoptosis can be carried out by two pathways: the extrinsic pathway and the intrinsic pathway. The extrinsic pathway is initiated through binding and activation of transmembrane proteins of the death receptor family (ex. FAS[76] and TNFR-1)[77,78]. Activation of these proteins results in the formation of the death-inducing signaling complex (DISC), comprised of FADD[79] and procaspases-8 and -10[76,80]. Procaspases-8 and -10 self-cleave due to induced proximity, followed by subsequent activation of downstream effector caspases. Additionally, caspase-8 can further amplify the apoptotic signal by cleaving BID to tBID[81,82], which engages the intrinsic pathway of apoptosis.

The intrinsic pathway is initiated by a wide variety of cellular stressors, including DNA damage, oxidative stress, cytosolic calcium ion overload, and ER stress[80]. These signals activate the BCL-2 family of proteins (discussed in detail below) to induce mitochondrial outer membrane permeabilization (MOMP). MOMP allows the release of cytochrome *c*[83,84] and other apoptogenic factors into the cytosol, where cytochrome *c*, apoptotic protease activating factor (APAF-1), and procaspase-9 assemble to form the apoptosome[85]. The apoptotsome then activates procaspase-9, which further cleaves downstream effector caspases such as caspase-3 and -7.

Should apoptosis be activated in error, a variety of proteins exist to inhibit the activated pathways. Unlike caspase-8, FLIPs (FADD-like ICE inhibitor proteins) bind available FADD cofactor but lack the essential catalytic residues to cleave downstream targets[86,87]. IAPs (inhibitors of apoptosis proteins) directly inhibit the effector caspases-3 and -7[88]. However, in most cases, once the onslaught of caspase activation begins and the mitochondria are compromised, apoptosis proceeds.

The BCL-2 family of proteins

The intrinsic pathway of apoptosis is tightly regulated by members of the BCL-2 family of proteins, which carefully control the induction or repression of mitochondrial outer membrane permeabilization (MOMP). The founding member of the family, BCL-2 (B-Cell Lymphoma 2) was discovered in the 1980s as an oncogene of unknown function activated by a chromosomal translocation in human lymphomas[24,89,90]. Further studies showed that overexpression of the gene product led to increased cell survival and tumorigenicity[91-93] without influencing levels of cellular proliferation[91]. Since that time, BCL-2 family members have become well-established as mediators of the intrinsic apoptotic pathway, with evolutionary conservation in a wide variety of organisms[72,94,95] and key roles in a broad array of human diseases. For example, the anti-apoptotic BCL-2 proteins MCL-1 and BCL-X_L are two of the most frequently upregulated genes across all human cancers, while the pro-apoptotic BCL-2 proteins BOK and PUMA are commonly deleted[25].

BCL-2 proteins are divided into three subclasses based on function and sequence homology[96,97] (**Figure 1-2**). The four regions of sequence homology are known as the BH (BCL-2 Homology) domains. Multidomain proapoptotic proteins contain BH domains 1-3 and include members BAX, BAK, and BOK. Upon induction of apoptosis, these death-promoting proteins localize to the mitochondrial membrane[98] and oligomerize to form pores[99], resulting in MOMP. Cytochrome *c* diffuses through these pores into the cytosol[100], activating downstream caspases and the apoptotic cascade[101]. Simultaneous deletion of *Bax* and *Bak* in mice severely impairs normal development, while generating lymphocytes highly resistant to apoptotic stimuli[102]. In contrast, the antiapoptotic proteins (e.g. BCL-2, BCL-w, and BCL-X_L) contain BH domains 1-4 and function to promote cellular survival[91-93,103,104]. Finally, the proapoptotic BH3-only proteins

Figure 1-2

Walensky, *CDD*, 2006

The BCL-2 family of apoptotic regulators can be separated into three families.

Antiapoptotic BCL-2 proteins share BCL-2 homology (BH) domains 1-4 and serve a pro-survival function. Proapoptotic BCL-2 proteins are further subdivided into two classes. The multidomain proapoptotic proteins share BH domains 1-3 and carry out the final steps of mitochondrial permeabilization. The BH3-only proteins contain only the third BH domain and relay signals of cellular stress to other family members.

contain only the BH3 domain and respond to a variety of stimuli to induce apoptosis, including cytokine withdrawal[105], calcium ion flux[105], DNA damage[106], and infrared radiation[107].

Two major models have been proposed to explain the manner in which these three classes of BCL-2 family members interact to regulate the induction of apoptosis. In the first model, known as the "direct activation" model[108,109], BH3-only proteins are divided into two classes: activators, which can bind directly to proapoptotic proteins, and sensitizers, which can bind only to antiapoptotic proteins. Apoptosis results from the binding of the BH3 domains of activators to BAX and BAK, causing BAX and BAK to permeabilize the mitochondrial membrane and activate the downstream apoptotic pathway. In healthy cells, this process is prevented by the presence of antiapoptotic factors which can sequester incoming BH3-only proteins. Apoptosis is activated only when sufficient levels of BH3-only proteins are present to saturate the antiapoptotic factors. Free activators are then able to bind directly to the death proteins, triggering the apoptotic cascade.

In contrast, in the "indirect activation" model[110,111], BAX and BAK are in a constitutively active state, blocked only by repressive binding of the antiapoptotic proteins. In this model, all BH3-only proteins bind only to antiapoptotic proteins. Apoptosis is activated when BH3-only proteins bind to the antiapoptotic proteins and trigger their release from the death proteins. The uninhibited death proteins are now able to permeabilize the membrane, causing the activation of apoptosis. Understanding how this family of proteins works together to respond properly to the cellular environment remains an active area of investigation.

p53 upregulated modulator of apoptosis (PUMA)

PUMA (p53 Upregulated Modulator of Apoptosis) belongs to the BH3-only class of the BCL-2 family and acts to promote the induction of apoptosis. *Puma* was first characterized as a transcriptional target of p53, showing rapid up-regulation upon p53 stimulation[112-114]. PUMA was

found to share functions with other BCL-2 family members, including localization to the mitochondrial membrane, the ability to induce the release of cytochrome *c* from mitochondria, and the capacity to initiate apoptosis in human cells. *Puma*$^{-/-}$ cells are less sensitive to a variety of both p53-dependent and independent insults, including irradiation, cytokine withdrawal, hypoxia, and DNA-damaging agents[106,107,115]. While *Puma*$^{-/-}$ knockout mice show little phenotype of their own, 50% of *Puma*$^{+/-}$*/Bim*$^{-/-}$ mice develop lymphomas, in comparison to only 20% of *Bim*$^{-/-}$ mice[116]. This implies that PUMA and BIM have overlapping but distinct functions. In addition to its role at the mitochondria, PUMA is necessary for the induction of ER stress-induced apoptosis[117,118]. Together, these data highlight the importance of PUMA's role in the regulation of apoptosis, both on its own and in conjunction with other BH3-only proteins. However, the mechanism by which PUMA induces apoptosis remains controversial.

As outlined above, the direct activation model divides the BH3-only class of proteins into broad categories: direct activators and sensitizers. While BIM[119,120] and BID[43] are accepted as direct activators, the role of PUMA as either a direct activator or a sensitizer remains unclear. Evidence to support PUMA as a direct activator comes from studies of both the PUMA BH3 domain and the full-length protein, in which the PUMA BH3 domain is shown to physically associate with and activate BAX[121-125]. This experimental evidence suggests that PUMA, like BIM and BID, may also directly activate BAX and BAK to induce apoptosis.

In contrast to this work, however, several groups have published evidence suggesting a role for PUMA exclusively as a sensitizer BH3-only protein. Attempts to characterize the BCL-2 family binding partners for PUMA have uniformly shown PUMA to be a pan-antiapoptotic binder [126-128]; however, the association between PUMA and BAX or BAK has proved difficult to confirm[129,130]. The discrepancies between these studies and those suggesting direct activation may result from the transient nature of a PUMA-BAX interaction or the lack of structure of the

PUMA BH3 peptides used. These contradictions necessitate further study of PUMA and its role in BAX/BAK activation.

PUMA and neuroblastoma

While BH3-only proteins frequently overlap in function[131], it is clear that some stress stimuli or cell types engage the pro-apoptotic function of some BH3-only proteins more than others. While PUMA broadly acts as a downstream effector of p53-driven apoptosis, it has also been show to have more selective roles in the activation of neuronal and neural precursor cell apoptosis. In particular, activation of apoptosis by proteasomal inhibitors[132], oxidative stress[123], or DNA damaging agents[133,134] in cells of neuroectodermal origin was dependent on the presence of PUMA. Interestingly, a study by Reimertz et al. in the human neuroblastoma SH-SY5Y cell line identified PUMA as the top upregulated pro-apoptotic gene following induction of ER stress and the ensuing apoptotic response[118]. Overexpression of PUMA in these cells was sufficient to induce apoptosis, suggesting that a PUMA mimetic could serve a therapeutic function in neuroblastoma cells.

Structural interaction of multidomain pro-apoptotics and BH3-only proteins

The first high resolution structure of a member of the BCL-2 family was that of BCL-X_L. This anti-apoptotic protein was structurally defined by a series of α-helices, two which were highly hydrophobic and localized at the core of the protein, surrounded by external amphipathic helices. Notably, three of the four conserved BCL-2 homology domains were spatially adjacent, forming a deep hydrophobic cleft[135]. This cleft was determined to be the site of interaction for binding the BH3 domain of the proapoptotic protein BAK[136], suggesting a mechanism by which anti-apoptotic proteins sequester pro-apoptotic proteins and thereby block their function. This

paradigm has held for the BH3 interactions of all proapoptotic proteins, both multidomain and BH3-only, to the anti-apoptotics proteins.

Based on the sequence similarity of the multidomain proapoptotics BAX and BAK with the antiapoptotic proteins, it has been hypothesized that if BH3-only proteins could in fact bind to BAX or BAK, the binding would occur in the same hydrophobic pocket. In an effort to resolve this question, NMR studies were performed with a stabilized version of the BH3 domain of BIM (BIM SAHB) and full-length BAX[119]. Surprisingly, rather than binding to the canonical hydrophobic groove, BIM SAHB bound to a more shallow hydrophobic binding site on the opposite face of the protein consisting of overlapping α-helices 1 and 6 (**Figure 1-3**). This new binding site was shown to be the site of direct activation of BAX by the BIM BH3 domain, and was thus named the "trigger site." This trigger site has since been the target of therapeutic development aimed at lowering the apoptotic threshold in cancer and other diseases of pathologic cellular excess[137].

Until recently, similar structural studies were difficult to perform on BAK, due to the challenge of producing full-length recombinant protein. However, recent work by Leshchiner et al. successfully generated a mutated version of full-length BAK that is amenable to large-scale recombinant protein production and purification[138]. To investigate the binding of BH3-only proteins on BAK, crosslinkable peptides of the BH3 domain of BID were incubated with the full-length recombinant BAK. Interestingly, these peptides bound exclusively to the canonical hydrophobic pocket, analogous to the binding of the BH3 domain on antiapoptotic proteins. Binding at this site caused activation of BAK in a variety of assays. These findings suggest that there may be two mechanisms of activation for the executioner proteins by the BH3-only class of proteins, one for cytosolic BAX and another for membrane-integrated BAK and perhaps BAX.

Figure 1-3

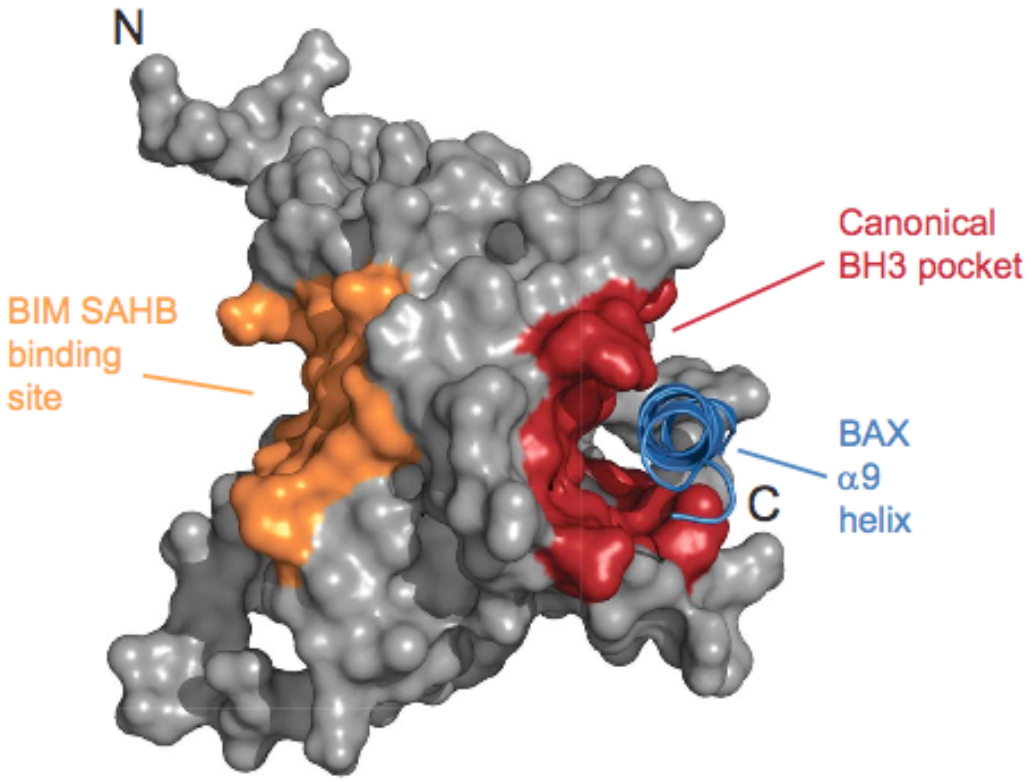

Gavathoitis, *Nature*, 2008

BIM SAHB directly binds BAX in a site directly opposite the canonical BH3 binding groove. On a structure of full-length BAX, the canonical binding groove, analogous to the BH3 binding groove on anti-apoptotic proteins, is shown in red, with the C-terminal α-helix 9 inserted into the groove of inactive BAX. The identified “trigger site” for BIM SAHB binding and activation, located on the opposite side of the protein, is shown in orange.

Summary

An organism's ability to carefully regulate the life and death of its cells is critical for growth and survival. Apoptosis, a form of programmed cell death, allows for the controlled destruction of unnecessary or deleterious cells, a process partially regulated by the BCL-2 family of proteins. Importantly, the BCL-2 family carefully integrates signals of cellular stress at the outer membrane of the mitochondria, where a balancing act between pro- and antiapoptotic proteins dictates the cellular outcome. Our understanding of the interactions among these proteins has grown enormously in the last two decades, providing novel opportunities for therapeutic targeting.

III. Transcription factor targeting

Transcription factors are fundamental regulators of cellular homeostasis, modulating with exquisite precision the timing and rate of gene expression. Despite their established pathogenic role in the development, progression, and maintenance of cancer[139], deregulated transcription factors have long been deemed "undruggable" due to the difficulty of targeting protein-protein and protein-DNA interactions, particularly within the nucleus. New pharmacologic strategies, including nucleic acid mimetics[140] and stabilized peptides[52,54,56], have reinvigorated efforts to address these formidable targets.

Overview of transcription factor targeting

Many of the most notorious oncogenes in cancer biology, such as RAS, AKT, and BCR-ABL, are protein kinases. These overactive, deregulated kinases ramp up the cellular signaling pathways that instruct a cell to grow, divide, and migrate. These proteins are also some of the most attractive targets from a therapeutic perspective. ATP binds to the vast majority of protein kinases through a deep hydrophobic cleft[141], providing an amenable site for traditional small

molecule targeting. Indeed, well-known cancer therapeutics including Imatinib (better known as Gleevec), Sunitinib, and Erlontinib all target a spectrum of protein kinases. Unfortunately, kinases represent only a small portion of known oncogenes. However, many of these kinase-driven signaling pathways converge on a smaller number of transcription factors, which serve as distinct nodes of regulation that can amplify diverse cellular signals: transcription factors.

There are three main classes of transcription factors important in human cancer[139]. In the first class, steroid receptors like estrogen and androgen receptors move to the nucleus and induce transcription upon binding of their respective ligands. A second class resides in the nucleus constitutively and become active only upon signaling from upstream kinase cascades. These resident nuclear proteins include c-JUN, E2F, and MYC. Finally, a third class of transcription factors are normally cytosolic and only move into the nucleus when a signal is received to activate transcription. Proteins like the STAT family and NF-kB fall into this group.

While these three classes of transcription factors all function in slightly different manners, their basic route to transcriptional output follows a similar path: nuclear localization, activation, association with co-factors and DNA binding, and transcription of downstream gene targets. Each of these steps offers possibilities for therapeutic targeting. Thus far, attempts have been made to modulate transcription factor activity with decoy oligonucleotide binding sites[142], DNA-binding sequence-specific polyamides[143], zinc finger nucleases[144], interfering RNA[145], and small molecules[146]. Additionally, many groups have made use of short, stabilized peptides (discussed in detail above) to disrupt interactions between transcription factors and other regulatory proteins, two examples of which are presented below.

- The protein Notch is a transmembrane protein that sits on the extracellular membrane. Ligand binding to the extracellular portion of the protein results in proteolytic cleavage of the receptor by γ-secretase, causing the release of an intracellular fragment called ICN1. ICN1 translocates to the nucleus, where it

engages two additional proteins, CSL and Mastermind (MAML). This complex is now sufficient to recruit core transcriptional machinery to activate Notch-dependent target genes[147]. Previously devised therapies include small molecule inhibitors of γ-secretase[148], but these molecules have a variety of off-target effects. In an effort to specifically target Notch, work by Moellering and colleagues examined known structures of the ICN1-CSL-MAML complex. Notably, an α-helical portion of MAML binds to a long groove formed by the juncture of ICN1 and CSL. Stapled peptides generated against this α-helical region inhibited formation of the ICN1-CSL-MAML complex, effectively turning off NOTCH-dependent transcription[56]. This peptide also showed *in vivo* efficacy in a mouse model of T-ALL.

- Myc (c-Myc, N-Myc, and L-Myc) is broadly expressed throughout development and in a subset of adult cells, regulating cellular proliferation, differentiation, and apoptosis[149]. A basic-helix-loop-helix leucine zipper (bHLH LZ) protein, Myc carries out its transcriptional activities through dimerization of its bHLH LZ region with the bHLH LZ region of its partner protein, Max. Notably, Myc is one of the mostly commonly overexpressed oncogenes in human cancers[25]. Despite this, there has been much hesitation about targeting Myc, due to its importance to normal and cancer cells alike. Additionally, it was unknown whether therapeutic modulation of Myc would be beneficial only to those tumors initially driven by Myc, or if it could also influence cancers of different origins. To address these questions, Soucek et al. generated an inducible, dominant negative form of Myc, termed “omoMyc”[150]. This mutant was installed into a preclinical mouse model of Ras-induced lung cancer, and both the therapeutic benefits and side effects were

monitored. Amazingly, upon induction of omoMyc, Ras-driven lung tumors disappeared. Additional effects were observed in other rapidly proliferating tissues (skin and bone marrow, for example), but these side effects were found to be completely reversible.

Myc inhibition has been approached in a number of ways, including both direct[151,152] and indirect[153] small molecule inhibition and short peptide inhibition[154,155]. These short peptides have targeted Myc's dimerization domain, which is predominantly made of two adjoined α-helices. However, none of these approaches have yet translated from the laboratory to the clinic.

Basic helix-loop-helix proteins

One of the largest classes of transcription factors is the basic helix-loop-helix (bHLH) family. These proteins are defined by the presence of an amino terminal basic region, followed by two amphipathic α-helices joined together by a small loop region[156-158]. bHLH proteins are critical for a variety of developmental processes throughout the tissues of an organism, including hematopoietic cells, cardiac muscle, skeleton, and both the peripheral and central nervous systems, and are of particular importance to the determination of cell-type specifications[159].

The first members of the bHLH family were discovered in 1989 by comparison of a variety of transcription factors that all bound to a common DNA consensus sequence known as an E-box (5'-CANNTG-3')[156]. Phylogenetic analyses have shown that the bHLH family is both expansive and ancient, with over 500 bHLH factors present in animals, plants and fungi[160-163]. The family can be divided into roughly 6 groups, based on specific E-box binding, conservation of residues in other parts of the bHLH motif, and the presence or absence of other domains[164]. Class I proteins (eg. E12, E47) are expressed in many tissues, while Class II proteins (eg. OLIG2, NeuroD) show a more tissue-restricted localization. Class III proteins (eg. MYC, TFE3)

are bHLH proteins with a leucine zipper motif just C-terminal to the bHLH, and Class IV proteins (eg. MAX, MAD) are those that can dimerize with Class III proteins. Class V proteins (eg. Id proteins) lack a basic region and therefore cannot bind to DNA, serving as cellular inhibitors of Class I and II proteins. Finally, Class VI proteins (eg. Hairy, Enhancer of split) are characterized by a proline residue in their basic region.

It is now known that the conserved basic region of bHLH proteins binds to the major groove of DNA at an E-box sequence. In particular, a conserved glutamic acid in the basic region binds to the 5'-CA-3' nucleotides of the E-box, while other residues in the basic region dictate specificity for various E-boxes[160]. For instance, a mutation in the basic region of the bHLH factor MyoD (L14R) alters the binding specificity for the protein from its traditional sequence (5'-CAGCTG-3') to that of c-Myc (5'-CACGTG-3')[165].

The second structural region of the domain, the helix-loop-helix region, allows for dimerization of these proteins[157]. Structural analyses have determined that these two α-helices dimerize in a parallel orientation[166,167], coiling around each other in a handshake pattern. In bHLH leucine zipper proteins (for instance, the proteins Myc and Max), the second α-helix is followed by a leucine zipper α-helical motif, increasing the region and specificity of dimerization. Dimerization is dependent upon the ability of α-helical pairings to line up in correct register with one another, placing hydrophobic residues adjacent to one another and allowing for the formation of stabilizing salt bridges[167,168]. bHLH proteins can form either homo- or heterodimeric pairs, and the choice of dimerization partners depends both on availability and sequence compatibility. This variability affords bHLH factor-driven transcription increased levels of flexibility and control.

The bHLH protein OLIG2

In 2000, a new family of bHLH transcription factors was discovered in a screen for bHLH proteins that are expressed in neural progenitor cells[169,170]. Located only 40kb apart on chromosome 21 and aptly named *Olig1* and *Olig2* (and later joined by *Olig3*[171]), both proteins are expressed during development of the central nervous system[172]. Together, OLIG1 and OLIG2 are critical for the development of oligodendrocytes, with a limited amount of functional redundancy between them[169,170]. OLIG2 alone is responsible for the differentiation of somatic motor neurons[170,171]. *Olig1*$^{-/-}$ knockout mice are viable and relatively normal, while *Olig2*$^{-/-}$ knockout mice die at birth and have no motor neurons or mature oligodendrocytes[173-175]. Taken together, these data suggest that while OLIG1 and OLIG2 each contribute to early neurodevelopment, OLIG2 clearly plays the predominant role. Additionally, in adults, OLIG2 expression is restricted to neural progenitor cells in the subventricular zone, NG2-positive glia, and mature myelinating oligodendrocytes[172,176].

Initially in development, anti-neural bHLH proteins expand the pool of progenitor cells, until pro-neural factors take over and induce differentiation. In contrast, OLIG2 plays both anti-neurogenic and pro-neurogenic roles during development. Early in development, OLIG2 assumes an anti-neurogenic role, keeping cells in a replication-competent stage. Later in development, OLIG2 becomes pro-neurogenic, pushing cells to exit the cell cycle and differentiate into motor neurons and oligodendrocytes[169,170]. The mechanisms by which OLIG2 can perform these diverse functions are still somewhat unclear. As a bHLH protein, OLIG2 can both homodimerize and heterodimerize with other bHLH factors to bind DNA, a capacity dependent on the integrity of the bHLH domain[177]. In some cases, OLIG2 is able to act as a transcriptional repressor. For example, expression of *Olig2* decreases expression of both *Hb9* and *p21*[177,178]. However, in other instances, OLIG2 can have a transcriptional activator

function[179]. These differences are likely dependent on other proteins that can complex with OLIG2 and affect its transcriptional control.

Like many proteins, OLIG2 is regulated by phosphorylation. Residues 77-88 of OLIG2 are a series of consecutive serines and threonines, some of which have been shown to be phosphorylated *in vitro*[176]. However, these phosphorylation events have yet to be identified in living cells. In contrast, phosphorylation of serine 147, located in Helix 2 of the bHLH domain, has been identified in embryonic mouse tissue and seems to direct OLIG2 function toward motor neuron specification[180]. Additionally, phosphorylation of serines 10, 13, and 14 has been identified in mouse neurospheres and glioma cell cultures[181]. Combined mutation of all three phosphorylation sites greatly reduces the proliferative impact of OLIG2, although it is still capable of inducing differentiation. This triple phosphorylation motif is also required for OLIG2's ability to inhibit p53 activity. This offers a potential mechanism for the proliferation effect of OLIG2, a capacity hypothesized to partially account for OLIG2's tumorigenic activity[181,182].

OLIG2 and glioma

In addition to its developmental functions, OLIG2 also plays a more insidious role in tumorigenesis of the brain. While gliomas account for less than 2% of all new cancer cases each year, they are the third leading cause of cancer-related death in men and the fourth leading cause of death in women aged 15-34 years[183]. Analysis of a variety of brain tumors has found that OLIG2 is expressed in 100% of diffuse gliomas, including astrocytomas, oligodendrogliomas, and oligoastrocytomas[184,185]. OLIG2 marks a subset of the tumor cells that have stem cell-like qualities[178,186]and are highly resistant to radiation and chemotherapy[187].

Importantly, in addition to serving as a marker for glioma stem cells, OLIG2 function is required for glioma formation in a mouse model[178]. Mouse neurospheres with background mutations in *Ink4a/ARF* and *EGFRvIII* engineered to be *Olig1*$^{+/-}$*/Olig2*$^{+/-}$ or *Olig1*$^{-/-}$*/Olig2*$^{-/-}$ were

injected into SCID mice, and the emergence of tumors was monitored. Strikingly, mice with at least one functional copy of *Olig2* (but not *Olig1)* formed tumors within three months, while those without *Olig2* remained tumor free for the length of the study (**Figure 1-4**). This dependence on OLIG2, as well as data suggesting that ablation of OLIG2 in adult mice is tolerable[188], makes OLIG2 and its transcriptional activities attractive targets for therapeutic intervention.

Summary

More than ten years ago, the basic helix-loop-helix transcription factors OLIG1 and OLIG2 were identified as the earliest known markers of oligodendrocyte precursor cells. A member of the basic helix-loop-helix (bHLH) transcription factor family, OLIG2 dimerizes through its bHLH domain in order to exert its transcriptional effects. OLIG2 is critical throughout development for the formation of somatic motor neurons and myelinating oligodendrocytes. In addition, it has a role in the proliferation of neural progenitor cells, with a pathobiological corollary in brain tumor growth. OLIG2 expression marks tumorigenic glioma stem cells and is required for the formation of gliomas in mouse models. Unfortunately, transcription factors have historically been resistant to therapeutic intervention due to the lack of deep binding grooves and the difficulty of targeting protein-DNA interactions in the nucleus. However, progress has recently been made in this area using novel techniques to disrupt protein-protein interactions, including the use of stapled peptides, reinvigorating efforts to target transcription factors in general and OLIG2 in particular.

Figure 1-4

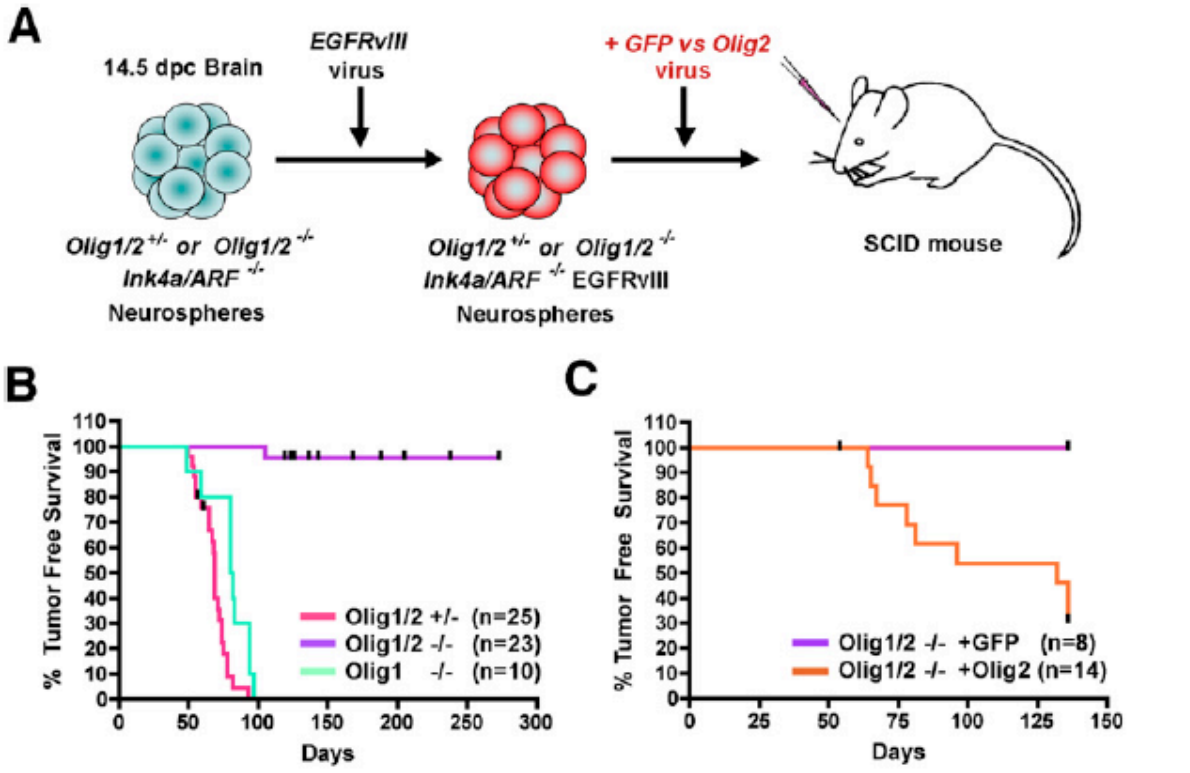

Ligon, *Neuron*, 2007

***Olig2* is required for the formation of gliomas in a mouse tumor model.** (A) *Olig1*$^{+/-}$*/Olig2*$^{+/-}$ or *Olig1*$^{-/-}$*/Olig2*$^{-/-}$ *Ink4a/ARF*$^{-/-}$ *EGFRvIII* neurospheres were generated and injected into the brains of SCID mice. (B) Kaplan-Meier survival analysis. While mice with at least one copy of *Olig2* formed tumors within three months, mice with homozygous deletion for *Olig2* remained tumor-free (96% survival at 273 days). (C) Restoration of *Olig2* restored tumorigenic capacity.

References

1. Braun, P. & Gingras, A.-C. History of protein-protein interactions: from egg-white to complex networks. *Proteomics* **12,** 1478–1498 (2012).

2. Kastle, J. H. ON THE VITAL ACTIVITY OF THE ENZYMES. *Science* **13,** 765–771 (1901).

3. Halperin, I., Wolfson, H. & Nussinov, R. Protein-protein interactions; coupling of structurally conserved residues and of hot spots across interfaces. Implications for docking. *Structure* **12,** 1027–1038 (2004).

4. Guharoy, M. & Chakrabarti, P. Conservation and relative importance of residues across protein-protein interfaces. *Proc Natl Acad Sci USA* **102,** 15447–15452 (2005).

5. Conte, Lo, L., Chothia, C. & Janin, J. The atomic structure of protein-protein recognition sites. *J Mol Biol* **285,** 2177–2198 (1999).

6. Jones, S. & Thornton, J. M. Principles of protein-protein interactions. *Proc Natl Acad Sci USA* **93,** 13–20 (1996).

7. Bogan, A. A. & Thorn, K. S. Anatomy of hot spots in protein interfaces. *J Mol Biol* **280,** 1–9 (1998).

8. Young, L., Jernigan, R. L. & Covell, D. G. A role for surface hydrophobicity in protein-protein recognition. *Protein Sci* **3,** 717–729 (1994).

9. Sheinerman, F. B., Norel, R. & Honig, B. Electrostatic aspects of protein-protein interactions. *Curr. Opin. Struct. Biol.* **10,** 153–159 (2000).

10. International Human Genome Sequencing Consortium. Finishing the euchromatic sequence of the human genome. *Nature* **431,** 931–945 (2004).

11. Legrain, P. *et al.* The human proteome project: current state and future direction. *Mol. Cell Proteomics* **10,** M111.009993 (2011).

12. Hopkins, A. L. & Groom, C. R. The druggable genome. *Nature Publishing Group* **1,** 727–730 (2002).

13. Wells, J. A. & McClendon, C. L. Reaching for high-hanging fruit in drug discovery at protein-protein interfaces. *Nature* **450,** 1001–1009 (2007).

14. Hofseth, L. J., Hussain, S. P. & Harris, C. C. p53: 25 years after its discovery. *Trends in Pharmacological Sciences* **25,** 177–181 (2004).

15. Hollstein, M., Sidransky, D., Vogelstein, B. & Harris, C. C. p53 mutations in human cancers. *Science* **253,** 49–53 (1991).

16. Vassilev, L. T. *et al.* In vivo activation of the p53 pathway by small-molecule antagonists of MDM2. *Science* **303,** 844–848 (2004).

17. Kussie, P. H. *et al.* Structure of the MDM2 oncoprotein bound to the p53 tumor suppressor transactivation domain. *Science* **274,** 948–953 (1996).

18. Yoakim, C. *et al.* Discovery of the first series of inhibitors of human papillomavirus type 11: inhibition of the assembly of the E1-E2-Origin DNA complex. *Bioorg. Med. Chem. Lett.* **13,** 2539–2541 (2003).

19. Goudreau, N. *et al.* Optimization and determination of the absolute configuration of a series of potent inhibitors of human papillomavirus type-11 E1-E2 protein-protein interaction: a combined medicinal chemistry, NMR and computational chemistry approach. *Bioorg Med Chem* **15,** 2690–2700 (2007).

20. Nelson, B. H. & Willerford, D. M. Biology of the interleukin-2 receptor. *Adv. Immunol.* **70,** 1–81 (1998).

21. Waldmann, T. A. The IL-2/IL-2 receptor system: a target for rational immune intervention. *Immunology today* **14,** 264–270 (1993).

22. Tilley, J. W. *et al.* Identification of a small molecule inhibitor of the IL-2/IL-2Ralpha receptor interaction which binds to IL-2. *J Am Chem Soc* **119,** 7589–7590 (1997).

23. Braisted, A. C. *et al.* Discovery of a potent small molecule IL-2 inhibitor through fragment assembly. *J Am Chem Soc* **125,** 3714–3715 (2003).

24. Pegoraro, L. *et al.* A 14;18 and an 8;14 chromosome translocation in a cell line derived from an acute B-cell leukemia. *Proc Natl Acad Sci USA* **81,** 7166–7170 (1984).

25. Beroukhim, R. *et al.* The landscape of somatic copy-number alteration across human cancers. *Nature* **463,** 899–905 (2010).

26. Oltersdorf, T. *et al.* An inhibitor of Bcl-2 family proteins induces regression of solid tumours. *Nat Cell Biol* **435,** 677–681 (2005).

27. Gandhi, L. *et al.* Phase I study of Navitoclax (ABT-263), a novel Bcl-2 family inhibitor, in patients with small-cell lung cancer and other solid tumors. *J. Clin. Oncol.* **29,** 909–916 (2011).

28. Carter, P. J. Potent antibody therapeutics by design. *Nat. Rev. Immunol.* **6,** 343–357 (2006).

29. Hudis, C. A. Trastuzumab--mechanism of action and use in clinical practice. *N. Engl. J. Med.* **357,** 39–51 (2007).

30. Brennan, P. J. *et al.* HER2/neu: mechanisms of dimerization/oligomerization. *Oncogene* **19,** 6093–6101 (2000).

31. Guharoy, M. & Chakrabarti, P. Secondary structure based analysis and classification of biological interfaces: identification of binding motifs in protein-protein interactions. *Bioinformatics* **23,** 1909–1918 (2007).

32. Simon, R. J. *et al.* Peptoids: a modular approach to drug discovery. *Proc Natl Acad Sci USA* **89,** 9367–9371 (1992).

33. Liskamp, R. M. J., Rijkers, D. T. S., Kruijtzer, J. A. W. & Kemmink, J. Peptides and proteins as a continuing exciting source of inspiration for peptidomimetics. *Chembiochem* **12,** 1626–1653 (2011).

34. Seebach, D. *et al.* β-Peptides: Synthesis by Arndt-Eistert homologation with concomitant peptide coupling. Structure determination by NMR and CD spectroscopy and by X-ray crystallography. Helical secondary structure of a β-hexapeptide in solution and its stability towards pepsin. *Helvetica chimica acta* **79,** 913–941 (2004).

35. Marqusee, S. & Baldwin, R. L. Helix stabilization by Glu-...Lys+ salt bridges in short peptides of de novo design. *Proc Natl Acad Sci USA* **84,** 8898–8902 (1987).

36. Ghadiri, M. R. & Fernholz, A. K. Peptide architecture. Design of stable. alpha.-helical metallopeptides via a novel exchange-inert ruthenium (III) complex. *J Am Chem Soc* **112,** 9633–9635 (1990).

37. Taylor, J. W. The synthesis and study of side-chain lactam-bridged peptides. *Biopolymers* **66,** 49–75 (2002).

38. Jackson, D. Y., King, D. S., Chmielewski, J., Singh, S. & Schultz, P. G. General approach to the synthesis of short. alpha.-helical peptides. *J Am Chem Soc* **113,** 9391–9392 (1991).

39. Toniolo, C., Crisma, M., Formaggio, F. & Peggion, C. Control of peptide conformation by the Thorpe-Ingold effect (Cα-tetrasubstitution). *Peptide Science* **60,** 396–419 (2002).

40. Blackwell, H. E. & Grubbs, R. H. Highly efficient synthesis of covalently cross-linked peptide helices by ring-closing metathesis. *Angewandte Chemie International Edition* **37,** 3281–3284 (1998).

41. Schafmeister, C. E., Po, J. & Verdine, G. L. An All-Hydrocarbon Cross-Linking System for Enhancing the Helicity and Metabolic Stability of Peptides. *J Am Chem Soc* **122,** 5891–5892 (2000).

42. Walensky, L. D. BCL-2 in the crosshairs: tipping the balance of life and death. *Cell Death Differ* **13,** 1339–1350 (2006).

43. Walensky, L. D. *et al.* A stapled BID BH3 helix directly binds and activates BAX. *Mol Cell* **24,** 199–210 (2006).

44. Danial, N. N. *et al.* Dual role of proapoptotic BAD in insulin secretion and beta cell survival. *Nat Med* **14,** 144–153 (2008).

45. Gavathiotis, E., Reyna, D., Davis, M., Bird, G. & Walensky, L. BH3-Triggered Structural Reorganization Drives the Activation of Proapoptotic BAX. *Mol Cell* **40,** 481–492 (2010).

46. Walensky, L., Kung, A., Escher, I., Malia, T. & Barbuto, S. Activation of apoptosis in vivo by a hydrocarbon-stapled BH3 helix. *Science* (2004).

47. Grossmann, T. N. & Yeh, J. Inhibition of oncogenic Wnt signaling through direct targeting of β-catenin. in (2012). doi:10.1073/pnas.1208396109/-/DCSupplemental

48. Stewart, M. L., Fire, E., Keating, A. E. & Walensky, L. D. The MCL-1 BH3 helix is an exclusive MCL-1 inhibitor and apoptosis sensitizer. *Nat Chem Biol* **6,** 595–601 (2010).

49. Green, B. R. *et al.* Cyclic analogs of galanin and neuropeptide Y by hydrocarbon stapling. *Bioorg Med Chem* **21,** 303–310 (2013).

50. Zhang, H. *et al.* A cell-penetrating helical peptide as a potential HIV-1 inhibitor. *J Mol Biol* **378,** 565–580 (2008).

51. Sviridov, D. O. *et al.* Helix stabilization of amphipathic peptides by hydrocarbon stapling increases cholesterol efflux by the ABCA1 transporter. *Biochem Biophys Res Commun* **410,** 446–451 (2011).

52. Takada, K. *et al.* Targeted disruption of the BCL9/β-catenin complex inhibits oncogenic Wnt signaling. *Science Translational Medicine* **4,** 148ra117 (2012).

53. Bird, G. H. *et al.* Hydrocarbon double-stapling remedies the proteolytic instability of a lengthy peptide therapeutic. *Proc Natl Acad Sci USA* **107,** 14093–14098 (2010).

54. Bernal, F., Tyler, A. F., Korsmeyer, S. J., Walensky, L. D. & Verdine, G. L. Reactivation of the p53 tumor suppressor pathway by a stapled p53 peptide. *J Am Chem Soc* **129,** 2456–2457 (2007).

55. Bernal, F. *et al.* A stapled p53 helix overcomes HDMX-mediated suppression of p53. *Cancer Cell* **18,** 411–422 (2010).

56. Moellering, R. E. *et al.* Direct inhibition of the NOTCH transcription factor complex. *Nature* **462,** 182–188 (2009).

57. Phillips, C. *et al.* Design and structure of stapled peptides binding to estrogen receptors. *J Am Chem Soc* **133,** 9696–9699 (2011).

58. Kerr, J. F., Wyllie, A. H. & Currie, A. R. Apoptosis: a basic biological phenomenon with wide-ranging implications in tissue kinetics. *British journal of cancer* **26,** 239–257 (1972).

59. Danial, N. N. & Korsmeyer, S. J. Cell death: critical control points. *Cell* **116,** 205–219 (2004).

60. Frindel, E., Malaise, E. & Tubiana, M. Cell proliferation kinetics in five human solid tumors. *Cancer* **22,** 611–620 (1968).

61. Clifton, K. H. & Yatvin, M. B. Cell population growth and cell loss in the MTG-B mouse mammary carcinoma. *Cancer Res* **30,** 658–664 (1970).

62. Weinstein, G. D. & Frost, P. Cell proliferation in human basal cell carcinoma. *Cancer Res* **30,** 724–728 (1970).

63. Meier, P., Finch, A. & Evan, G. Apoptosis in development. *Nature* **407,** 796–801 (2000).

64. Norbury, C. J. & Zhivotovsky, B. DNA damage-induced apoptosis. *Oncogene* **23,** 2797–2808 (2004).

65. Williams, G. T., Smith, C. A., Spooncer, E., Dexter, T. M. & Taylor, D. R. Haemopoietic colony stimulating factors promote cell survival by suppressing apoptosis. *Nature* **343,** 76–79 (1990).

66. Yamaguchi, Y. *et al.* Analysis of the survival of mature human eosinophils: interleukin-5 prevents apoptosis in mature human eosinophils. *Blood* **78,** 2542–2547 (1991).

67. Puthalakath, H. *et al.* Bmf: a proapoptotic BH3-only protein regulated by interaction with the myosin V actin motor complex, activated by anoikis. *Science* **293,** 1829–1832 (2001).

68. Evan, G. I. *et al.* Induction of apoptosis in fibroblasts by c-myc protein. *Cell* **69,** 119–128 (1992).

69. Mayo, M. W. *et al.* Requirement of NF-kappaB activation to suppress p53-independent apoptosis induced by oncogenic Ras. *Science* **278,** 1812–1815 (1997).

70. Hengartner, M. O. The biochemistry of apoptosis. *Nature* **407,** 770–776 (2000).

71. Ellis, H. M. & Horvitz, H. R. Genetic control of programmed cell death in the nematode C. elegans. *Cell* **44,** 817–829 (1986).

72. Hengartner, M. O. & Horvitz, H. R. Activation of C. elegans cell death protein CED-9 by an amino-acid substitution in a domain conserved in Bcl-2. *Nature* **369,** 318–320 (1994).

73. Thornberry, N. A. & Lazebnik, Y. Caspases: enemies within. *Science* **281,** 1312–1316 (1998).

74. Enari, M. *et al.* A caspase-activated DNase that degrades DNA during apoptosis, and its inhibitor ICAD. *Nature* **391,** 43–50 (1998).

75. Orth, K., Chinnaiyan, A. M., Garg, M., Froelich, C. J. & Dixit, V. M. The CED-3/ICE-like protease Mch2 is activated during apoptosis and cleaves the death substrate lamin A. *J Biol Chem* **271,** 16443–16446 (1996).

76. Wajant, H. The Fas signaling pathway: more than a paradigm. *Science* **296,** 1635–1636 (2002).

77. Yonehara, S., Ishii, A. & Yonehara, M. A cell-killing monoclonal antibody (anti-Fas) to a cell surface antigen co-downregulated with the receptor of tumor necrosis factor. *J Exp Med* **169,** 1747–1756 (1989).

78. Cleveland, J. L. & Ihle, J. N. Contenders in FasL/TNF death signaling. *Cell* **81,** 479–482 (1995).

79. Chinnaiyan, A. M., O'Rourke, K., Tewari, M. & Dixit, V. M. FADD, a novel death domain-containing protein, interacts with the death domain of Fas and initiates apoptosis. *Cell* **81,** 505–512 (1995).

80. Galluzzi, L., Kepp, O., Trojel-Hansen, C. & Kroemer, G. Mitochondrial control of cellular life, stress, and death. *Circ. Res.* **111,** 1198–1207 (2012).

81. Li, H., Zhu, H., Xu, C. J. & Yuan, J. Cleavage of BID by caspase 8 mediates the mitochondrial damage in the Fas pathway of apoptosis. *Cell* **94,** 491–501 (1998).

82. Luo, X., Budihardjo, I., Zou, H., Slaughter, C. & Wang, X. Bid, a Bcl2 interacting protein, mediates cytochrome c release from mitochondria in response to activation of cell surface death receptors. *Cell* **94,** 481–490 (1998).

83. Liu, X., Kim, C. N., Yang, J., Jemmerson, R. & Wang, X. Induction of apoptotic program in cell-free extracts: requirement for dATP and cytochrome c. *Cell* **86,** 147–157 (1996).

84. Kluck, R. M., Bossy-Wetzel, E., Green, D. R. & Newmeyer, D. D. The release of cytochrome c from mitochondria: a primary site for Bcl-2 regulation of apoptosis. *Science* **275,** 1132–1136 (1997).

85. Bratton, S. B. & Salvesen, G. S. Regulation of the Apaf-1-caspase-9 apoptosome. *J Cell Sci* **123,** 3209–3214 (2010).

86. Shu, H. B., Halpin, D. R. & Goeddel, D. V. Casper is a FADD- and caspase-related inducer of apoptosis. *Immunity* **6,** 751–763 (1997).

87. Scaffidi, C., Schmitz, I., Krammer, P. H. & Peter, M. E. The role of c-FLIP in modulation of CD95-induced apoptosis. *J Biol Chem* **274,** 1541–1548 (1999).

88. Deveraux, Q. L., Takahashi, R., Salvesen, G. S. & Reed, J. C. X-linked IAP is a direct inhibitor of cell-death proteases. *Nature* **388,** 300–304 (1997).

89. Cleary, M. L. & Sklar, J. Nucleotide sequence of a t(14;18) chromosomal breakpoint in follicular lymphoma and demonstration of a breakpoint-cluster region near a transcriptionally active locus on chromosome 18. *Proc Natl Acad Sci USA* **82,** 7439–7443 (1985).

90. Bakhshi, A. *et al.* Cloning the chromosomal breakpoint of t(14;18) human lymphomas: clustering around JH on chromosome 14 and near a transcriptional unit on 18. *Cell* **41,** 899–906 (1985).

91. McDonnell, T. J. *et al.* bcl-2-immunoglobulin transgenic mice demonstrate extended B cell survival and follicular lymphoproliferation. *Cell* **57,** 79–88 (1989).

92. Reed, J. C., Cuddy, M., Slabiak, T., Croce, C. M. & Nowell, P. C. Oncogenic potential of bcl-2 demonstrated by gene transfer. *Nature* **336,** 259–261 (1988).

93. Vaux, D. L., Cory, S. & Adams, J. M. Bcl-2 gene promotes haemopoietic cell survival and cooperates with c-myc to immortalize pre-B cells. *Nature* **335,** 440–442 (1988).

94. Colussi, P. A. *et al.* Debcl, a proapoptotic Bcl-2 homologue, is a component of the Drosophila melanogaster cell death machinery. *The Journal of Cell Biology* **148,** 703–714 (2000).

95. Kratz, E. *et al.* Functional characterization of the Bcl-2 gene family in the zebrafish. *Cell Death Differ* **13,** 1631–1640 (2006).

96. Chan, S.-L. & Yu, V. C. Proteins of the bcl-2 family in apoptosis signalling: from mechanistic insights to therapeutic opportunities. *Clin Exp Pharmacol Physiol* **31,** 119–128 (2004).

97. Youle, R. J. & Strasser, A. The BCL-2 protein family: opposing activities that mediate cell death. *Nat Rev Mol Cell Biol* **9,** 47–59 (2008).

98. Wolter, K. G. *et al.* Movement of Bax from the cytosol to mitochondria during apoptosis. *The Journal of Cell Biology* **139,** 1281–1292 (1997).

99. Nechushtan, A., Smith, C. L., Lamensdorf, I., Yoon, S. H. & Youle, R. J. Bax and Bak coalesce into novel mitochondria-associated clusters during apoptosis. *The Journal of Cell Biology* **153,** 1265–1276 (2001).

100. Dejean, L. M. *et al.* Oligomeric Bax is a component of the putative cytochrome c release channel MAC, mitochondrial apoptosis-induced channel. *Mol Biol Cell* **16,** 2424–2432 (2005).

101. Kim, C. N. *et al.* Overexpression of Bcl-X(L) inhibits Ara-C-induced mitochondrial loss of cytochrome c and other perturbations that activate the molecular cascade of apoptosis. *Cancer Res* **57,** 3115–3120 (1997).

102. Lindsten, T. *et al.* The combined functions of proapoptotic Bcl-2 family members bak and bax are essential for normal development of multiple tissues. *Mol Cell* **6,** 1389–1399 (2000).

103. Boise, L. H. *et al.* bcl-x, a bcl-2-related gene that functions as a dominant regulator of apoptotic cell death. *Cell* **74,** 597–608 (1993).

104. Reynolds, J. E. *et al.* Mcl-1, a member of the Bcl-2 family, delays apoptosis induced by c-Myc overexpression in Chinese hamster ovary cells. *Cancer Res* **54,** 6348–6352 (1994).

105. Bouillet, P. *et al.* Proapoptotic Bcl-2 relative Bim required for certain apoptotic responses, leukocyte homeostasis, and to preclude autoimmunity. *Science* **286,** 1735–1738 (1999).

106. Villunger, A. *et al.* p53- and drug-induced apoptotic responses mediated by BH3-only proteins puma and noxa. *Science* **302,** 1036–1038 (2003).

107. Jeffers, J. R. *et al.* Puma is an essential mediator of p53-dependent and -independent apoptotic pathways. *Cancer Cell* **4,** 321–328 (2003).

108. Letai, A. *et al.* Distinct BH3 domains either sensitize or activate mitochondrial apoptosis, serving as prototype cancer therapeutics. *Cancer Cell* **2,** 183–192 (2002).

109. Kuwana, T. *et al.* BH3 domains of BH3-only proteins differentially regulate Bax-mediated mitochondrial membrane permeabilization both directly and indirectly. *Mol Cell* **17,** 525–535 (2005).

110. Uren, R. T. *et al.* Mitochondrial permeabilization relies on BH3 ligands engaging multiple prosurvival Bcl-2 relatives, not Bak. *The Journal of Cell Biology* **177,** 277–287 (2007).

111. Willis, S. N. *et al.* Apoptosis initiated when BH3 ligands engage multiple Bcl-2 homologs, not Bax or Bak. *Science* **315,** 856–859 (2007).

112. Han, J. *et al.* Expression of bbc3, a pro-apoptotic BH3-only gene, is regulated by diverse cell death and survival signals. *Proc Natl Acad Sci USA* **98,** 11318–11323 (2001).

113. Yu, J., Zhang, L., Hwang, P. M., Kinzler, K. W. & Vogelstein, B. PUMA induces the rapid apoptosis of colorectal cancer cells. *Mol Cell* **7,** 673–682 (2001).

114. Nakano, K. & Vousden, K. H. PUMA, a novel proapoptotic gene, is induced by p53. *Mol Cell* **7,** 683–694 (2001).

115. Yu, J., Wang, Z., Kinzler, K. W., Vogelstein, B. & Zhang, L. PUMA mediates the apoptotic response to p53 in colorectal cancer cells. *Proc Natl Acad Sci USA* **100,** 1931–1936 (2003).

116. Erlacher, M. *et al.* Puma cooperates with Bim, the rate-limiting BH3-only protein in cell death during lymphocyte development, in apoptosis induction. *J Exp Med* **203,** 2939–2951 (2006).

117. Luo, X., He, Q., Huang, Y. & Sheikh, M. S. Transcriptional upregulation of PUMA modulates endoplasmic reticulum calcium pool depletion-induced apoptosis via Bax activation. *Cell Death Differ* **12,** 1310–1318 (2005).

118. Reimertz, C., Kögel, D., Rami, A., Chittenden, T. & Prehn, J. H. M. Gene expression during ER stress-induced apoptosis in neurons: induction of the BH3-only protein Bbc3/PUMA and activation of the mitochondrial apoptosis pathway. *The Journal of Cell Biology* **162,** 587–597 (2003).

119. Gavathiotis, E. *et al.* BAX activation is initiated at a novel interaction site. *Nature* **455,** 1076–1081 (2008).

120. Merino, D. *et al.* The role of BH3-only protein Bim extends beyond inhibiting Bcl-2-like prosurvival proteins. *The Journal of Cell Biology* **186,** 355–362 (2009).

121. Cartron, P.-F. *et al.* The first alpha helix of Bax plays a necessary role in its ligand-induced activation by the BH3-only proteins Bid and PUMA. *Mol Cell* **16,** 807–818 (2004).

122. Gallenne, T. *et al.* Bax activation by the BH3-only protein Puma promotes cell dependence on antiapoptotic Bcl-2 family members. *The Journal of Cell Biology* **185,** 279–290 (2009).

123. Steckley, D. *et al.* Puma is a dominant regulator of oxidative stress induced Bax activation and neuronal apoptosis. *J Neurosci* **27,** 12989–12999 (2007).

124. Zhang, Y., Xing, D. & Liu, L. PUMA promotes Bax translocation by both directly interacting with Bax and by competitive binding to Bcl-X L during UV-induced apoptosis. *Mol Biol Cell* **20,** 3077–3087 (2009).

125. Kim, H. *et al.* Hierarchical regulation of mitochondrion-dependent apoptosis by BCL-2 subfamilies. *Nat Cell Biol* **8,** 1348–1358 (2006).

126. Willis, S. N. & Adams, J. M. Life in the balance: how BH3-only proteins induce apoptosis. *Curr Opin Cell Biol* **17,** 617–625 (2005).

127. Chipuk, J. E. & Green, D. R. PUMA cooperates with direct activator proteins to promote mitochondrial outer membrane permeabilization and apoptosis. *Cell Cycle* **8,** 2692–2696 (2009).

128. Certo, M. *et al.* Mitochondria primed by death signals determine cellular addiction to antiapoptotic BCL-2 family members. *Cancer Cell* **9,** 351–365 (2006).

129. Callus, B. A. *et al.* Triggering of Apoptosis by Puma Is Determined by the Threshold Set by Prosurvival Bcl-2 Family Proteins. *J Mol Biol* **384,** 313–323 (2008).

130. Jabbour, A. M. *et al.* Puma indirectly activates Bax to cause apoptosis in the absence of Bid or Bim. *Cell Death Differ* **16,** 555–563 (2009).

131. Erlacher, M. *et al.* BH3-only proteins Puma and Bim are rate-limiting for gamma-radiation- and glucocorticoid-induced apoptosis of lymphoid cells in vivo. *Blood* **106,** 4131–4138 (2005).

132. Concannon, C. G. *et al.* Apoptosis induced by proteasome inhibition in cancer cells: predominant role of the p53/PUMA pathway. *Oncogene* **26,** 1681–1692 (2007).

133. Wyttenbach, A. & Tolkovsky, A. M. The BH3-only protein Puma is both necessary and sufficient for neuronal apoptosis induced by DNA damage in sympathetic neurons. *J Neurochem* **96,** 1213–1226 (2006).

134. Akhtar, R. S. *et al.* BH3-only proapoptotic Bcl-2 family members Noxa and Puma mediate neural precursor cell death. *J Neurosci* **26,** 7257–7264 (2006).

135. Muchmore, S. W. *et al.* X-ray and NMR structure of human Bcl-xL, an inhibitor of programmed cell death. *Nature* **381,** 335–341 (1996).

136. Sattler, M. *et al.* Structure of Bcl-xL-Bak peptide complex: recognition between regulators of apoptosis. *Science* **275,** 983–986 (1997).

137. Gavathiotis, E., Reyna, D. E., Bellairs, J. A., Leshchiner, E. S. & Walensky, L. D. Direct and selective small-molecule activation of proapoptotic BAX. *Nat Chem Biol* **8,** 639–645 (2012).

138. Leshchiner, E. S., Braun, C. R., Bird, G. H. & Walensky, L. D. Direct activation of full-length proapoptotic BAK. *Proc Natl Acad Sci USA* (2013). doi:10.1073/pnas.1214313110

139. Darnell, J. E. Transcription factors as targets for cancer therapy. *Nat Rev Cancer* **2,** 740–749 (2002).

140. Dickinson, L. *et al.* Arresting cancer proliferation by small-molecule gene regulation. *Chemistry & Biology* **11,** 1583–1594 (2004).

141. Fabbro, D. *et al.* Protein kinases as targets for anticancer agents: from inhibitors to useful drugs. *Pharmacol. Ther.* **93,** 79–98 (2002).

142. Mann, M. J. & Dzau, V. J. Therapeutic applications of transcription factor decoy oligonucleotides. *J Clin Invest* **106,** 1071–1075 (2000).

143. Dervan, P. B. & Edelson, B. S. Recognition of the DNA minor groove by pyrrole-imidazole polyamides. *Curr. Opin. Struct. Biol.* **13,** 284–299 (2003).

144. Beerli, R. R., Segal, D. J., Dreier, B. & Barbas, C. F. Toward controlling gene expression at will: specific regulation of the erbB-2/HER-2 promoter by using polydactyl zinc finger proteins constructed from modular building blocks. *Proc Natl Acad Sci USA* **95,** 14628–14633 (1998).

145. Fire, A. *et al.* Potent and specific genetic interference by double-stranded RNA in Caenorhabditis elegans. *Nature* **391,** 806–811 (1998).

146. Koehler, A. N. A complex task? Direct modulation of transcription factors with small

molecules. *Current Opinion in Chemical Biology* **14,** 331–340 (2010).

147. Bray, S. J. Notch signalling: a simple pathway becomes complex. *Nat Rev Mol Cell Biol* **7,** 678–689 (2006).

148. Seiffert, D. Presenilin-1 and -2 Are Molecular Targets for gamma -Secretase Inhibitors. *Journal of Biological Chemistry* **275,** 34086–34091 (2000).

149. Pelengaris, S., Khan, M. & Evan, G. c-MYC: more than just a matter of life and death. *Nat Rev Cancer* **2,** 764–776 (2002).

150. Soucek, L., Whitfield, J., Martins, C., Finch, A. & Murphy, D. Modelling Myc inhibition as a cancer therapy. *Nature* (2008).

151. Yin, X., Giap, C., Lazo, J. & Prochownik, E. Low molecular weight inhibitors of Myc–Max interaction and function. *Oncogene* **22,** 6151–6159 (2003).

152. Berg, T. *et al.* Small-molecule antagonists of Myc/Max dimerization inhibit Myc-induced transformation of chicken embryo fibroblasts. *Proc Natl Acad Sci USA* **99,** 3830–3835 (2002).

153. Delmore, J. E. *et al.* BET bromodomain inhibition as a therapeutic strategy to target c-Myc. *Cell* **146,** 904–917 (2011).

154. Draeger, L. J. & Mullen, G. P. Interaction of the bHLH-zip domain of c-Myc with H1-type peptides. Characterization of helicity in the H1 peptides by NMR. *J Biol Chem* **269,** 1785–1793 (1994).

155. D'Agnano, I., Valentini, A., Gatti, G., Chersi, A. & Felsani, A. Oligopeptides impairing the Myc-Max heterodimerization inhibit lung cancer cell proliferation by reducing Myc transcriptional activity. *Journal of Cellular Physiology* **210,** 72–80 (2007).

156. Murre, C., McCaw, P. & Baltimore, D. A new DNA binding and dimerization motif in immunoglobulin enhancer binding, daughterless, MyoD, and myc proteins. *Cell* **56,** 777–783 (1989).

157. Murre, C. *et al.* Interactions between heterologous helix-loop-helix proteins generate complexes that bind specifically to a common DNA sequence. *Cell* **58,** 537–544 (1989).

158. Jones, S. An overview of the basic helix-loop-helix proteins. *Genome Biol* (2004).

159. Guillemot, F. Vertebrate bHLH genes and the determination of neuronal fates. *Exp Cell Res* **253,** 357–364 (1999).

160. Robinson, K. A. & Lopes, J. M. SURVEY AND SUMMARY: Saccharomyces cerevisiae basic helix-loop-helix proteins regulate diverse biological processes. *Nucleic Acids Res* **28,** 1499–1505 (2000).

161. Ledent, V. & Vervoort, M. The basic helix-loop-helix protein family: comparative

genomics and phylogenetic analysis. *Genome Res* **11,** 754–770 (2001).

162. Ledent, V., Paquet, O. & Vervoort, M. Phylogenetic analysis of the human basic helix-loop-helix proteins. *Genome Biol* (2002).

163. Stevens, J. D., Roalson, E. H. & Skinner, M. K. Phylogenetic and expression analysis of the basic helix-loop-helix transcription factor gene family: genomic approach to cellular differentiation. *Differentiation* **76,** 1006–1022 (2008).

164. Massari, M. E. & Murre, C. Helix-Loop-Helix Proteins: Regulators of Transcription in Eucaryotic Organisms. *Mol Cell Biol* **20,** 429–440 (2000).

165. Blackwell, T. K. *et al.* Binding of myc proteins to canonical and noncanonical DNA sequences. *Mol Cell Biol* **13,** 5216–5224 (1993).

166. Longo, A., Guanga, G. P. & Rose, R. B. Crystal structure of E47-NeuroD1/beta2 bHLH domain-DNA complex: heterodimer selectivity and DNA recognition. *Biochemistry* **47,** 218–229 (2008).

167. Nair, S. K. & Burley, S. K. X-ray structures of Myc-Max and Mad-Max recognizing DNA. Molecular bases of regulation by proto-oncogenic transcription factors. *Cell* **112,** 193–205 (2003).

168. Baxevanis, A. D. & Vinson, C. R. Interactions of coiled coils in transcription factors: where is the specificity? *Curr Opin Genet Dev* **3,** 278–285 (1993).

169. Lu, Q. R. *et al.* Sonic hedgehog--regulated oligodendrocyte lineage genes encoding bHLH proteins in the mammalian central nervous system. *Neuron* **25,** 317–329 (2000).

170. Zhou, Q., Wang, S. & Anderson, D. J. Identification of a novel family of oligodendrocyte lineage-specific basic helix-loop-helix transcription factors. *Neuron* **25,** 331–343 (2000).

171. Takebayashi, H. *et al.* Dynamic expression of basic helix-loop-helix Olig family members: implication of Olig2 in neuron and oligodendrocyte differentiation and identification of a new member, Olig3. *Mechanisms of development* **99,** 143–148 (2000).

172. Rowitch, D. H., Lu, Q. R., Kessaris, N. & Richardson, W. D. An 'oligarchy' rules neural development. *Trends Neurosci* **25,** 417–422 (2002).

173. Takebayashi, H. *et al.* The basic helix-loop-helix factor olig2 is essential for the development of motoneuron and oligodendrocyte lineages. *Curr Biol* **12,** 1157–1163 (2002).

174. Lu, Q. R. *et al.* Common developmental requirement for Olig function indicates a motor neuron/oligodendrocyte connection. *Cell* **109,** 75–86 (2002).

175. Zhou, Q. & Anderson, D. J. The bHLH transcription factors OLIG2 and OLIG1 couple neuronal and glial subtype specification. *Cell* **109,** 61–73 (2002).

176. Meijer, D. H. *et al.* Separated at birth? The functional and molecular divergence of OLIG1 and OLIG2. 1–13 (2012). doi:10.1038/nrn3386

177. Lee, S., Lee, B., Ruiz, E. & Pfaff, S. Olig2 and Ngn2 function in opposition to modulate gene expression in motor neuron progenitor cells. *Genes Dev* **19,** 282 (2005).

178. Ligon, K. L. *et al.* Olig2-regulated lineage-restricted pathway controls replication competence in neural stem cells and malignant glioma. *Neuron* **53,** 503–517 (2007).

179. Küspert, M., Hammer, A., Bösl, M. R. & Wegner, M. Olig2 regulates Sox10 expression in oligodendrocyte precursors through an evolutionary conserved distal enhancer. *Nucleic Acids Res* **39,** 1280–1293 (2011).

180. Li, H., de Faria, J. P., Andrew, P., Nitarska, J. & Richardson, W. D. Phosphorylation Regulates OLIG2 Cofactor Choice and the Motor Neuron-Oligodendrocyte Fate Switch. *Neuron* **69,** 918–929 (2011).

181. Sun, Y., Meijer, D., Alberta, J., Mehta, S. & Kane, M. Phosphorylation State of Olig2 Regulates Proliferation of Neural Progenitors. *Neuron* (2011).

182. Mehta, S. *et al.* The central nervous system-restricted transcription factor Olig2 opposes p53 responses to genotoxic damage in neural progenitors and malignant glioma. *Cancer Cell* **19,** 359–371 (2011).

183. Kesari, S. & Stiles, C. D. The bad seed: PDGF receptors link adult neural progenitors to glioma stem cells. *Neuron* **51,** 151–153 (2006).

184. Ligon, K. L. *et al.* The oligodendroglial lineage marker OLIG2 is universally expressed in diffuse gliomas. *J. Neuropathol. Exp. Neurol.* **63,** 499–509 (2004).

185. Bouvier, C. *et al.* Shared oligodendrocyte lineage gene expression in gliomas and oligodendrocyte progenitor cells. *J. Neurosurg.* **99,** 344–350 (2003).

186. Jackson, E. L. *et al.* PDGFR alpha-positive B cells are neural stem cells in the adult SVZ that form glioma-like growths in response to increased PDGF signaling. *Neuron* **51,** 187–199 (2006).

187. Stiles, C. D. & Rowitch, D. H. Glioma stem cells: a midterm exam. *Neuron* **58,** 832–846 (2008).

188. Cai, J. *et al.* A crucial role for Olig2 in white matter astrocyte development. *Development* **134,** 1887–1899 (2007).

Chapter 2

Multimodal Interaction with BCL-2 Family Proteins Underlies the Pro-Apoptotic Activity of PUMA BH3

Abstract

PUMA is a pro-apoptotic BCL-2 family member first discovered as a transcriptional target of p53 and has since been implicated in driving the apoptotic response to a diversity of p53-dependent and independent cellular insults. As such, deciphering the spectrum of PUMA interactions that confer its context-dependent pro-apoptotic properties remains a high priority goal. The BH3 interaction domain of PUMA is well known to broadly engage the diversity of anti-apoptotic targets, but its ability to directly bind and activate pro-apoptotic effectors such as BAX remains unresolved. We generated PUMA SAHB, a structurally-stabilized PUMA BH3 helix that, in addition to targeting anti-apoptotic proteins, directly binds to BAX. Multidisciplinary analyses revealed that PUMA SAHB engages an α1/α6 trigger site on BAX, inducing its functional activation. Both PUMA SAHB and PUMA protein pull-downs confirmed interaction with native pro- and anti-apoptotic targets. As PUMA has been implicated in driving apoptosis in a variety of neuronal cell types, we further demonstrated the therapeutic potential of PUMA SAHB in neuroblastoma. Thus, PUMA BH3 is a dual anti-apoptotic inhibitor and pro-apoptotic direct activator, and its mimetics may serve as effective pharmacologic triggers of apoptosis in cancers of neural origin.

Introduction

The cellular decision to live or die is controlled by members of the BCL-2 protein family, which executes the activation or suppression of mitochondrial apoptosis[1]. BCL-2 proteins are classified into three groups based on sequence homology and function. Anti-apoptotic members such as BCL-2 contain up to four BCL-2 Homology (BH) domains, whereas the multidomain pro-apoptotic proteins, including BAX and BAK, contain three BH domains. A heterogeneous group of proteins that contain only the BH3 motif function as afferent sensors of stress. These so called "BH3-only" proteins relay pro-apoptotic signals to the multidomain members, which ultimately render a life or death decision based upon the overall balance between the degree of stress and the anti-apoptotic reserve.

PUMA (p53-Upregulated Modulator of Apoptosis) is one such BH3-only protein that was first identified as a transcriptional target of p53[2-4]. p53 deletion and mutagenesis can effectively blunt PUMA upregulation, contributing to the pathogenesis, maintenance, and chemoresistance of human cancer; reconstituting PUMA function in this context can effectively reactivate apoptosis[4,5]. *Puma*$^{-/-}$ cells have since been shown to manifest reduced sensitivity to a variety of p53-dependent and independent insults, including irradiation, DNA-damaging agents, cytokine withdrawal, hypoxia, and endoplasmic-reticulum stress[4,6-10]. These data highlight the importance of PUMA's role in apoptosis regulation in health and disease, and the potential of PUMA-based therapeutics to alternatively enhance chemo- and radiosensitivity in the context of cancer treatment and mitigate damage to host tissues through targeted PUMA inhibition[11]. Thus, deciphering the spectrum of PUMA interactions that confer its context-dependent pro-apoptotic properties remains a high priority goal.

The BH3-only protein interaction circuit is believed to induce apoptosis by two complementary mechanisms. The first is by BH3-only protein-mediated "inhibition of the inhibitors" of cell death[12,13]. That is, the BH3 motif of BH3-only proteins engages the canonical

BH3-binding groove of anti-apoptotic targets to neutralize their capacity to bind and block the multidomain pro-apoptotic effectors BAX and BAK. In addition, select members of the BH3-only class of apoptotic proteins have been shown to directly bind and activate BAK and BAX at discrete canonical[14] and non-canonical[15] BH3-binding sites on these proteins, respectively.

Whereas structural and biochemical data support direct and functional interactions for the BH3 domains of BIM and BID with BAX and BAK[15-18], the direct binding capability of the PUMA BH3 helix is unresolved. A series of studies that employed *in vitro* functional assays, and cellular and *in vivo* analyses, have yielded conflicting results regarding the existence and potential mechanistic role of direct PUMA interactions with BAX and/or BAK. A physical association between PUMA protein and BAX has been shown in bacterial two-hybrid assays[19], yeast cells[20], *in vitro* and mammalian cell co-immunoprecipitation studies[21-23], and by FRET analysis[23], indicating that the two proteins can interact. *Puma*$^{-/-}$*Bim*$^{-/-}$*Bid*$^{-/-}$ knockout (TKO) mice show developmental defects that are reminiscent of, although perhaps less severe than[24], those observed in *Bax*$^{-/-}$*Bak*$^{-/-}$ mice, suggesting that eliminating key direct activators may be tantamount to knocking out BAX and BAK altogether[25].

However, a series of studies document that the pro-apoptotic activity of PUMA instead derives from exclusive anti-apoptotic inhibition, citing the lack of direct interaction between PUMA and BAX upon co-immunoprecipitation from cells exposed to discrete stress stimuli[13,26,27]. In addition, a C-terminally truncated form of PUMA that manifests decreased BAX-binding activity retained pro-apoptotic potency equivalent to that of full-length PUMA, suggestive that the contribution of PUMA-BAX engagement, at least in this experimental context, was not essential[22]. Such cellular analyses are made all-the-more challenging by the proposed “hit and run” nature of the transient interactions between direct BH3 activators and BAX/BAK, potentially confounding co-immunoprecipitation-based studies. Even liposomal release assays, which probe functional activation of BAX and BAK upon administration of discrete

agonists/antagonists, have had mixed results with PUMA BH3[28,29]. Thus, we undertook a biochemical, structural, and cellular study to interrogate the capacity of PUMA BH3 to directly and functionally engage BAX, and thereby contribute to its pro-apoptotic activity *in vitro* and in cells.

Results

Design, synthesis, and anti-apoptotic binding activity of hydrocarbon-stapled PUMA BH3 helices

Whereas select BH3-only proteins, like BID, are highly structured and maintain an α-helical BH3 domain in the unbound state, others are intrinsically disordered[30] but undergo α-helical folding of the BH3 domain upon binding to compatible anti-apoptotic grooves[31]. In dissecting the mechanism of BH3-mediated direct BAX activation, we determined that a helical BID or BIM BH3 peptide, but not unfolded ones, were capable of engaging and activating BAX[18]. As synthetic PUMA BH3 peptides are predominantly unstructured in solution[32] (**Figure 2-1**), we first sought to stabilize the physiologically-relevant α-helical structure by insertion of an all-hydrocarbon crosslink. By replacing *i, i+4* pairs of native residues with non-natural amino acids bearing olefin tethers followed by ruthenium-catalyzed olefin metathesis, we previously generated a variety of stabilized alpha-helices of BCL-2 domains (SAHBs) modeled after the BH3 motifs of BCL-2 family proteins[33-35]. In designing stapled peptides - whether for *in vitro* binding studies, cellular localization analyses, structure determination, cellular signal transduction studies, or *in vivo* activity analyses - synthetic iteration is required to achieve optimal solubility, structural stability, cell permeability, and biological activity for the desired application. In the case of our prototype BIM $SAHB_A$[18], which potently bound to and activated BAX, adjustments in both sequence and charge were required to enhance solubility and weaken binding potency in order to capture the transient “hit and run” interactions[15,17]. In contrast, for

Figure 2-1

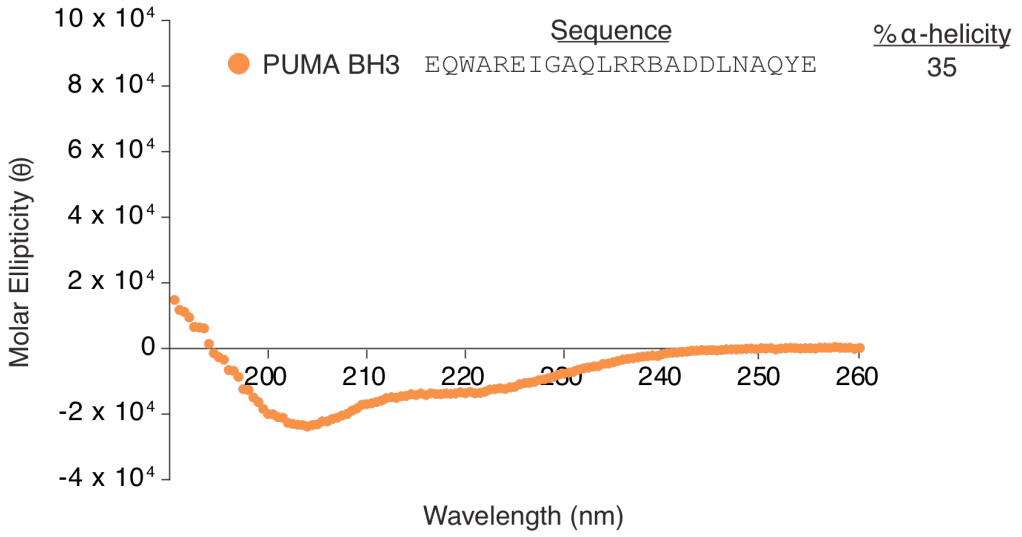

Circular dichroism analysis of PUMA BH3. A PUMA BH3 peptide composed of residues 131-153 is relatively unstructured in solution, as reflected by the circular dichroism spectra and the percent α-helical content.

cellular work performed in the low micromolar range, the prototype BIM SAHB$_A$ (+2 charge) was optimal[15,36], given its enhanced target binding potency and capacity to penetrate intact cells.

Thus, as for our development of BIM and MCL-1 SAHBs for a diversity of applications[15,18,34,36], we initiated our synthetic efforts here by generating a panel of PUMA SAHB constructs (designated PUMA SAHBs A1-A8*)* of differential sequence composition, length, and charge. In a screening fluorescence polarization binding assay against anti-apoptotic BCL-X_LΔC, we observed a binding affinity range of 2.6-13 nM for this panel of PUMA SAHB$_{A1}$ peptides (**Figure 2-2A**). Guided by our learnings from BIM SAHB$_A$, we selected a relatively low affinity compound bearing the most negative charge for *in vitro* biochemical and structural analyses, given our goal of evaluating functional interactions with BAX, in addition to the anti-apoptotic targets.

For optimal comparison, we aimed to examine a PUMA SAHB bearing a staple in the same location used for our prior studies with BIM SAHB$_A$. However, as for BIM SAHBs[15], we also wanted to confirm that any single staple location did not independently impact biochemical activity. Therefore, we also generated a panel of PUMA SAHBs A-L with differential localization of the hydrocarbon staple (**Figure 2-2B**). This “staple scanning” approach not only serves to dissociate any individual staple location from overall observed biochemical activity but also identifies the best binders and, importantly, those key residues and interfaces to avoid for staple placement, providing valuable structure-activity relationship information[15,34]. In each case, PUMA SAHBs with hydrocarbon staple placements that avoid the core hydrophobic binding interface and conserved BH3 residues, exhibit nanomolar BCL-X_LΔC binding affinity in the 4-21 nM range. In contrast, staples that replace key hydrophobic or charged residues of the binding interface, as found in PUMA SAHBs C, E, I, and J, manifest relatively impaired binding activity. As would be predicted, positioning the staple directly at the binding interface while also replacing the universally conserved leucine residue, as in PUMA SAHB$_H$, is most detrimental.

Figure 2-2

A

PUMA SAHB	Sequence	Sequence	Charge	K_D (nM)
A1	EQWAREIGAQLRXBADXLNAQYE	131-153	-2	12 ± 1.2
A2	QWAREIGAQLRXBADXLNAQYERR	130-155	+1	9.7 ± 1.1
A3	QWAREIGAQLRXBADXLNAQY	132-152	0	2.1 ± 0.5
A4	EEQWAREIGAQLRXBADXLNAQYERR	132-155	-1	10 ± 16
A5	REIGAQLRXBADXLNAQYERR	135-155	+1	13 ± 1.4
A6	REIGAQLRXBADXLNAQYERRR	135-156	+2	3.2 ± 0.8
A7	EIGAQLRXBADXLNAQYERR	136-155	0	13 ± 1.4
A8	EIGAQLRXBADXLNAQYERRR	136-156	+1	17 ± 2.0
A9	EIGAQLRXBADXLNAQYERRRQEE	136-159	-1	10 ± 1.0

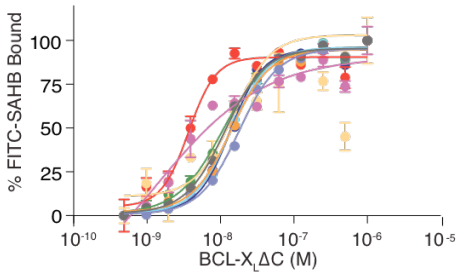

B

PUMA SAHB	Sequence	Staple Position	Charge	K_D (nM)
A1	EQWAREIGAQLRXBADXLNAQYE	143, 147	-2	17 ± 2.9
B1	XQWAXEIGAQLRRBADDLNAQYE	131, 135	-2	5.3 ± 1.2
C1	EXWARXIGAQLRRBADDLNAQYE	132, 136	-1	41 ± 4.9
D1	EQXAREXGAQLRRBADDLNAQYE	133, 137	-2	7.9 ± 1.6
E1	EQWXREIXAQLRRBADDLNAQYE	134, 138	-2	49 ± 6.1
F1	EQWARXIGAXLRRBADDLNAQYE	136, 140	-1	9.0 ± 1.1
G1	EQWAREIGAXLRRXADDLNAQYE	140, 144	-2	21 ± 3.6
H1	EQWAREIGAQXRRBXDDLNAQYE	141, 145	-2	>400
I1	EQWAREIGAQLRRXADDXNAQYE	144, 148	-2	45 ± 7.9
J1	EQWAREIGAQLRRBAXDLNXQYE	146, 150	-1	97 ± 13
K1	EQWAREIGAQLRRBADXLNAXYE	147, 151	-1	11 ± 4.0
L1	EQWAREIGAQLRRBADDLXAQYX	149, 153	-1	4.0 ± 0.9

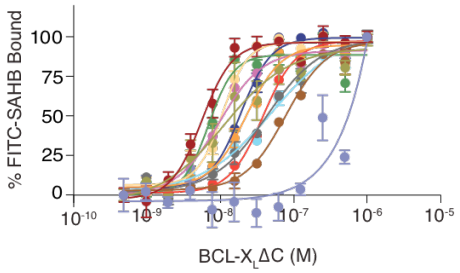

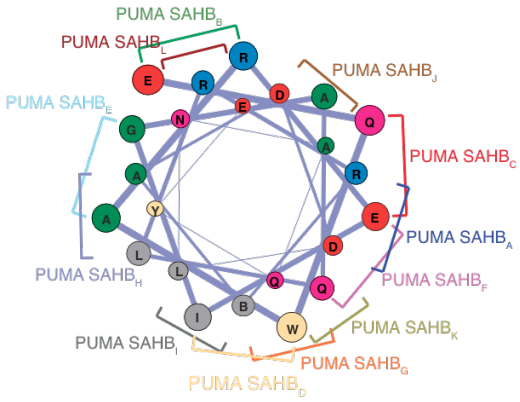

Sequence composition and anti-apoptotic binding activity of a panel of hydrocarbon-stapled PUMA BH3 peptides. (**A**) A series of FITC-PUMA SAHB$_A$ peptides of differential BH3 domain length and (**B**) FITC-PUMA BH3 (131-153) constructs with varying staple positions (as reflected by the "staple walk" along the pictured helical wheel) were synthesized and screened for BCL-X_LΔC binding activity by fluorescence polarization assay.

Biophysical and anti-apoptotic binding characterizations of PUMA SAHB$_{A1}$ and its negative control point mutant

Based on the above analysis, we chose PUMA SAHB$_{A1}$ to advance our *in vitro* studies of PUMA's pro-apoptotic activity due to the construct's (1) high affinity for known anti-apoptotic targets, (2) negative charge (which enhances solubility and optimized *in vitro* behavior for biochemical and structural studies), , and (3) similarity to a stapled BIM peptide previously used in BAX activation studies. Using this peptide as a starting reagent, we also generated a negative control construct for PUMA SAHB$_{A1}$ by swapping the location of an alanine residue at position 139 with the universally conserved leucine at position 141. Importantly, PUMA SAHB$_{A1}$ and its A139L/L141A double point mutant, designated PUMA SAHB$_{A1}$mut, exhibit similar, high percentage α-helical content, as assessed by circular dichroism (**Figure 2-3A**).

When the corresponding FITC-derivatized analogs were subjected to anti-apoptotic protein binding analyses, PUMA SAHB$_{A1}$ engaged BCL-2ΔC, BCL-X$_L$ΔC, BCL-wΔC, MCL-1ΔNΔC, and BFL-1ΔC with dissociation constants in the 20-35 nM range, whereas A139L/L141A mutagenesis uniformly impaired binding activity, consistent with disruption of a major BH3 binding determinant (**Figure 2-3B)**. Thus, we find that hydrocarbon stapling of the PUMA BH3 domain can potently enforce α-helical structure and the library of constructs obey predicted structure-activity relationships based upon BH3 sequence composition. Notably, PUMA SAHB$_{A1}$ engages in high affinity, sequence-specific binding interactions with all anti-apoptotic targets.

PUMA SAHB directly binds to BAX by initial interaction at the α1/α6 trigger site

To determine if a PUMA BH3 helix could likewise directly bind to the pro-apoptotic class of BCL-2 family proteins, as previously observed for BIM SAHB, we undertook an NMR analysis

Figure 2-3

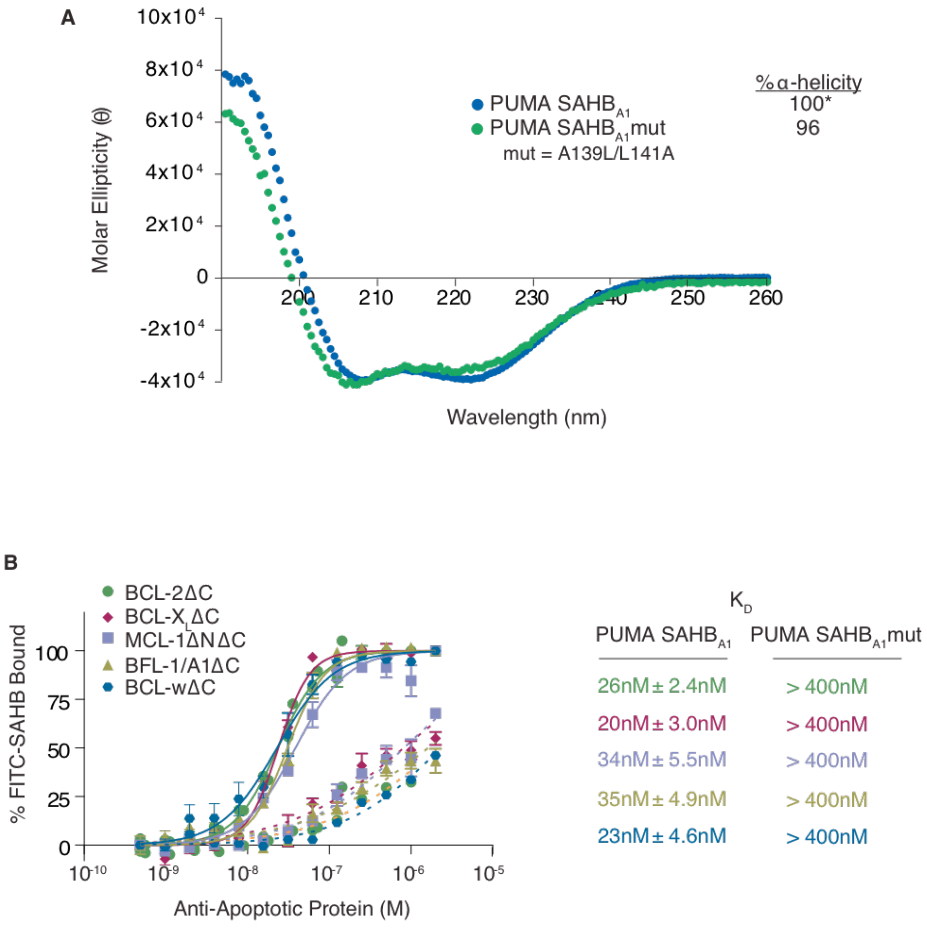

Helicity and anti-apoptotic binding activity of PUMA SAHB$_{A1}$ and its negative control point mutant. (**A**) Circular dichroism of PUMA SAHB$_{A1}$ and its A139L/L141A mutant demonstrated the marked α-helical structure of both stapled peptides in aqueous solution. *, exceeds the calculated ideal α-helicity of an undecapeptide standard[60]. (**B**) FITC-PUMA SAHB$_{A1}$ (solid lines) exhibits high affinity binding to the diversity of anti-apoptotic BCL-2 family proteins, whereas A139L/L141A point mutagenesis (dashed lines) markedly impairs binding activity, highlighting the BH3 sequence-dependence of PUMA SAHB$_{A1}$ engagement. Data are mean ± S.D. for experiments performed in triplicate. X, stapling amino acid; B, norleucine.

of ^{15}N-BAX upon PUMA SAHB titration. Of note, the BAX-activating BIM BH3 interaction is transient, making the structural analysis of this dynamic process especially challenging[15]. We thus employed PUMA SAHB$_{A1}$, a relatively weaker binding PUMA SAHB$_A$ that also possessed the most negative charge (-2) to enhance solubility for high concentration NMR experiments, as described above. We observed weak but dose-responsive backbone amide chemical shift changes in a discrete subset of BAX residues localized within α1, the α1-α2 loop, and α6, corresponding to the previously identified binding site for a stapled BIM BH3 helix[15] (**Figure 2-4**). Upon increasing the PUMA SAHB:^{15}N-BAX ratio from 1:1 to 4:1 (**Figure 2-4A, B**), a series of chemical shift changes became more prominent in the α1-α2 loop (yellow), α2 (BH3) (teal), and α9 (pink), three regions previously implicated in BIM BH3-triggered N-terminal loop opening, BAX BH3 exposure, and C-terminal helix mobilization, respectively[17]. These PUMA SAHB-induced allosteric changes are consistent with induction of a major conformational change that is transmitted from the N-terminal face through the hydrophobic core to the C-terminal face, resulting in functional activation of BAX.

To probe the PUMA SAHB interaction site on BAX by a second and completely distinct experimental approach, we developed and applied photoreactive PUMA SAHBs (pSAHBs). pSAHBs contain differentially localized benzophenone moieties, which covalently trap both static and dynamic protein interactors upon UV irradiation and enable the explicit localization of intercalation sites using mass spectrometry methods, as previously reported[37]. To validate the binding specificity of PUMA pSAHBs-1 and -2, we first conducted crosslinking analysis with anti-apoptotic BFL-1/A1ΔC, for which definitive structures are known. We found that the differentially-placed benzophenone moieties in each PUMA pSAHB crosslinked to discrete sub-regions of the canonical BH3 binding pocket (**Figure 2-5**), precisely corresponding to the established structure of a PUMA BH3/BFL-1/A1ΔC complex[38] (PDB ID# 2VOF). Having

Figure 2-4 (next page)

NMR analysis of ^{15}N-BAX upon PUMA SAHB$_{A1}$ titration. (**A**) At a 1:1 ratio of ^{15}N-PUMA SAHB$_{A1}$/BAX, a series of chemical shift changes localize to surface residues of a1 and a6, corresponding to the previously defined trigger site (purple) for BIM BH3-induced direct BAX activation. Allosteric changes involving residues of the α1-α2 loop (yellow), α2 (teal), and α9 (pink), as transmitted through the hydrophobic core (α4, α5), are also evident, and become more prominent upon titration up to a PUMA SAHB$_{A1}$/BAX ratio of 4:1 (**B**). Ca atoms of BAX residues that undergo significant chemical shift change upon exposure to PUMA SAHB$_{A1}$ are represented as orange bars on the plot (top) and orange spheres on the ribbon diagrams of monomeric BAX protein (calculated significance threshold >0.007 p.p.m. for 1:1 titration and >0.011 for 4:1 titration).

(**Figure 2-4**, cont.)

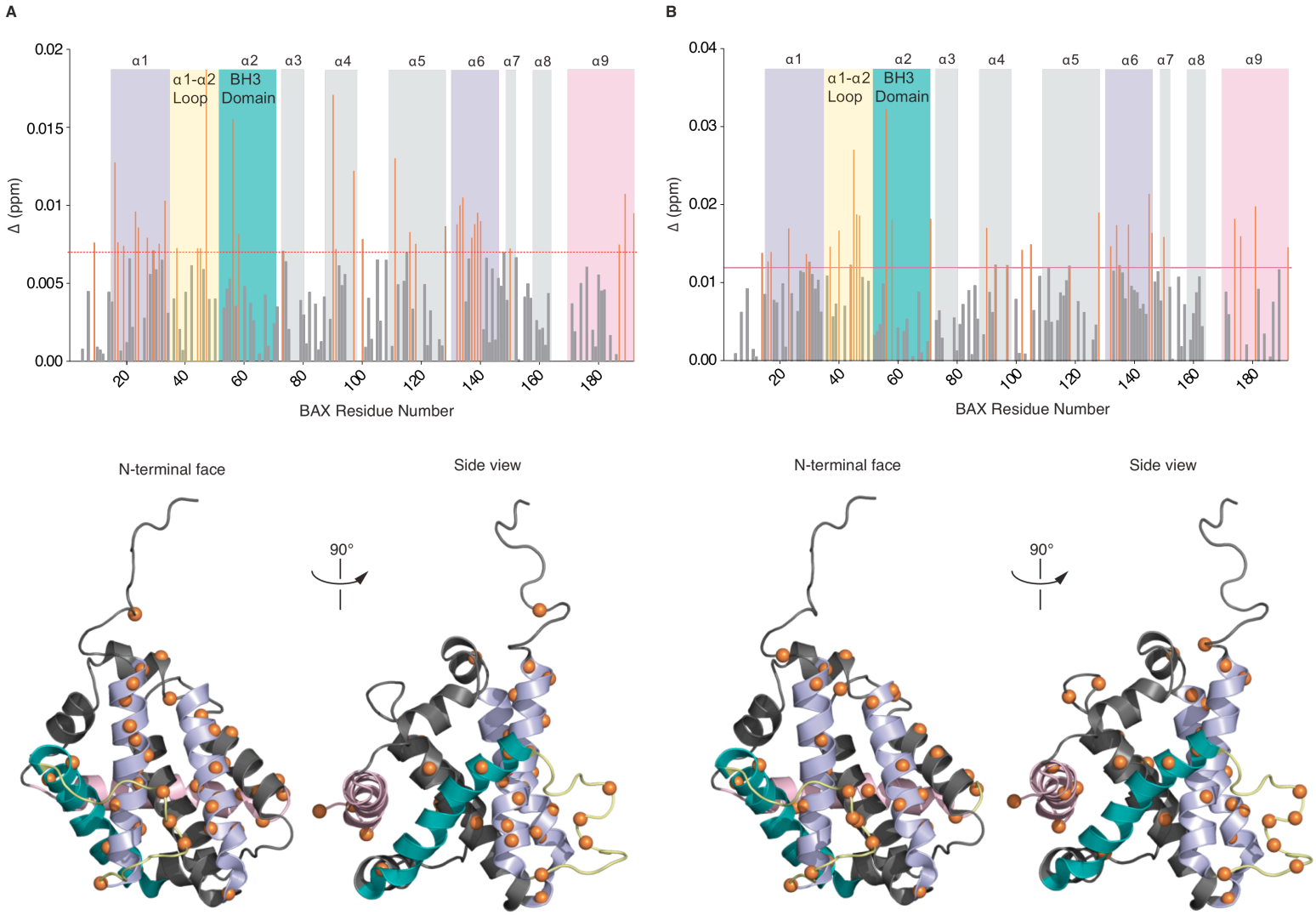

Figure 2-5

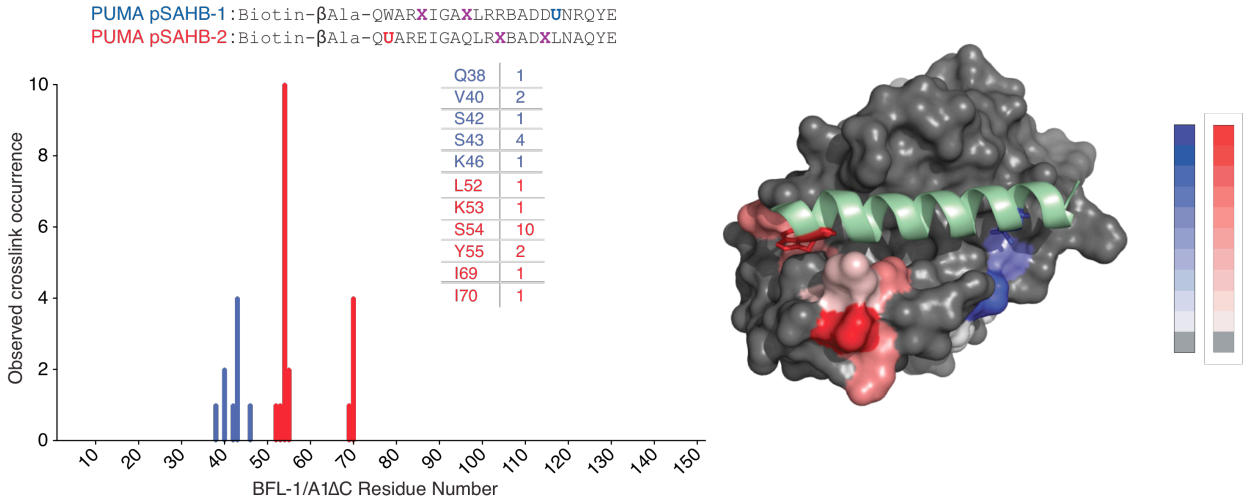

Photoreactive PUMA SAHBs localize the BH3 interaction site on BFL-1/A1ΔC with high fidelity. PUMA pSAHBs-1 and -2 were incubated individually with anti-apoptotic BFL-1/A1ΔC and the mixtures subjected to UV irradiation, electrophoresis, excision of the crosslinked protein, trypsin proteolysis, and LC-MS/MS analysis. The plot (left) depicts the frequency of crosslinked sites identified across the BFL-1/A1ΔC polypeptide sequence for PUMA pSAHB-1 (blue) and PUMA pSAHB-2 (red). Mapping of PUMA pSAHB-crosslinked amino acids onto the BFL-1/A1ΔC structure (PDB ID# 2VOF) highlighted the capacity of PUMA pSAHBs to precisely localize the site of interaction at the canonical BH3-binding pocket. The frequency of crosslinking occurrence is reflected on the BFL-1/A1ΔC structure by the color scale for each PUMA pSAHB (1, blue; 2, red).

validated the fidelity of PUMA pSAHBs-1 and -2, we subjected full-length BAX to the crosslinking analysis. We found that PUMA pSAHB-1 almost exclusively crosslinked to BAX residues of the α1/α6 trigger site (**Figure 2-6A**), whereas PUMA pSAHB-2 reacted with residues at both the α1/α6 trigger site and α3 residues of the canonical BH3-binding pocket (**Figure 2-6B**). BAX α9 effectively occludes the canonical BH3-binding pocket in the protein's inactive state[39] and our NMR study only detects protein surface chemical shift changes involving the α1/α6 site upon ligand binding. Thus, the identified canonical pocket crosslinks are most likely indicative of a compatible secondary binding interaction that ensues upon allosteric release of α9 from the canonical pocket, which is induced by initial BH3 engagement of the α1/α6 trigger site.

To explore this hypothesis, we repeated the PUMA pSAHB crosslinking studies on a mutant form of BAX in which the C-terminus was deleted (BAXΔC), thus exposing the canonical BH3-binding pocket from the outset. Strikingly, the balance of crosslinks completely shifted for both PUMA pSAHBs in favor of canonical pocket residues (**Figure 2-7A, B**). These data support a model in which exposure of the canonical BH3-binding pocket upon allosteric release of α9 reveals a secondary PUMA BH3 interaction site that may be reflective of a sequential BH3-mediated direct BAX activation mechanism.

PUMA SAHB directly activates BAX-mediated pore formation

To link the direct interaction between PUMA SAHB and BAX to its functional activation, we employed a reductionist liposomal system that measures BAX pore formation in a membrane environment upon the addition of discrete reagents. Whereas treatment with BAX, PUMA $SAHB_{A1}$, or its A139L/L141A mutant alone had little to no effect on the liposomes, the combination of BAX and PUMA $SAHB_{A1}$ yielded dose-responsive liposomal release of entrapped fluorophore (**Figure 2-8A**). Point mutagenesis of the PUMA BH3 interacting surface completely

Figure 2-6

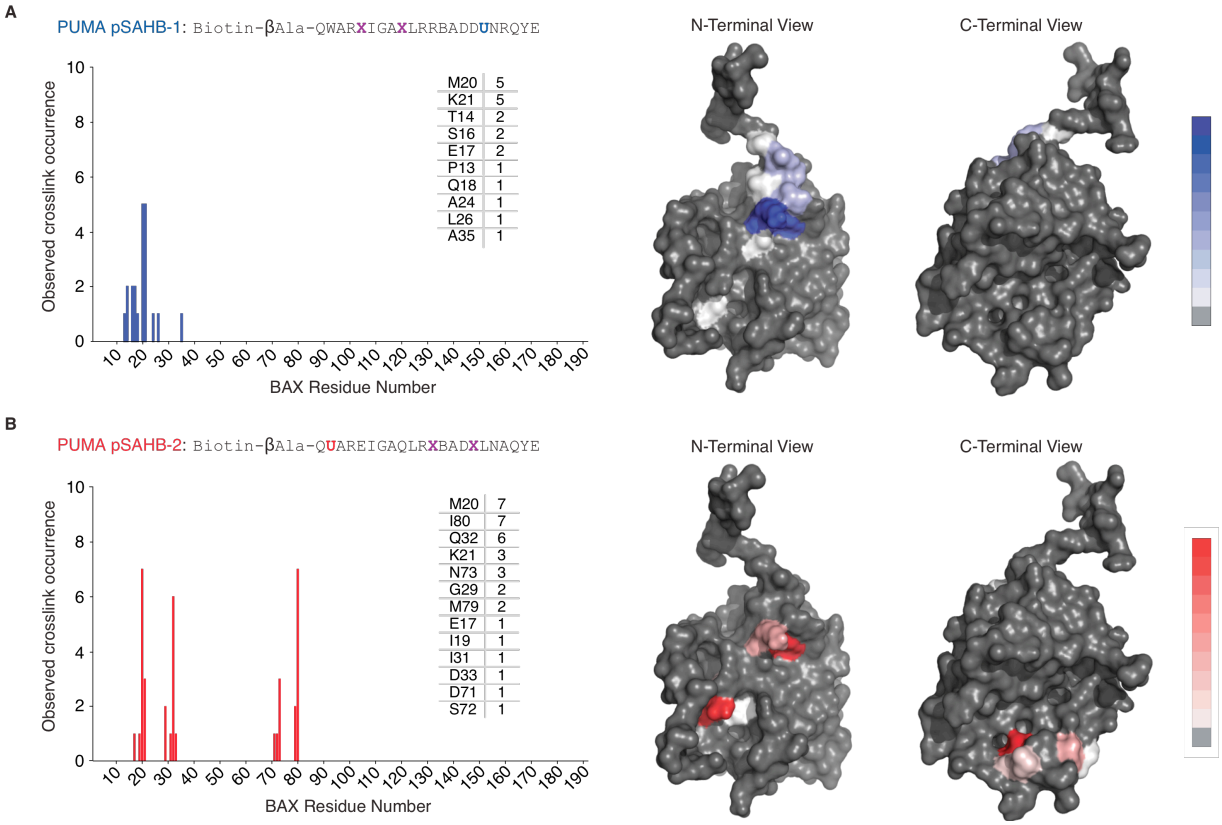

BAX interaction site analysis by PUMA SAHB photoaffinity labeling and mass spectrometry. (**A**) PUMA pSAHB-1 was incubated with full-length BAX and the mixture subjected to UV irradiation, streptavidin (SA) pulldown, electrophoresis, excision of the crosslinked protein, trypsin proteolysis, and LC-MS/MS analysis. A single arginine substitution (A150R) was made in PUMA pSAHB-1 to facilitate tryptic digestion into shorter and more identifiable fragments by MS. The plot (left) depicts the frequency of crosslinked sites identified across the BAX polypeptide sequence, with crosslinked residues mapped onto the solution structure of monomeric BAX (PDB ID 2K7W) (right) and colored according to the frequency of occurrence. The C-terminal α9 helix of BAX has been removed from the structure to better visualize the crosslinked residues of the canonical BH3-binding pocket. The corresponding analysis was also performed for PUMA pSAHB-2 with full-length BAX (**B**).

Figure 2-7

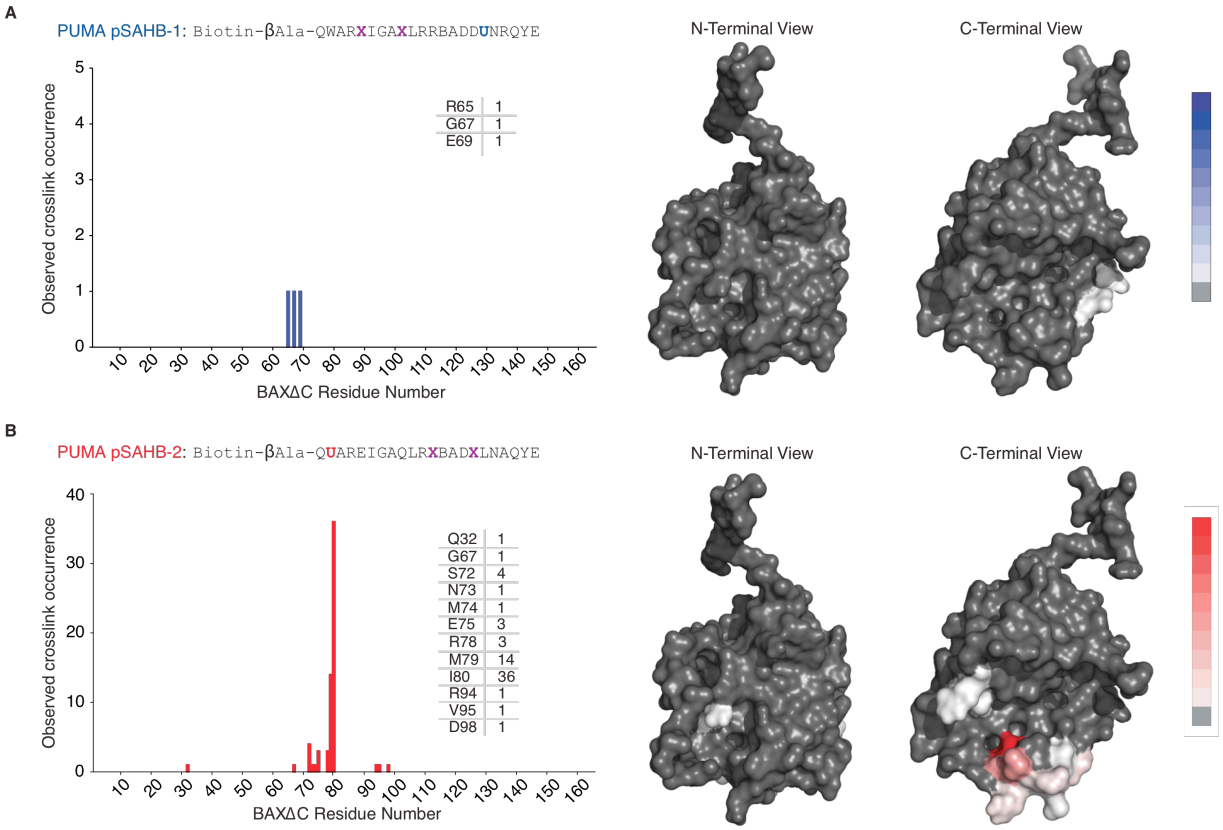

Deletion of the C-terminal α9 helix of BAX increases PUMA SAHB photoaffinity labeling to the canonical BH3 binding pocket. (**A**) PUMA pSAHB-1 was incubated with BAXΔC and the mixture subjected to UV irradiation, streptavidin (SA) pulldown, electrophoresis, excision of the crosslinked protein, trypsin proteolysis, and LC-MS/MS analysis. A single arginine substitution (A150R) was made in PUMA pSAHB-1 to facilitate tryptic digestion into shorter and more identifiable fragments by MS. The plot (left) depicts the frequency of crosslinked sites identified across the BAXΔC polypeptide sequence, with crosslinked residues mapped onto the solution structure of monomeric BAXΔC (PDB ID 2K7W) (right) and colored according to the frequency of occurrence. The corresponding analysis was also performed for PUMA pSAHB-2 with BAXΔC (**B**).

abrogated the effect (**Figure 2-8B**), underscoring the sequence-based specificity of PUMA SAHB$_{A1}$ activity.

Likewise, in the context of BAX/BAK-deficient mitochondria isolated from *Alb-cre*^{pos}*Bax*$^{flox/-}$*Bak*$^{-/-}$ mice, dose-responsive release of cytochrome *c* was only observed upon incubation with the combination of BAX and PUMA SAHB$_{A1}$. Again, the specificity of PUMA SAHB$_{A1}$ activity was confirmed by the inability of the mutant construct to activate BAX-mediated cytochrome *c* release. Whereas in the mitochondrial assay, the effect of PUMA SAHB$_{A1}$ on BAX activity can be amplified by simultaneous inhibition of membrane-embedded anti-apoptotic proteins, the requirement of PUMA SAHB$_{A1}$ to initiate BAX activation in both assays underscores the functional role of the direct PUMA SAHB/BAX binding interaction in triggering the membrane release activity of BAX.

Generation of a cell permeable PUMA SAHB

We next aimed to correlate our *in vitro* biochemical and structural findings to PUMA BH3 activity in cells. Among the BH3-only proteins, PUMA has been implicated as a major driver of apoptosis induction in neurons and neuronal precursor cells[8,39-41]. Therefore, we examined the pro-apoptotic activity of PUMA SAHB$_{A1}$ in neuroblastoma cells, which can mount a substantial and clinically-relevant apoptotic blockade[42]. We first screened PUMA SAHB$_{A1}$ for cellular uptake by treating SH SY5Y neuroblastoma cells with the FITC-derivatized analog of PUMA SAHB$_{A1}$ for six hours, followed by trypsinization, repeated washing, cellular lysis, electrophoresis, and fluorescence scan detection. A comparison of lysates from cells treated with the unmodified FITC-PUMA BH3 peptide and the corresponding A-stapled analog revealed no intracellular peptide fluorescence (**Figure 2-9A**), consistent with our prior observations that stapling of peptides alone does not uniformly confer cellular penetrance[43], particularly when the overall charge of the construct is less than zero[15,34,44], as is the case with PUMA SAHB$_{A1}$.

Figure 2-8

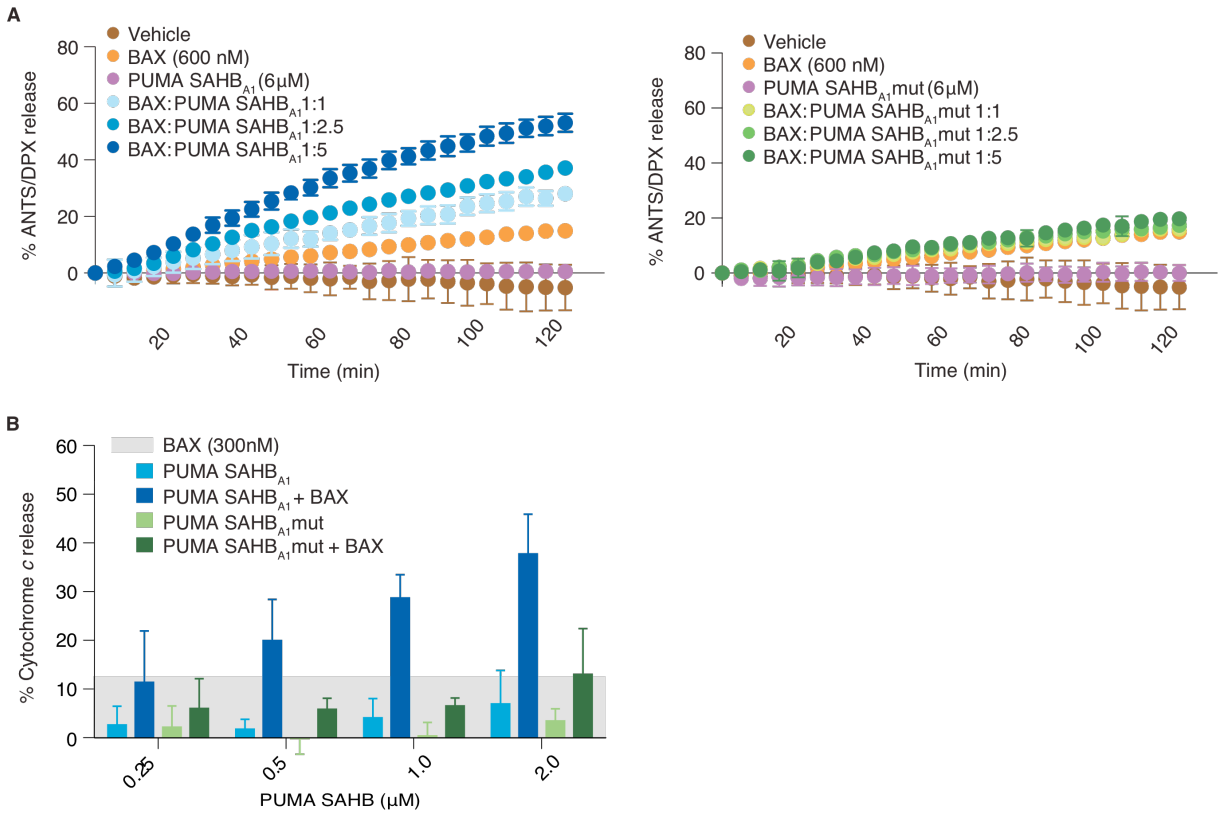

PUMA SAHB$_{A1}$ triggers BAX-mediated liposomal and cytochrome *c* release. (**A**) PUMA SAHB$_{A1}$ triggered dose-responsive BAX-mediated liposomal release of entrapped fluorophore (left), whereas BAX or PUMA SAHBs alone, or the combination of PUMA SAHB$_{A1}$mut with BAX (right), had little to no effect. Data are mean ± S.D. for experiments performed in triplicate and repeated twice. (**B**) BAX/BAK-deficient mitochondria dose-responsively released cytochrome *c* upon incubation with recombinant BAX and increasing amounts of PUMA SAHB$_{A1}$, whereas BAX or PUMA SAHBs alone, or the combination of PUMA SAHB$_{A1}$mut with BAX, had little to no effect. Data are mean ± S.D. for experiments performed in sextuplicate and repeated three times.

Figure 2-9

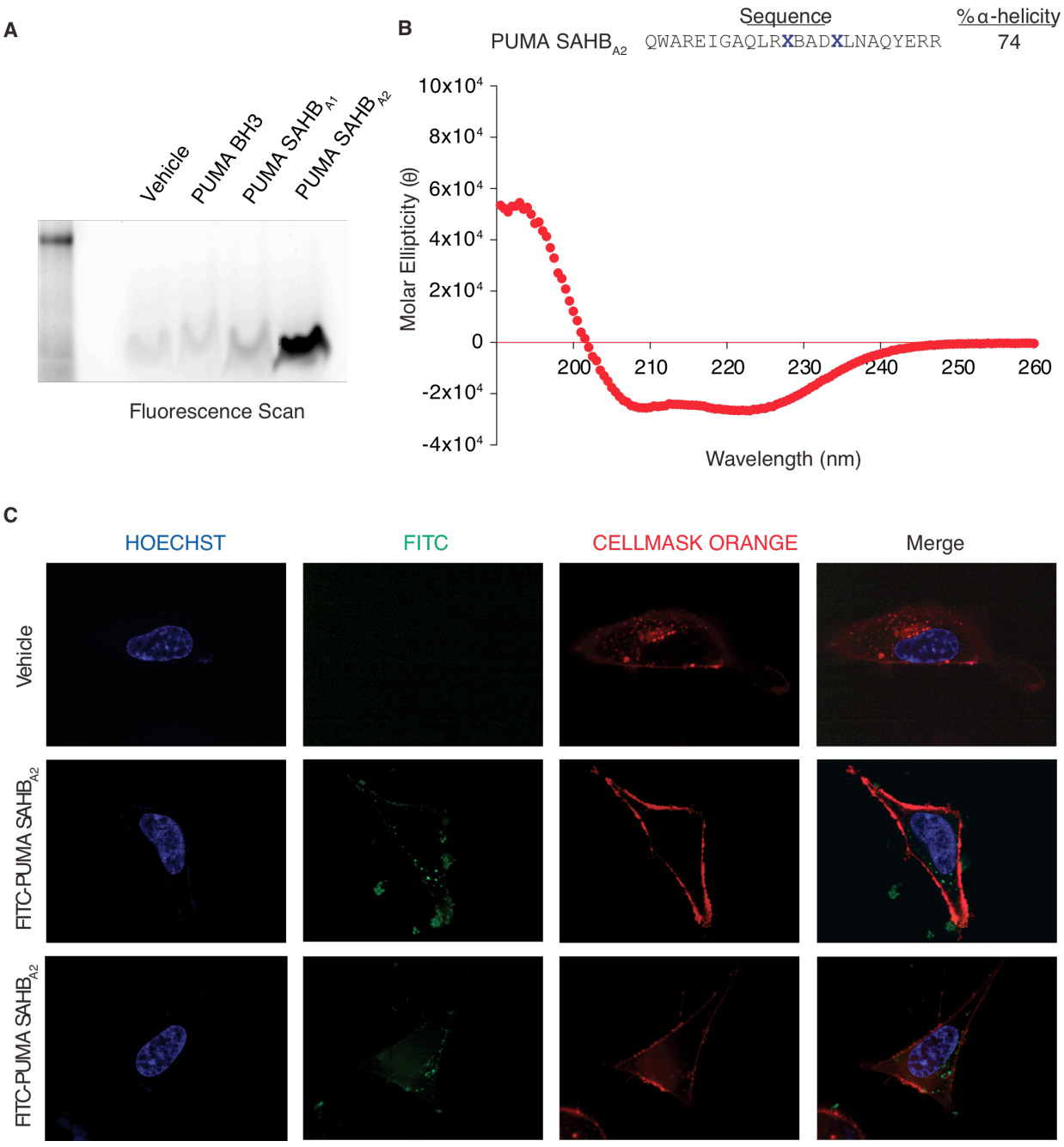

Characterization of cell permeable PUMA SAHB$_{A2}$. (**A**) SH SY5Y cells were treated with FITC-PUMA BH3 peptides (5 μM), followed by washing, trypsinization, cellular lysis, electrophoresis of the isolated supernatant, and fluorescence detection. Whereas little to no unmodified PUMA BH3 peptide or PUMA SAHB$_{A1}$ fluorescence was detected in the

(**Figure 2-9**, cont.)

corresponding cellular lysates, PUMA $SAHB_{A2}$ demonstrated robust fluorescence. (**B**) Circular dichroism demonstrated that, like PUMA $SAHB_{A1}$ and its A139L/L141/A mutant, PUMA $SAHB_{A2}$ is predominantly α-helical in solution, with a calculated percent α-helicity of 74% based on the observed molar ellipticity at 222 nm. (**C**) Live cell confocal microscopy of SH SY5Y cells treated with FITC- PUMA $SAHB_{A2}$ demonstrated its intracellular distribution. Prior to imaging, the cells were treated with Hoechst dye (blue) to label nuclei and CellMask Orange (orange-red) to delineate the plasma membrane. Original magnification, *100x*.

To facilitate cellular penetrance, we previously adjusted the overall charge of α-helical stapled peptides from <0 to the 0 to +2 range either by converting aspartic and glutamic acid residues to asparagines and glutamines[45], or by shifting the sequence composition to eliminate N- or C-terminal negatively charged residues and/or include N- or C-terminal positively charged residues[15,34,35]. Thus, we eliminated the N-terminal glutamic acid of PUMA SAHB$_{A1}$ and appended two native C-terminal arginines, converting the overall peptide charge from -1 to +2, while maintaining high α-helical content (**Figure 2-9B**) and analogous binding activity (see **Figure 2-2A**). When the FITC-derivatized analog of this alternate construct, PUMA SAHB$_{A2}$, was subjected to cellular uptake analysis, a robust fluorescent band was detected in the lysate of treated cells (**Figure 2-9A**). Live cell confocal microscopy of FITC-PUMA SAHB$_{A2}$-treated SH SY5Y cells further confirmed peptide uptake and its intracellular distribution (**Figure 2-9C**).

PUMA SAHB induces caspase 3/7 activation and cell death by engagement of anti- and pro-apoptotic targets

With a cell permeable version of PUMA SAHB in hand, we treated a series of neuroblastoma cells, including SH SY5Y, Kelly, and IMR5, and measured cell viability at 24 hours. In each case, a dose-responsive impairment in cell viability was observed (**Figure 2-10, A-C, left**), which correlated with dose-responsive caspase 3/7 activation, as measured at eight hours (**Figure 2-10, A-C, right**). To investigate whether the observed caspase 3/7 activation and cell death correlated with PUMA SAHB engagement of BCL-2 family targets, we incubated cellular lysates from each of the three cell lines with an N-terminal biotinylated analog of PUMA SAHB$_A$, followed by streptavidin pull-down, and western analysis. In each case, a diverse spectrum of BCL-2 family targets was engaged, as reflected by PUMA SAHB pull-down of anti-apoptotic BCL-2 and MCL-1, and pro-apoptotic BAX (**Figure 2-11, A-C**). Taken together, these data demonstrate that cell permeable PUMA SAHB$_{A2}$ can activate the death pathway in

Figure 2-10 (next page)

Cell permeable PUMA SAHB$_{A2}$ engages a diversity of BCL-2 family targets, activates caspase 3/7, and decreases the viability of neuroblastoma cells. (**A-C**) PUMA SAHB$_{A2}$ dose-responsively impaired the viability of a series of neuroblastoma cell lines including SH SY5Y, Kelly, and IMR5, as measured by CellTiter-Glo at 24 hours after treatment (left). The observed decrease in cell viability corresponded to dose-responsive caspase 3/7 activation, as measured by Caspase-Glo at eight 8 hours after treatment (right). Data are mean $\pm$ S.D. for experiments performed in triplicate.

(**Figure 2-10**, cont.)

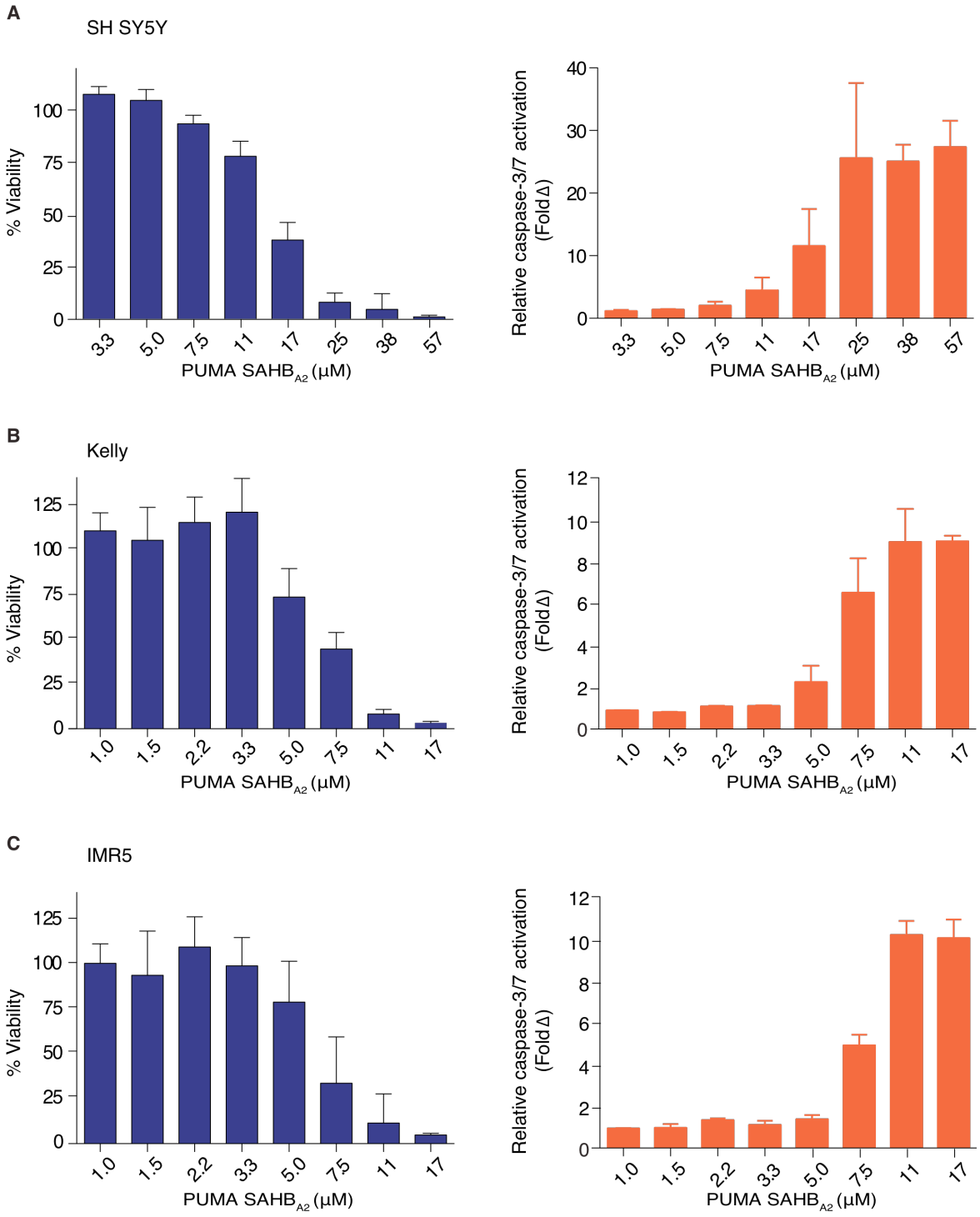

Figure 2-11

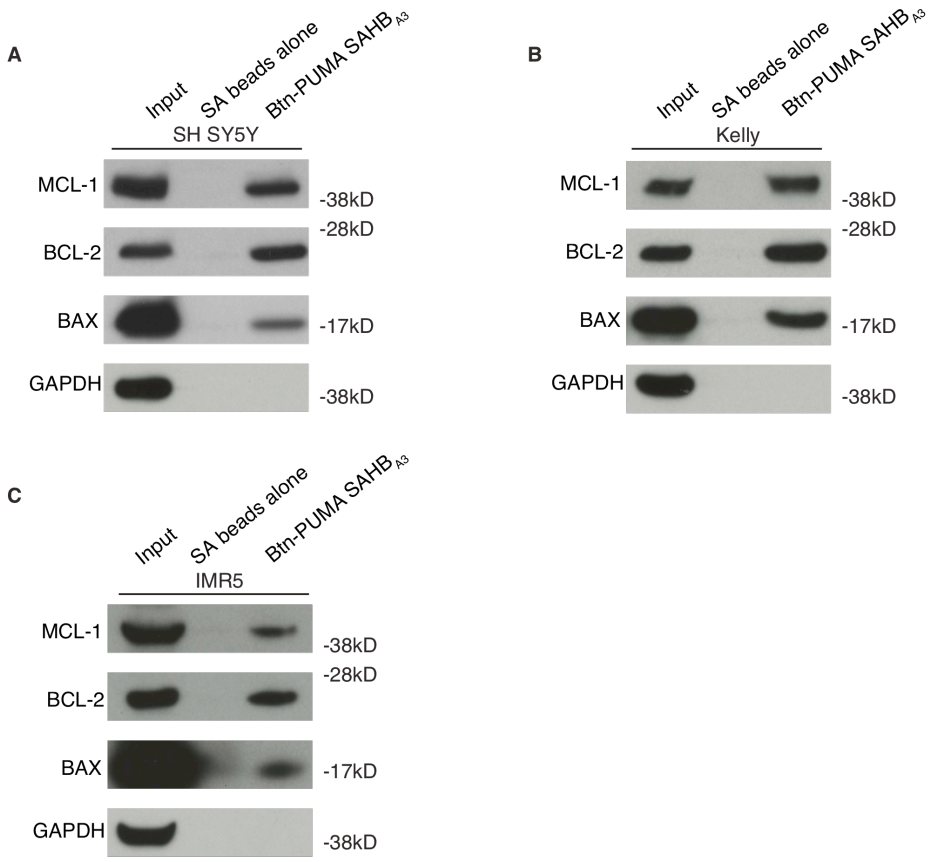

A biotinylated version of PUMA SAHB co-precipitates native anti- and pro-apoptotic BCL-2 family proteins. Incubation of cellular lystates with biotinylated PUMA SAHB$_{A3}$, followed by streptavidin pull-down, washing, electrophoresis of eluates, and BCL-2 family western analysis, documented engagement of native MCL-1, BCL-2, and BAX in all three neuroblastoma lines (**A-C**).

neuroblastoma cells, and this biological activity correlates with the capacity of a biotinylated PUMA BH3 helix to bind both anti- and pro-apoptotic BCL-2 family members.

Specificity and physiologic relevance of PUMA SAHB activity

An important measure of pro-apoptotic specificity for ligands designed to operate via the BCL-2 family pathway is whether death induction occurs in a BAX/BAK-dependent fashion. Thus, we treated wild-type and *Bax*$^{-/-}$*Bak*$^{-/-}$ mouse embryonic fibroblasts (MEFs) with PUMA SAHB$_{A2}$ and measured cell viability and caspase 3/7 activation, as performed for the neuroblastoma cell lines. Albeit at a higher dosing range, PUMA SAHB$_{A2}$ dose-responsively impaired cell viability of wild-type MEFs, with caspase 3/7 activation observed at the corresponding doses that induced cell death (**Figure 2-12A**). In contrast, little to no effect of PUMA SAHB$_{A2}$ was observed in *Bax*$^{-/-}$*Bak*$^{-/-}$ MEFs, with cell viability maintained in the 80-100% range and no activation of caspase 3/7 (**Figure 2-12B**).

Finally, we explored whether or not the protein interactions of stapled PUMA BH3 helices, and their observed functional consequences, bear on the physiologic interactions of full-length PUMA protein. Flag-PUMAα was transiently transfected into human embryonic kidney 293T cells and immunoprecipitated using anti-Flag resin. As observed for biotinylated PUMA SAHB$_{A3}$, Flag-PUMA engaged a diversity of anti- and pro-apoptotic BCL-2 family targets, as reflected by western analysis detection of BCL-2, MCL-1, and BAX (**Figure 2-13**). As for the PUMA SAHB pull down, the relative ratio of Flag-PUMA pull down to protein input was greater for anti-apoptotic BCL-2 and MCL-1 than pro-apoptotic BAX, reflecting either (1) the more stable nature of BH3/anti-apoptotic interactions compared to BH3/pro-apoptotic interactions or (2) a frank preference for PUMA BH3 engagement of anti-apoptotic targets and once this reservoir is saturated, direct activation of pro-apoptotic targets can ensue.

Figure 2-12

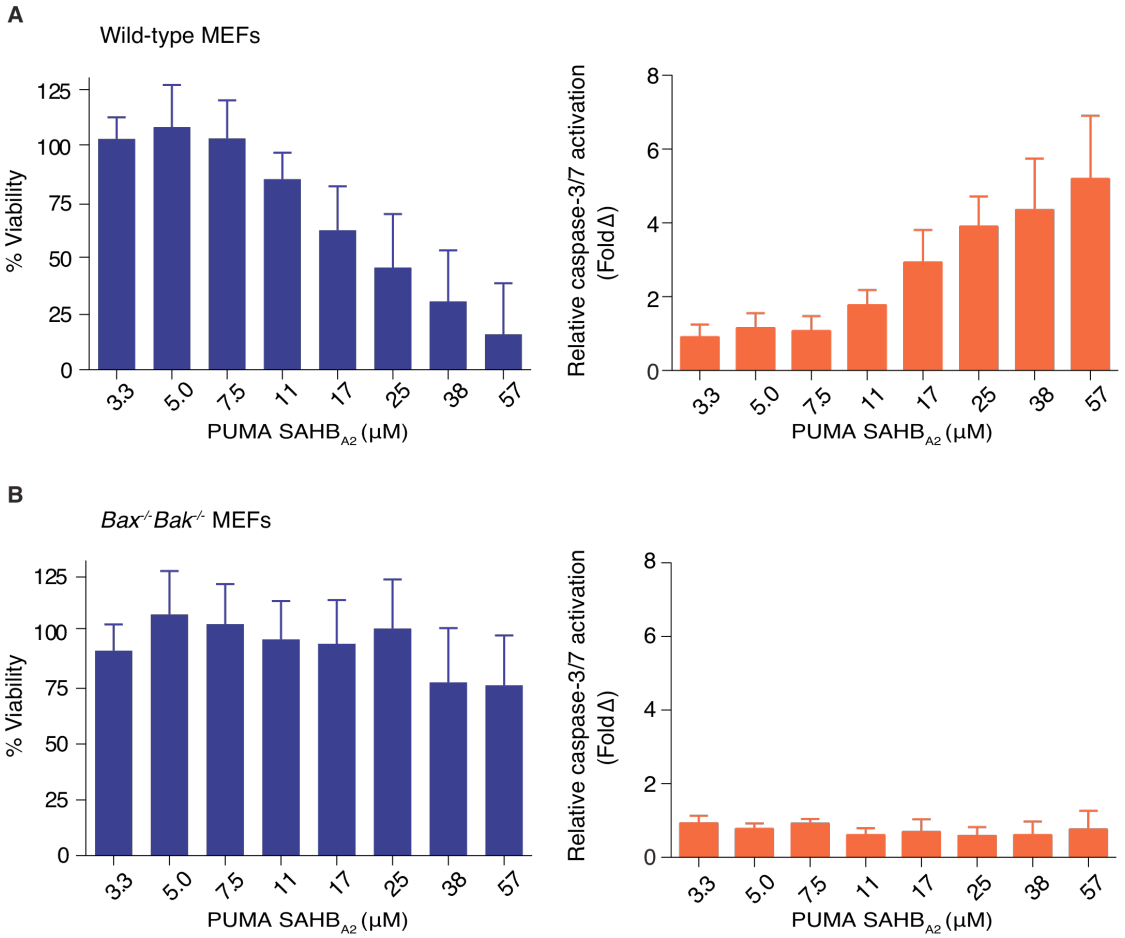

PUMA SAHB$_{A2}$ activity is BAX/BAK-dependent. (**A-B**) PUMA SAHB$_{A2}$ dose-responsively impaired the viability of wild-type mouse embryonic fibroblasts (MEFs), but had little to no effect on *Bax*$^{-/-}$*Bak*$^{-/-}$ MEFs, as measured by CellTiter-Glo at 24 hours after treatment (left column). Correspondingly, dose-responsive caspase 3/7 was observed in wild-type MEFs but not in *Bax*$^{-/-}$ *Bak*$^{-/-}$ MEFs, as measured by Caspase-Glo at 8 hours after treatment (right column). Data are mean ± S.D. for experiments performed in triplicate and repeated four times.

Figure 2-13

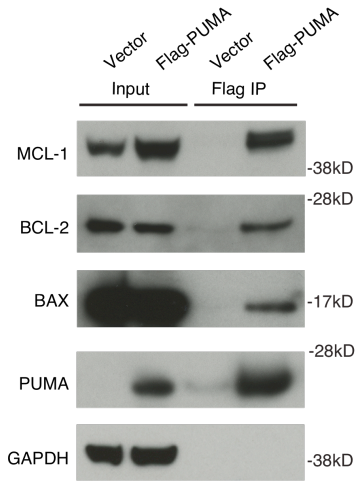

Full-length PUMA protein, expressed in HEK 293T cells, targets native anti- and pro-apoptotic BCL-2 family proteins. Flag-Puma α or vector control was transiently transfected into human embryonic kidney 293T (HEK 293T) cells and lysates subjected to immunoprecipitation using Flag affinity beads, followed by washing, and electrophoresis of eluates. Western analysis of MCL-1, BCL-2, BAX, PUMA, and GAPDH confirmed PUMA pulldown of both anti- and pro-apoptotic proteins.

Taken together, these data demonstrate that PUMA BH3 harbors the biochemical capacity to engage both anti- and pro-apoptotic BCL-2 family proteins and, depending on the cellular context, may harness this multimodal interaction potential to activate the apoptotic pathway.

Discussion

PUMA is a potent pro-apoptotic BH3-only protein implicated in a variety of apoptotic signaling pathways and subject to transcriptional and post-translational regulation[6]. Like BIM, PUMA broadly interacts with BCL-2 family anti-apoptotic proteins, and the two proteins have been shown to compensate for and cooperate with one another in a variety of physiologic death pathways[42,45-47]. Published biochemical, cellular, and *in vivo* studies differ, however, on whether a component of PUMA's pro-apoptotic potency also derives from its capacity to directly engage pro-apoptotic proteins, as demonstrated for BID and BIM. Notably, alignment of BCL-2 family BH3 domains reveals that PUMA BH3 is most similar to the BH3 domains of BIM and BAX in that very region implicated in direct interaction at the recently identified α1/α6 trigger site of BAX[15,17], with a highly homologous hydrophobic and electrostatic distribution reflected by the consensus LRR(I/M)(A/G)D(D/E) (**Figure 2-14**). Thus, based on the defined BIM BH3 triggering and BAX BH3 auto-propagating interactions at the α1/α6 site, it seemed likely that PUMA BH3 could likewise bind BAX at this same location.

Indeed, by two separate methods, NMR and mass spectrometry analysis of PUMA pSAHB-labeled BAX, we identified PUMA BH3 interaction at the α1/α6 interface. We linked this binding event to direct and functional activation of BAX in both liposomal and mitochondrial assay systems, in which PUMA SAHB dose-responsively triggered BAX-mediated release activity in a BH3 sequence-dependent manner. The physiologic relevance of these structural and biochemical findings are supported by the capacity of PUMA SAHB and PUMA protein to

Figure 2-14

Sequence homology of BIM, BAX, and PUMA BH3 domains. Alignment of the human BH3 domains of BIM, BAX, and PUMA demonstrates the high degree of sequence homology in the core BH3 region that engages in complementary hydrophobic and electrostatic interactions at the BAX α1/α6 trigger site. Hydrophobic, acidic, and basic residues of the consensus sequence are shown in yellow, red, and blue, respectively.

likewise engage native anti-apoptotic BCL-2 family proteins and BAX in cells. Taken together, these data support a model in which PUMA can function as a direct activator of BAX, consistent with a recent study documenting that in the absence of the direct activators BID, BIM, and p53, PUMA was sufficient to activate BAX[45].

In mapping the PUMA BH3 interaction site by pSAHB-based photoaffinity labeling, the majority of crosslinked residues in full-length BAX localized to the α1/α6 trigger site, yet a small subset included residues of the canonical BH3-binding pocket. As the chemical shift changes observed by NMR upon PUMA $SAHB_{A1}$ binding primarily involved surface residues of the α1/α6 trigger site, we suggest that allosteric release of α9 upon triggering at the N-terminal site exposes the canonical pocket, which is likewise compatible with PUMA BH3 binding. Indeed, when we performed the site identification analyses with C-terminally deleted BAX, the PUMA pSAHB crosslinking pattern shifted to predominantly involve residues of the canonical pocket. A similar compatibility for activator BH3 domains at the traditional BH3-binding pocket was also observed for C-terminally deleted BAK[14], which naturally resides in the mitochondrial membrane. These data suggest that activator BH3-engagement at the canonical pocket may represent a common mechanism for maintaining mitochondrial-localized BAK and BAX in an activation-competent state, with the α1/α6 triggering mechanism of BAX representing a unique afferent step required to regulate the activation and mitochondrial translocation of cytosolic BAX.

The stability and high affinity of BH3-only interactions with anti-apoptotic BCL-2 family proteins suggests that upon BH3-only deployment in response to cellular stress, the principal wrestling site between pro-life and pro-death forces may reside in these neutralizing complexes. However, with continued pro-apoptotic signaling, displacement of activator BH3-only proteins from anti-apoptotics or depletion of the anti-apoptotic reservoir, produces a BID/BIM/PUMA overflow that directly activates BAX and BAK at their respective BH3 trigger sites (**Figure 2-15**). Importantly, the very potency of PUMA and the capacity of its BH3 helix to engage native anti-

Figure 2-15

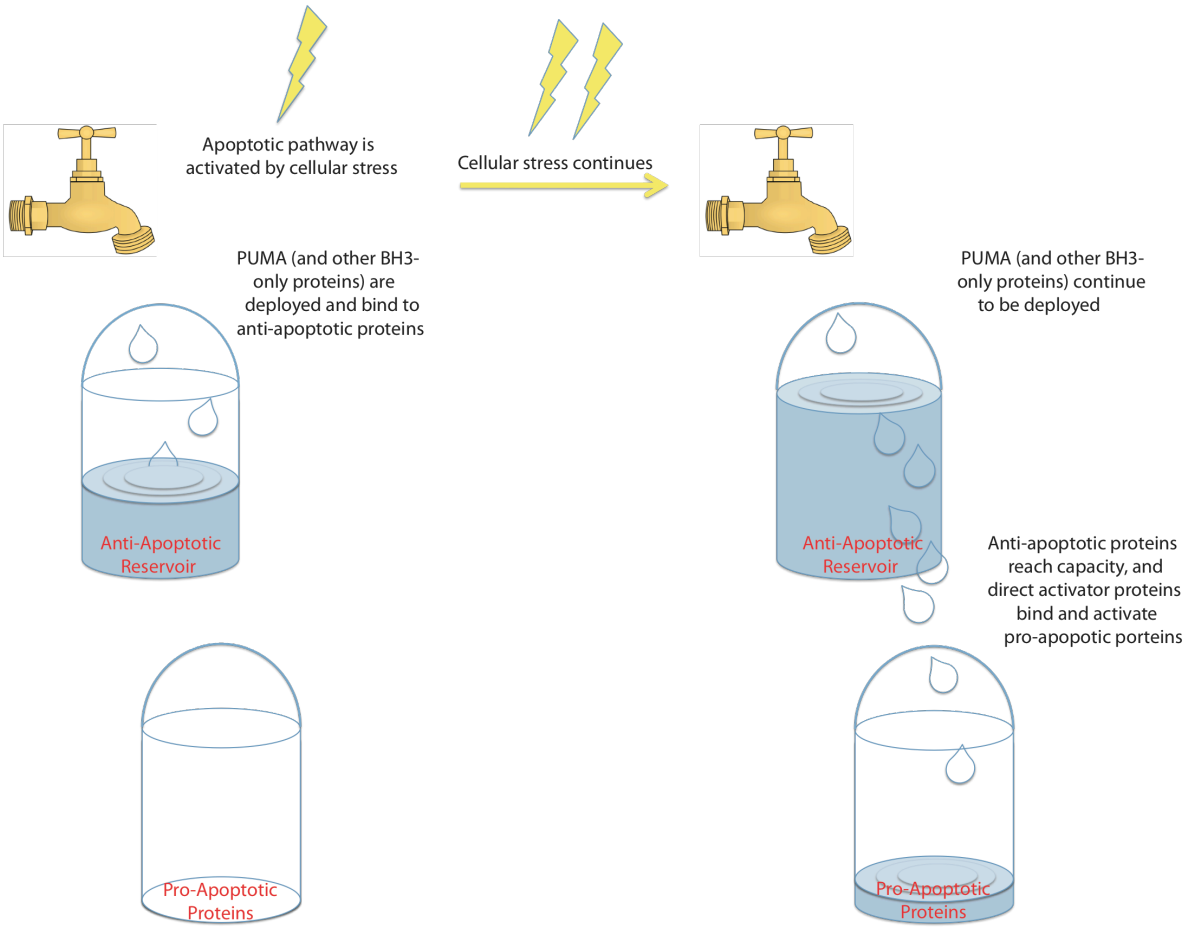

A model for multimodal activation of BCL-2 family proteins by PUMA. Cellular stresses activate BH3-only proteins, including both direct and indirect activators. Both sets of proteins bind to and deplete the anti-apoptotic protein reservoir, thereby lowering the apoptotic threshold. As long as the burden of anti-apoptotic proteins outweighs that of the pro-apoptotics, cellular viability is maintained. If persistent stress is incurred, additional BH3-only proteins are activated. The anti-apoptotic reservoirs become fully neutralized, and direct activators BID, BIM, and PUMA bind and directly activate pro-apoptotic BAX and BAK, inducing apoptosis.

and pro-apoptotic BH3-binding pockets, suggests that pharmacologic mimicry of this functionality carries the potential to reactivate apoptosis in the context of resistant cancer, as observed here for neuroblastoma. Indeed, the BH3-binding pockets of both anti- and pro-apoptotic BCL-2 family proteins are *bona fide* drug targets. Whereas therapeutic targeting of the anti-apoptotic BCL-2/BCL-X_L canonical groove in the form of ABT-737, -263, and -199 has led the way for "inhibiting the inhibitors" of apoptosis[48], new approaches to "activating the activators" by simulating BIM and PUMA engagement of BH3 trigger sites on BAX/BAK are underway[36,49] and may add a new dimension to the growing arsenal of BCL-2 family modulators.

Methods

Stapled peptide synthesis and characterization. SAHBs were synthesized, derivatized, purified to >95% homogeneity by LC/MS, quantified by amino acid analysis, and subjected to circular dichroism (Aviv Biomedical spectrophotometer) in 5 mM potassium phosphate buffer, pH 7.4, as previously described[43,50,51]. X = (S)-N-Fmoc-2-(4'-pentylenyl)alanine [S5]; U = 4-benzoylphenylalanine, B = norleucine.

Recombinant protein production. BCL-2ΔC, BCL-X_LΔC, BCL-wΔC, MCL-1ΔNΔC, BFL1ΔC, and BAX were produced and purified as described[15,36]. Briefly, BCL-2ΔC, BCL-X_LΔC, BCL-wΔC, and MCL-1ΔNΔC were expressed as glutathione-S-transferase (GST) fusion proteins in *Escherichia coli BL21* (DE3) from the pGEX2T vector (Pharmacia Biotech) and purified by affinity chromatography using glutathione sepharose beads (GE Healthcare), followed by thrombin cleavage of the GST tag. GB1-BFL1ΔC-His was similarly expressed in *Escherichia coli* BL21 (DE3) from the pGEV2 vector, purified by affinity chromatography using nickel-NTA agarose beads (Qiagen), and eluted according to the manufacturer's instructions. BAX was expressed in *Escherichia coli* BL21 (DE3) from the pTYB1 vector and purified by affinity

chromatography using chitin beads (New England BioLabs), and the chitin tag cleaved by overnight incubation in 50 mM dithiothreitol. In each case, pure, monomeric protein was isolated by gel filtration FPLC.

Fluorescence polarization binding assay. FITC-PUMA SAHBs (50 nM) were added to serial dilutions of recombinant protein in binding buffer (100 mM NaCl, 50 mM Tris, pH 8.0) in 96-well black opaque plates. The plates were incubated in the dark at room temperature until equilibrium was reached, and then fluorescence polarization was measured by a microplate reader (Spectramax M5 Microplate Reader, Molecular Devices). Dissociation constants (K_D) were calculated by nonlinear regression analysis of dose-response curves with Prism software 5.0 (GraphPad).

NMR analysis. Uniformly ^{15}N-labeled full-length human BAX was generated as previously described[15,52]. Protein samples were prepared in 25 mM sodium acetate, 50 mM NaCl solution at pH 6.0 in 5% D_2O. PUMA $SAHB_{A1}$ (6 mM stock) was titrated into a solution of 50 mM BAX to achieve the indicated molar ratios. Correlation ^{1}H-^{15}N HSQC spectra[53] were acquired at 25°C on a Bruker 800 MHz NMR spectrometer equipped with a cryogenic probe, processed using NMRPipe[54], and analyzed with NMRView[55]. The weighted average chemical shift difference Δ at the indicated molar ratio was calculated as $[\{(\Delta H)^2 + (\Delta N/5)^2\}/2]^{1/2}$ in p.p.m. The absence of a bar indicates no chemical shift difference, or the presence of a proline or residue that is overlapped or not assigned. BAX cross-peak assignments were applied as previously reported[52]. The significance threshold for backbone amide chemical shift changes was calculated based on the average chemical shift across all residues plus the standard deviation, in accordance with standard methods[56].

Binding site identification by pSAHB photoaffinity labeling and mass spectrometry. Recombinant protein (10 mM) and biotinylated pSAHB (30 mM) were mixed and then irradiated (365 nm, Spectroline Handheld UV Lamp Model En280L, Spectronics Corp.) for 1.5 hours on ice. Unreacted peptide was removed from the irradiated samples by overnight dialysis at 4°C in dialysis buffer (200 mM NaCl, 50 mM Tris, pH 7.5) using 6–8 kD molecular weight cutoff D-Tube dialyzers (EMD Biosciences). Biotinylated species were captured by incubation with high-capacity streptavidin agarose (Thermo) for 2 hours at 4°C. Streptavidin beads were sequentially washed at room temperature three times each in 1% SDS in PBS, 1 M NaCl in PBS, and 10% ethanol in PBS, boiled 2 x 10 minutes in a 10% SDS solution (Promega) containing D-biotin (10 mg/ml), the eluates electrophoresed using 4%-12% gradient Bis-Tris gels (Invitrogen), and then stained for protein content by Coomassie Blue. The crosslinked bands were excised and prepared for mass spectrometry analysis as previously described[37]. Samples were subjected to LC-MS/MS in an LTQ Orbitrap XL hybrid mass spectrometer (ThermoFisher, San Jose, CA). MS/MS spectra were searched using the SEQUEST algorithm[57] against a partially tryptic database of the relevant protein. Benzophenone-crosslinked tryptic fragments were identified by using the mass of the tryptic fragment of the pSAHB peptide as a required modification. Reversed protein sequences were used to generate an estimate of the false discovery rate. Identified crosslinked peptides were filtered based on tryptic state, charge state, mass accuracy, and number of crosslinks per peptide.

Liposomal release assay. Liposomes were generated and applied in BAX-mediated release assays as described[17,58]. Briefly, a lipid mixture composed of a 48:28:10:10:4 molar ratio of phosphatidylcholine, phosphatidylethanolamine, phosphatidylinositol, dioleoyl phosphatidylserine, and tetraoleolyl cardiolipin (Avanti Polar Lipids) in chloroform was generated to mimic the lipid composition of the outer mitochondrial membrane. Solvent was removed by

evaporation under nitrogen gas and then by vacuum for two hours. Lipid films were hydrated in liposome buffer (150 mM KCl, 20 mM HEPES, pH 7.0) and mixed with 12.5 mM ANTS fluorophore and 45 mM DPX quencher. After five freeze-thaw cycles, the mixture was extruded through 100 nm nucleopore polycarbonate membranes (Avestin) and intact liposomes purified by gel filtration chromatography using a 10 mL Sepharose CL2B column (GE Healtcare). To monitor ligand-triggered BAX-mediated release, liposomes were incubated in liposome buffer with the indicated amounts of recombinant monomeric BAX and PUMA SAHBs in black opaque 96 well plates (total reaction volume, 100 mL). ANTS/DPX release was monitored over a 120 minute period in a spectrofluorometer (Tecan Infinite M1000) using an excitation wavelength of 355 nm, an emission wavelength of 540 nm, and a bandwidth of 20 nm. Maximal release was determined by addition of Triton X-100 to a final concentration of 0.2% (v/v). Percent release was calculated as $[(F-F_0)/(F_{Triton}-F_0)]$ x100, where F is the observed release, and F_0 and F_{100} are baseline and maximal fluorescence, respectively.

Cytochrome c release assay. Mouse liver mitochondria (1.0 mg/mL) were isolated from *Alb-cre*^{pos}*Bax*$^{fl/-}$*Bak*$^{-/-}$ mice as described[33], and incubated with the indicated combinations of recombinant BAX and PUMA SAHBs at 37°C for 40 minutes. The pellet and supernatant fractions were isolated by centrifugation, and released cytochrome *c* was quantitated using a colorimetric ELISA assay (R&D Systems). Percent cytochrome *c* released into the supernatant (%cytoc_{sup}) from releasable mitochondrial pools was calculated according to the following equation: %cyto*c*=[(cytoc_{sup}-cytoc_{backgr})/(cytoc_{total}-cytoc_{backgr})]x100, where background release represents cytochrome *c* detected in the supernatant of vehicle-treated samples and total release represents cytochrome *c* measured in 1% Triton X-100-treated samples.

Cell culture. Wild-type (WT) and *Bax*$^{-/-}$*Bak*$^{-/-}$ (DKO) mouse embryonic fibroblasts (MEFs) and human embryonic kidney (HEK) 293T cells were maintained in DMEM (Invitrogen) supplemented with 10% FBS, 100 U/mL penicillin/streptomycin, 2 mM L-glutamine, 0.1 mM nonessential amino acids, and 50 mM b-mercaptoethanol. Neuroblastoma cell lines SH SY5Y, Kelly, and IMR5 were maintained in RPMI 1640 GlutaMAX (Invitrogen) supplemented with 10% FBS and 100 U/mL penicillin/streptomycin.

Cellular uptake analysis. SH SY5Y cells were plated in 6-well plates at 5x10^5 cells per well and, after overnight incubation, full media was removed and replaced with OptiMEM (Invitrogen) containing 100 U/mL penicillin/streptomycin. FITC-PUMA peptide (1 mM stock in DMSO) or vehicle was diluted into 1 mL cultures for a final treatment concentration of 5 mM and incubated at 37°C for 6 hours, followed by washing twice in PBS, trypsinizing for 10 minutes to remove any surface-bound peptide, and washing in PBS twice more. Cells were then lysed in 1% CHAPS buffer on ice and incubated for 20 minutes. Supernatants were collected after table top centrifugation, electrophoresed, and intracellular FITC peptide detected by fluorescence imaging using a Typhoon 9400 (GE Healthcare Life Sciences). For live cell confocal microscopy, SH SY5Y cells were plated in poly-D-lysine-coated culture plates (MatTek Corporation) at 2x10^5 cells per well and, after overnight incubation, full media was replaced with OptiMEM (Invitrogen) containing 100 U/mL penicillin/streptomycin. FITC-PUMA peptide (1 mM stock in DMSO) or vehicle was diluted into 1 mL cultures for a final treatment concentration of 10 mM and incubated at 37°C. After 6 hours, cells were incubated with CellMask Orange (5 μg/mL) and Hoeschst 33342 (5 μg/mL, Invitrogen) for 10 minutes, followed by washing three times with PBS and incubation with DMEM media lacking phenol red. Confocal images were acquired on a Yokogawa CSU-X1 spinning disk confocal system (Andor Technology) attached to a Nikon Ti-E

inverted microscope (Nikon Instruments). Excitation of the three fluorophores was performed sequentially using 405 nm, 488 nm, and 561 nm lasers. Images were acquired using a 100x Plan Apo objective lens with a Hamamatsu OrcaER camera (Hamamatsu Photonics). Acquisition parameters, shutters, filter positions, and focus were controlled by Andor iQ software (Andor Technology).

Cell viability and caspase-3/7 activation assays. Cells were plated in 96-well plates at $2.5x10^3$ cells per well and, after overnight incubation, full media was replaced with OptiMEM containing 100 U/mL penicillin/streptomycin. A serial dilution of PUMA $SAHB_{A2}$ from a 1 mM DMSO stock or vehicle was added to the cells in a final volume of 100 mL and incubated at 37°C for 6 hours, followed by addition of 10 mL FBS. To measure caspase-3/7 activation, cells were analyzed after eight hours of total treatment using the Caspase-Glo 3/7 chemiluminescence reagent (Promega). For cell viability analysis, cells were analyzed after 24 hours of total treatment using the CellTiter-Glo chemiluminescence reagent (Promega). Luminescence was detected by a microplate reader (Spectramax M5 Microplate Reader, Molecular Devices).

PUMA SAHB co-precipitation from cellular lysates. Neuroblastoma cells were trypsinized, collected by centrifugation, washed twice in cold PBS, and lysed in a 1% CHAPS buffer (50 mM Tris [pH 7.5], 200 mM NaCl, 1% [w/v] CHAPS, 1mM EDTA, 1.5 mM $MgCl_2$, complete protease inhibitor tablet [Roche]), on ice for 20 minutes. Lysates were isolated after table top centrifugation and then incubated (1.25 mg) with 50 nmol biotinylated-PUMA $SAHB_{A3}$ in lysis buffer overnight at 4°C. Biotin pull down was accomplished by incubation with high-capacity streptavidin agarose (Thermo) for 2 hours at 4°C, followed by washing the beads with 3 x 500 mL lysis buffer. Precipitated proteins were eluted by treating the beads with 4x LDS buffer

containing 50 mM DTT for 10 minutes at 70°C, and then subjected to electrophoresis (25 mg protein/lane) and western blotting using the following antibodies: BAX N-20 (1:2000) (sc-493, Santa Cruz Biotechnology), BCL-2 (1:200) (sc-509, Santa Cruz Biotechnology), MCL-1 s-19 (1:200) (sc-819, Santa Cruz Biotechnology).

Cell transfection and Flag-PUMA co-immunoprecipitation. HEK 293T cells were transiently transfected with pcDNA3 plasmid containing Flag-PUMAa using polyethylenimine[59] (PEI) at a 4:1 PEI:DNA ratio. Two days following transfection, cells were lysed in 1% CHAPS buffer (as above) and isolated lysate (2 mg) was incubated with 30 mL of anti-Flag magnetic affinity beads (Sigma) in lysis buffer overnight at 4°C. The beads were washed with 3 x 500 mL lysis buffer, and immunoprecipitated proteins eluted by incubation with 4x LDS containing 50 mM DTT for 10 minutes at 70°C. The immunoprecipitates were subjected to electrophoresis and analyzed by western blot using the above-described BAX, BCL-2, and MCL-1 antibodies.

Table 2-1: PUMA BH3 peptides.

Peptide	Sequence	N-terminus
PUMA BH3	EQWAREIGAQLRRMADDLNAQYE	Ac
PUMA SAHB$_{A1}$	EQWAREIGAQLR**X**BAD**X**LNAQYE	Ac, Fitc-βAla
PUMA SAHB$_{A2}$	QWAREIGAQLR**X**BAD**X**LNAQYERR	Ac, Fitc-βAla
PUMA SAHB$_{A3}$	QWAREIGAQLR**X**BAD**X**LNAQY	Fitc-βAla, Btn-βAla
PUMA SAHB$_{A4}$	EEQWAREIGAQLR**X**BAD**X**LNAQYERR	Fitc-βAla
PUMA SAHB$_{A5}$	REIGAQLR**X**BAD**X**LNAQYERR	Fitc-βAla
PUMA SAHB$_{A6}$	REIGAQLR**X**BAD**X**LNAQYERRR	Fitc-βAla
PUMA SAHB$_{A7}$	EIGAQLR**X**BAD**X**LNAQYERR	Fitc-βAla
PUMA SAHB$_{A8}$	EIGAQLR**X**BAD**X**LNAQYERRR	Fitc-βAla
PUMA SAHB$_{A9}$	EIGAQLR**X**BAD**X**LNAQYERRRQEE	Fitc-βAla
PUMA SAHB$_{B}$	**X**QWA**X**EIGAQLRRBADDLNAQYE	Fitc-βAla
PUMA SAHB$_{C}$	E**X**WAR**X**IGAQLRRBADDLNAQYE	Fitc-βAla
PUMA SAHB$_{D}$	EQ**X**ARE**X**GAQLRRBADDLNAQYE	Fitc-βAla
PUMA SAHB$_{E}$	EQW**X**REI**X**AQLRRBADDLNAQYE	Fitc-βAla
PUMA SAHB$_{F}$	EQWAR**X**IGA**X**LRRBADDLNAQYE	Fitc-βAla
PUMA SAHB$_{G}$	EQWAREIGA**X**LRR**X**ADDLNAQYE	Fitc-βAla
PUMA SAHB$_{H}$	EQWAREIGAQ**X**RRB**X**DDLNAQYE	Fitc-βAla
PUMA SAHB$_{I}$	EQWAREIGAQLRR**X**ADD**X**NAQYE	Fitc-βAla
PUMA SAHB$_{J}$	EQWAREIGAQLRRBA**X**DLN**X**QYE	Fitc-βAla
PUMA SAHB$_{K}$	EQWAREIGAQLRRBAD**X**LNA**X**YE	Fitc-βAla
PUMA SAHB$_{L}$	EQWAREIGAQLRRBADDL**X**AQY**X**	Fitc-βAla
PUMA SAHB$_{A1}$mut	EQWAREIG**L**Q**A**R**X**BAD**X**LNAQYE	Ac, Fitc-βAla
PUMA pSAHB-1	QWAR**X**IGA**X**LRRBADD**U**NRQYE	Btn-βAla
PUMA pSAHB-2	Q**U**AREIGAQLR**X**BAD**X**LNAQYE	Btn-βAla

X, stapling amino acid; B, norleucine; U, 4-benzoyl-phenylalanine (Bpa)

Attributions

Contributions to this part of the thesis were made by Amanda L. Edwards, Evripdis Gavathiotis, Kwadwo Opoku-Nsiah, Gregory H. Bird, and Loren D. Walensky.

A.L.E. and L.D.W. designed all PUMA SAHB constructs and experiments. A.L.E. and G.H.B. synthesized all peptides. E.G. performed the NMR experiments, and K.O. performed the confocal experiments. A.L.E. performed all fluorescence polarization binding experiments, pSAHB crosslinking experiments, liposomal and cytochrome *c* release assays, cellular viability experiments, and protein and peptide pulldowns.

References

1. Llambi, F. *et al.* A unified model of mammalian BCL-2 protein family interactions at the mitochondria. *Mol Cell* **44,** 517–531 (2011).

2. Han, J. *et al.* Expression of bbc3, a pro-apoptotic BH3-only gene, is regulated by diverse cell death and survival signals. *Proc Natl Acad Sci USA* **98,** 11318–11323 (2001).

3. Nakano, K. & Vousden, K. H. PUMA, a novel proapoptotic gene, is induced by p53. *Mol Cell* **7,** 683–694 (2001).

4. Yu, J., Zhang, L., Hwang, P. M., Kinzler, K. W. & Vogelstein, B. PUMA induces the rapid apoptosis of colorectal cancer cells. *Mol Cell* **7,** 673–682 (2001).

5. Yu, J. PUMA Sensitizes Lung Cancer Cells to Chemotherapeutic Agents and Irradiation. *Clinical Cancer Research* **12,** 2928–2936 (2006).

6. Jeffers, J. R. *et al.* Puma is an essential mediator of p53-dependent and -independent apoptotic pathways. *Cancer Cell* **4,** 321–328 (2003).

7. Luo, X., He, Q., Huang, Y. & Sheikh, M. S. Transcriptional upregulation of PUMA modulates endoplasmic reticulum calcium pool depletion-induced apoptosis via Bax activation. *Cell Death Differ* **12,** 1310–1318 (2005).

8. Reimertz, C., Kögel, D., Rami, A., Chittenden, T. & Prehn, J. H. M. Gene expression during ER stress-induced apoptosis in neurons: induction of the BH3-only protein Bbc3/PUMA and activation of the mitochondrial apoptosis pathway. *The Journal of Cell Biology* **162,** 587–597 (2003).

9. Villunger, A. *et al.* p53- and drug-induced apoptotic responses mediated by BH3-only

proteins puma and noxa. *Science* **302,** 1036–1038 (2003).

10. Yu, J. & Zhang, L. PUMA, a potent killer with or without p53. **27,** S71–S83 (2009).

11. Mustata, G. *et al.* Development of small-molecule PUMA inhibitors for mitigating radiation-induced cell death. *Curr Top Med Chem* **11,** 281–290 (2011).

12. Uren, R. T. *et al.* Mitochondrial permeabilization relies on BH3 ligands engaging multiple prosurvival Bcl-2 relatives, not Bak. *The Journal of Cell Biology* **177,** 277–287 (2007).

13. Willis, S. N. *et al.* Apoptosis initiated when BH3 ligands engage multiple Bcl-2 homologs, not Bax or Bak. *Science* **315,** 856–859 (2007).

14. Dai, H. *et al.* Transient binding of an activator BH3 domain to the Bak BH3-binding groove initiates Bak oligomerization. *The Journal of Cell Biology* **194,** 39–48 (2011).

15. Gavathiotis, E. *et al.* BAX activation is initiated at a novel interaction site. *Nature* **455,** 1076–1081 (2008).

16. Moldoveanu, T. *et al.* The X-Ray Structure of a BAK Homodimer Reveals an Inhibitory Zinc Binding Site. *Mol Cell* **24,** 677–688 (2006).

17. Gavathiotis, E., Reyna, D., Davis, M., Bird, G. & Walensky, L. BH3-Triggered Structural Reorganization Drives the Activation of Proapoptotic BAX. *Mol Cell* **40,** 481–492 (2010).

18. Walensky, L. D. *et al.* A stapled BID BH3 helix directly binds and activates BAX. *Mol Cell* **24,** 199–210 (2006).

19. Cartron, P.-F. *et al.* The first alpha helix of Bax plays a necessary role in its ligand-induced activation by the BH3-only proteins Bid and PUMA. *Mol Cell* **16,** 807–818 (2004).

20. Gallenne, T. *et al.* Bax activation by the BH3-only protein Puma promotes cell dependence on antiapoptotic Bcl-2 family members. *The Journal of Cell Biology* **185,** 279–290 (2009).

21. Kim, H. *et al.* Stepwise activation of BAX and BAK by tBID, BIM, and PUMA initiates mitochondrial apoptosis. *Mol Cell* **36,** 487–499 (2009).

22. Yee, K. S. & Vousden, K. H. Contribution of membrane localization to the apoptotic activity of PUMA. *Apoptosis* **13,** 87–95 (2008).

23. Zhang, Y., Xing, D. & Liu, L. PUMA promotes Bax translocation by both directly interacting with Bax and by competitive binding to Bcl-X L during UV-induced apoptosis. *Mol Biol Cell* **20,** 3077–3087 (2009).

24. Villunger, A., Labi, V., Bouillet, P., Adams, J. & Strasser, A. Can the analysis of BH3-only protein knockout mice clarify the issue of 'direct versus indirect' activation of Bax and Bak? *Cell Death Differ* **18,** 1545–1546 (2011).

25. Ren, D. *et al.* BID, BIM, and PUMA Are Essential for Activation of the BAX- and BAK-Dependent Cell Death Program. *Science* **330,** 1390–1393 (2010).

26. Callus, B. A. *et al.* Triggering of Apoptosis by Puma Is Determined by the Threshold Set by Prosurvival Bcl-2 Family Proteins. *J Mol Biol* **384,** 313–323 (2008).

27. Jabbour, A. M. *et al.* Puma indirectly activates Bax to cause apoptosis in the absence of Bid or Bim. *Cell Death Differ* **16,** 555–563 (2009).

28. Du, H. *et al.* BH3 Domains other than Bim and Bid Can Directly Activate Bax/Bak. *Journal of Biological Chemistry* **286,** 491 (2011).

29. Kuwana, T. *et al.* BH3 domains of BH3-only proteins differentially regulate Bax-mediated mitochondrial membrane permeabilization both directly and indirectly. *Mol Cell* **17,** 525–535 (2005).

30. Hinds, M. G. *et al.* Bim, Bad and Bmf: intrinsically unstructured BH3-only proteins that undergo a localized conformational change upon binding to prosurvival Bcl-2 targets. *Cell Death Differ* **14,** 128–136 (2006).

31. Day, C. L. *et al.* Structure of the BH3 Domains from the p53-Inducible BH3-Only Proteins Noxa and Puma in Complex with Mcl-1. *J Mol Biol* **380,** 958–971 (2008).

32. Letai, A. *et al.* Distinct BH3 domains either sensitize or activate mitochondrial apoptosis, serving as prototype cancer therapeutics. *Cancer Cell* **2,** 183–192 (2002).

33. Pitter, K., Bernal, F., Labelle, J. & Walensky, L. D. Dissection of the BCL-2 family signaling network with stabilized alpha-helices of BCL-2 domains. *Meth Enzymol* **446,** 387–408 (2008).

34. Stewart, M. L., Fire, E., Keating, A. E. & Walensky, L. D. The MCL-1 BH3 helix is an exclusive MCL-1 inhibitor and apoptosis sensitizer. *Nat Chem Biol* **6,** 595–601 (2010).

35. Walensky, L. D. *et al.* Activation of apoptosis in vivo by a hydrocarbon-stapled BH3 helix. *Science* **305,** 1466–1470 (2004).

36. Labelle, J. L. *et al.* A stapled BIM peptide overcomes apoptotic resistance in hematologic cancers. *J Clin Invest* **122,** 2018–2031 (2012).

37. Braun, C. R. *et al.* Photoreactive stapled BH3 peptides to dissect the BCL-2 family interactome. *Chemistry & Biology* **17,** 1325–1333 (2010).

38. Smits, C., Czabotar, P. E., Hinds, M. G. & Day, C. L. Structural plasticity underpins promiscuous binding of the prosurvival protein A1. *Structure* **16,** 818–829 (2008).

39. Akhtar, R. S. *et al.* BH3-only proapoptotic Bcl-2 family members Noxa and Puma mediate neural precursor cell death. *J Neurosci* **26,** 7257–7264 (2006).

40. Steckley, D. *et al.* Puma is a dominant regulator of oxidative stress induced Bax activation and neuronal apoptosis. *J Neurosci* **27,** 12989–12999 (2007).

41. Wyttenbach, A. & Tolkovsky, A. M. The BH3-only protein Puma is both necessary and sufficient for neuronal apoptosis induced by DNA damage in sympathetic neurons. *J*

Neurochem **96,** 1213–1226 (2006).

42. Erlacher, M. *et al.* Puma cooperates with Bim, the rate-limiting BH3-only protein in cell death during lymphocyte development, in apoptosis induction. *J Exp Med* **203,** 2939–2951 (2006).

43. Bird, G. H., Christian Crannell, W. & Walensky, L. D. Chemical Synthesis of Hydrocarbon‐Stapled Peptides for Protein Interaction Research and Therapeutic Targeting. *Current Protocols in Chemical Biology* 99–117 (2011). doi:10.1002/9780470559277.ch110042

44. Bernal, F., Tyler, A. F., Korsmeyer, S. J., Walensky, L. D. & Verdine, G. L. Reactivation of the p53 tumor suppressor pathway by a stapled p53 peptide. *J Am Chem Soc* **129,** 2456–2457 (2007).

45. Garrison, S. P. *et al.* Genetically defining the mechanism of Puma- and Bim-induced apoptosis. *Cell Death Differ* **19,** 642–649 (2012).

46. Erlacher, M. *et al.* BH3-only proteins Puma and Bim are rate-limiting for gamma-radiation- and glucocorticoid-induced apoptosis of lymphoid cells in vivo. *Blood* **106,** 4131–4138 (2005).

47. Gray, D. H. D. *et al.* The BH3-Only Proteins Bim and Puma Cooperate to Impose Deletional Tolerance of Organ-Specific Antigens. *Immunity* **37,** 451–462 (2012).

48. Oltersdorf, T. *et al.* An inhibitor of Bcl-2 family proteins induces regression of solid tumours. *Nat Cell Biol* **435,** 677–681 (2005).

49. Gavathiotis, E., Reyna, D. E., Bellairs, J. A., Leshchiner, E. S. & Walensky, L. D. Direct and selective small-molecule activation of proapoptotic BAX. *Nat Chem Biol* **8,** 639–645 (2012).

50. Braun, P. & Gingras, A.-C. History of protein-protein interactions: from egg-white to complex networks. *Proteomics* **12,** 1478–1498 (2012).

51. Bird, G. H., Bernal, F., Pitter, K. & Walensky, L. D. Synthesis and biophysical characterization of stabilized alpha-helices of BCL-2 domains. *Meth Enzymol* **446,** 369–386 (2008).

52. Suzuki, M., Youle, R. J. & Tjandra, N. Structure of Bax: coregulation of dimer formation and intracellular localization. *Cell* **103,** 645–654 (2000).

53. Waltz, I. The Importance of Not Saturating HzO in Protein NMR. Application to Sensitivity Enhancement and NOE Measurements. *J Am Chem Soc* **115,** 12593–12594 (1993).

54. Delaglio, F. *et al.* NMRPipe: a multidimensional spectral processing system based on UNIX pipes. *J. Biomol. NMR* **6,** 277–293 (1995).

55. Johnson, B. A. Using NMRView to visualize and analyze the NMR spectra of macromolecules. *Methods Mol. Biol.* **278,** 313–352 (2004).

56. Marintchev, A., Frueh, D. & Wagner, G. NMR methods for studying protein–protein interactions involved in translation initiation. *Meth Enzymol* **430,** 283–331 (2007).

57. Yates, J. R., Eng, J. K., McCormack, A. L. & Schieltz, D. Method to correlate tandem mass spectra of modified peptides to amino acid sequences in the protein database. *Anal Chem* **67,** 1426–1436 (1995).

58. Yethon, J., Epand, R., Leber, B., Epand, R. & Andrews, D. Interaction with a membrane surface triggers a reversible conformational change in Bax normally associated with induction of apoptosis. *Journal of Biological Chemistry* **278,** 48935 (2003).

59. Ehrhardt, C. *et al.* Polyethylenimine, a cost-effective transfection reagent. *Signal Transduction* **6,** 179–184 (2006).

60. Forood, B., Feliciano, E. J. & Nambiar, K. P. Stabilization of alpha-helical structures in short peptides via end capping. *Proc Natl Acad Sci USA* **90,** 838–842 (1993).

Chapter 3

Targeting of OLIG2 Using Stapled Alpha-Helical Peptides

Abstract

The protein OLIG2 plays a fundamental role in central nervous system development, regulating the differentiation of progenitor cells into neuronal subtypes and oligodendrocytes. Early in development, OLIG2 preserves these cells in a replication-competent state. OLIG2 also plays a similar role in tumor “stem cells,” serving to perpetually repopulate human gliomas. As a basic helix-loop-helix (bHLH) transcription factor, OLIG2 dimerizes through the interaction of two α-helices to carry out its downstream functions. We generated a series of stabilized alpha-helices (SAHs) mimicking helical segments of the OLIG2 bHLH domain in an effort to inhibit dimer formation and potentially OLIG2 function. While hydrocarbon stapling successfully produced a number of α-helical peptides corresponding to the endogenous domain, none of the SAH-OLIG2 peptides specifically and potently disrupted OLIG2 dimerization or its subsequent binding to DNA, as assessed by EMSA assay. As an alternative approach to direct OLIG2 targeting, we undertook a whole human genome yeast two-hybrid study of full-length OLIG2 to identify novel OLIG2 interaction partners. Several intriguing candidates, including the Wnt effector protein DVL3 and the regulator of embryonic neurogenesis LNX2, were identified and merit further study, both for their potential roles in OLIG2 biology and as alternate targets for indirect modulation of OLIG2.

Introduction

Transcription factors dictate the expression and stoichiometry of cellular proteins, making them master regulators of cell and tissue physiology. It is therefore not surprising that such control points are frequently mutated and deregulated in disease[1], making transcription factors potentially ideal targets for therapeutic intervention. However, transcription factors have long frustrated pharmacologic efforts due to the difficulty of targeting their protein-protein and protein-DNA interaction surfaces. Recently, strides have been made in modulating both of these classes of transcription factor interactions. For example, polyamides[2] and zinc finger nucleases[3] have been used to target specific DNA binding sequences, while small molecules[4,5] and short peptides[6-11] have been designed to disrupt specific transcription factor-based protein binding interfaces.

Basic helix-loop-helix (bHLH) proteins are a large and diverse class of transcription factors that regulate numerous processes during the cellular life span. The canonical bHLH domain consists of a basic stretch of amino acids that contact the DNA, typically at an E-box consensus site[12], followed by two α-helices joined with a variable loop region. Homologous α-helices of two transcription factor molecules can dimerize in a parallel orientation, stabilizing the dimer on the DNA and enabling downstream transcription[12,13]. Many bHLH transcription factors can pair with a variety of partners, thereby exerting precise control over a range of diverse targets.

The bHLH protein OLIG2 was discovered over a decade ago as a critical mediator of oligodendrocyte and somatic motor neuron differentiation[14-16]. While the majority of OLIG2 protein is downregulated following development, OLIG2 remains active in a subset of adult neural precursor cells and in mature myelinating oligodendrocytes[17,18]. OLIG2 functionally regulates both p21[19] and p53[20,21], allowing it to control entry into the cell cycle and cellular proliferation.

In addition to its developmental functions, OLIG2 is also a pathogenic factor in brain tumorigenesis. OLIG2 is expressed in 100% of diffuse gliomas, irrespective of grade[22,23], where it marks a subset of stem cell-like populations[19,24] that are highly resistant to radiation and chemotherapy[25]. Notably, OLIG2 is not merely present in these cells but is strictly required for the development of glioma in a mouse model[19]. Therapeutic disruption of OLIG2 function could thus be highly advantageous in the treatment of refractory gliomas.

Nature has already provided a solution for disrupting bHLH function. The Id proteins, which have a helix-loop-helix domain but lack a basic region and thus cannot bind to DNA, serve as natural dominant negatives in the cell through the formation of nonfunctional heterodimers[26]. Several approaches have been made to artificially reproduce this disruption through the generation of bHLH domain peptide mimetics. Short peptides designed against Helix 2 of the bHLH protein E47 were able to disrupt E47 homodimerzation *in vitro* at low micromolar doses[7], while peptides designed against Helix 1 or the leucine zipper domain of the MYC/MAX heterodimer have also shown some efficacy in cellular systems[6,8,11].

To evaluate the ability of short peptides to disrupt OLIG2 dimerization and DNA binding (**Figure 3-1**), we generated peptides designed against Helix 1, Helix 2, and the bHLH domains of OLIG2. Notably, in the studies described above, challenges in three areas emerged: successful mimicry of the native α-helical binding interface (shown to confer enhanced binding efficacy[6]); prolonged proteolytic stability in a cellular environment[8]; and selection of the optimal region to create a specific dominant negative peptide. To address the first two questions, we made use of a hydrocarbon crosslinking technique in which *i,i+4* residues of the peptide are replaced with non-natural amino acids bearing terminal olefins that are covalently crosslinked by ruthenium-catalyzed olefin metathesis[27,28]. This “stapling” approach frequently restores the native α-helicity of the peptide, as well as increasing proteolytic stability and cell penetrance[29]. Using this approach, stabilized alpha-helices (SAHs) of OLIG2 domains were synthesized for

Figure 3-1

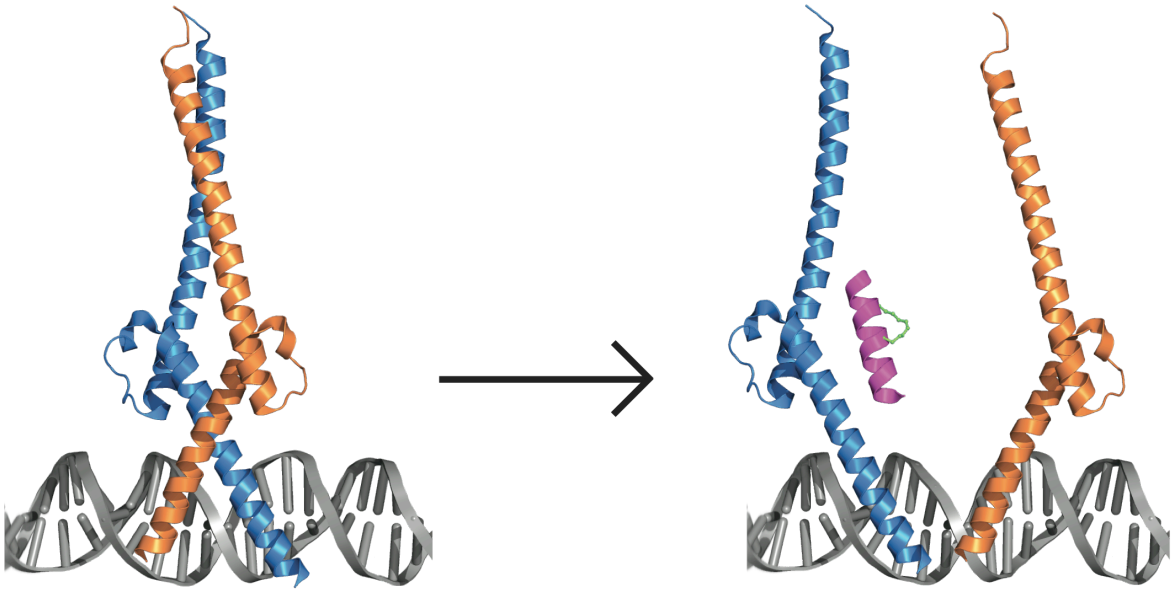

Schematic of bHLH dimerization disruption using stapled peptides. Basic helix-loop-helix transcription factors dimerize through their bHLH domains and engage target DNA (bHLH heterodimer of E47 and NeuroD1[30] shown here as an example). Addition of a dominant negative stapled peptide could disrupt an OLIG2 dimer, preventing downstream transcription.

biochemical analysis. To address the third area of difficulty, we generated panels of SAH-OLIG2 peptides for each domain (Helix 1, Helix 2, or bHLH) in order to comprehensively test a variety of peptides lengths, compositions, and charges. These peptides were then evaluated for their capacity to disrupt OLIG2 dimerization and DNA binding, in an effort to identify novel research tools and prototype therapeutics for disrupting pathologic OLIG2 activity *in vitro* and *in vivo*.

Results

Design, synthesis, and biophysical characterization of SAH-OLIG2 peptides

In order to investigate the ability of short peptides to inhibit OLIG2 transcription factor activity, we designed and synthesized a panel of compounds corresponding to the α-helical segments of the bHLH domain of OLIG2 (**Figure 3-2A,B**). In addition, based on preliminary evidence that E12 is a binding partner of OLIG2 (C. Stiles, personal communication), peptides based on the bHLH domain of E12 were also generated to compare the efficacy of E12 and OLIG2 peptides in disrupting OLIG2 interactions (**Figure 3-2C**). The designed constructs vary in their staple position, charge, and sequence coverage of the indicated helical domains.

In order to reinforce the native α-helicity of the bHLH sequences, non-natural amino acids were inserted into the peptides one α-helical turn apart (*i,i+4)* and chemically crosslinked by ruthenium-catalyzed olefin metathesis, yielding stabilized α-helices of OLIG2 and E12 peptides. Circular dichroism analysis demonstrated a range of α-helical stabilization from installation of the various staples, spanning 23%-100% α-helical induction (**Figure 3-2, A-C**). In comparison, native peptides of either Helix 1 or Helix 2 sequences of OLIG2 were unstructured in solution, as determined by circular dichroism (**Figure 3-2D**). Thus, this preliminary library of peptides provided a range of SAH-OLIG2 and -E12 α-helical peptides for further evaluation.

Figure 3-2 (next page)

A panel of SAH-OLIG2 and -E12 peptides with varying lengths and staple positions show a range of α-helical stabilization. Stapled SAH-OLIG2.1 (**A**) and 2.2 (**B**) peptides and SAH-E12.1 and 2.2 peptides (**C**) demonstrate a wide range of α-structural stabilization spanning 23-100% α-helicity, as measured by circular dichroism analysis. In contrast, native, unstapled OLIG2 Helix 1 and Helix 2 peptides are relatively unstructured in solution (**D**). *, exceeds the calculated ideal α-helicity of an undecapeptide standard[31]. X = S5 non-natural stapling amino acid, B = norleucine.

(**Figure 3-2**, cont.)

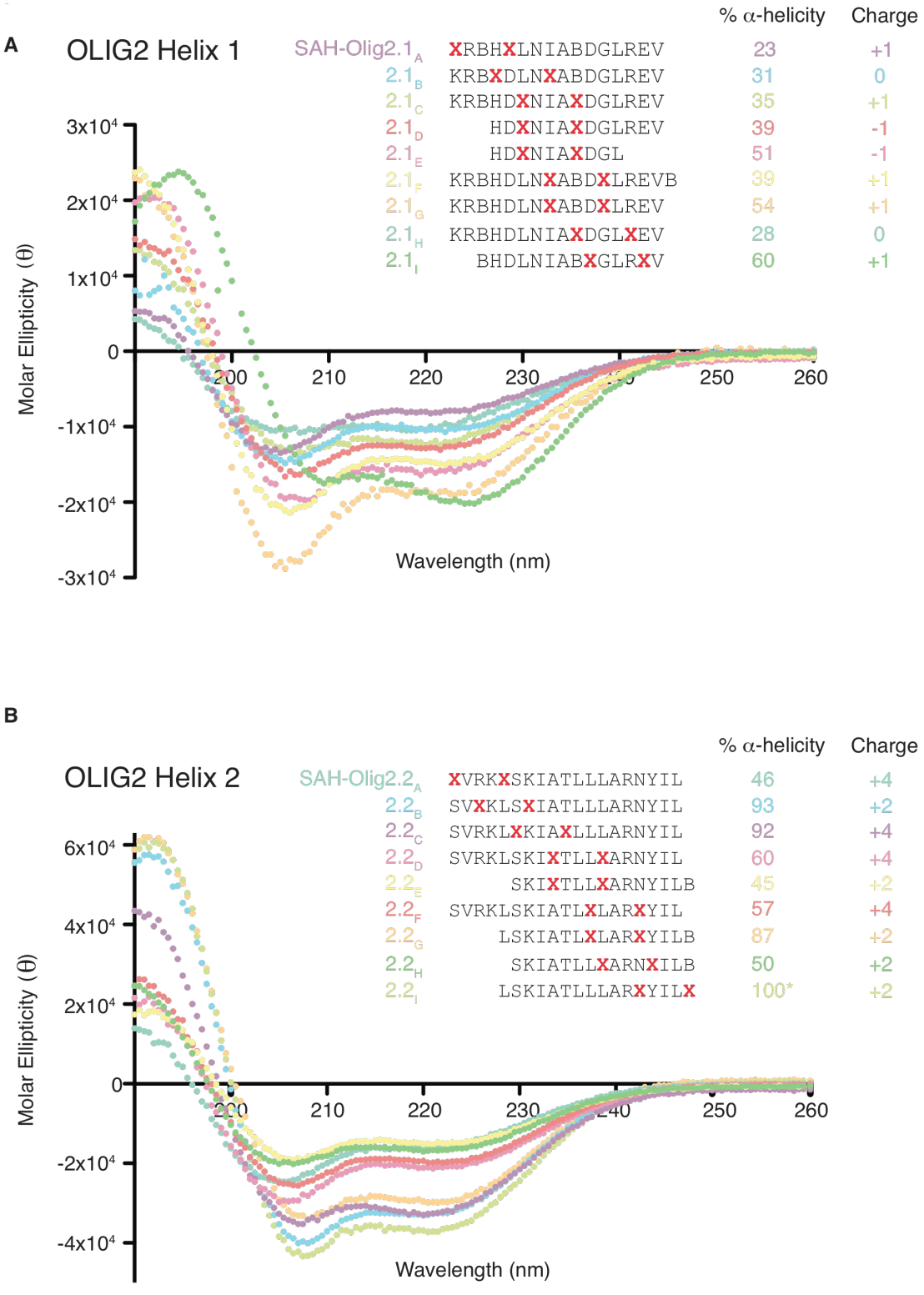

(**Figure 3-2**, cont.)

C

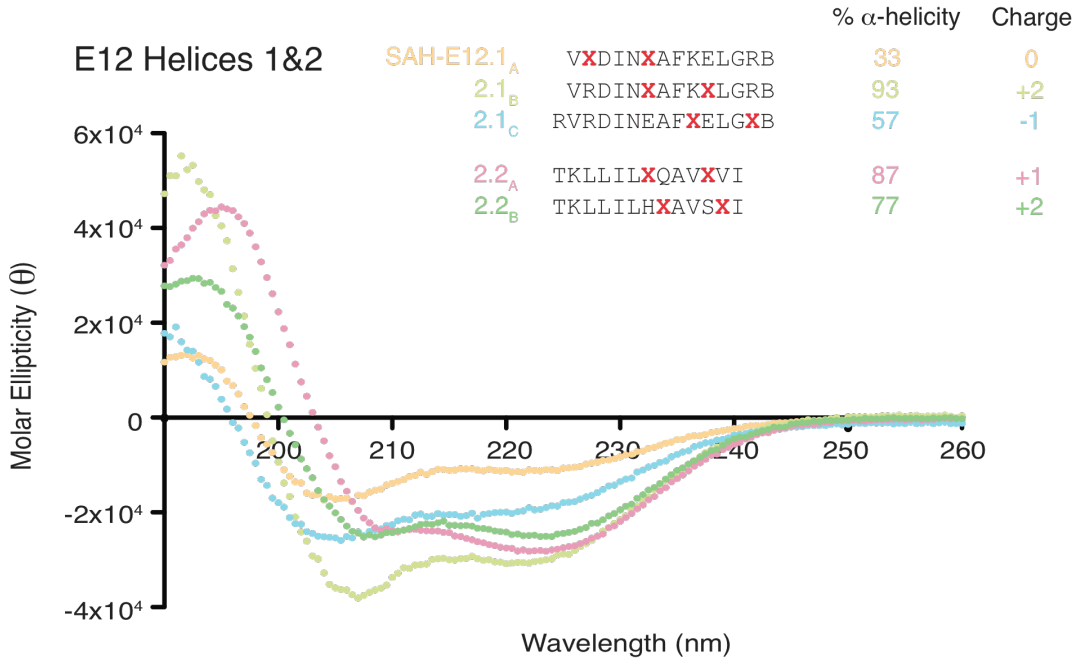

D

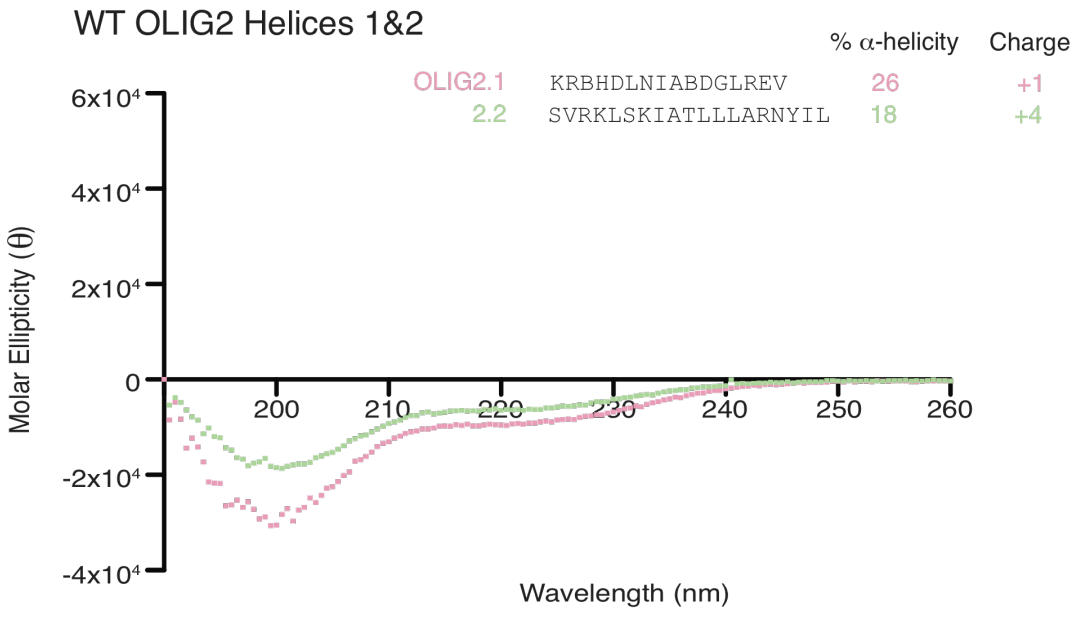

Functional evaluation of SAH-OLIG2 peptides using electrophoretic mobility shift assays

The SAH-OLIG2 peptides were screened for their ability to impact the formation of an OLIG2/DNA complex (and ultimately downstream transcriptional activity) by electrophoretic mobility shift assays (EMSAs). In these experiments, purified OLIG2 protein from COS-7 cells was pre-incubated with varying concentrations of SAH-OLIG2 and -E12 peptides, and the mixtures added to a ^{32}P-labelled double-stranded DNA probe containing an OLIG2 binding site. The proportion of DNA probe bound to OLIG2 was evaluated by polyacrylamide gel electrophoresis. Whereas peptides modeled after the Helix 1 portion of OLIG2's bHLH domain (SAH-OLIG2.1$_{A-I}$) or Helices 1 or 2 of E12 (SAH-E12.1$_{A-C}$ and SAH-E12.2$_{A,B}$) showed no effect on complex formation, several peptides modeled after the OLIG2 bHLH Helix 2 (SAH-OLIG2.2$_{A-I}$) caused an unexpected increase, rather than decrease, in complex formation (**Figure 3-3, A-C**).

OLIG2 belongs to a family of highly homologous bHLH transcription factors, and it was therefore important to determine the specificity of the observed Helix 2 effects. Thus, peptides modeled after Helix 2 of the MYC and MAX bHLH leucine zipper proteins (SAH-MYC2$_A$ and SAH-MAX2$_A$) were tested in the OLIG2 EMSA. While SAH-OLIG2.2$_D$ showed strong stabilization of the OLIG2/DNA complex, neither SAH-MYC2$_A$ nor SAH-MAX2$_A$ altered the dynamics of the complex (**Figure 3-4A**).

To rule out the possibility that hydrophobic or charge effects could account for the observed result, as opposed to sequence-specific binding, a scrambled version of SAH-OLIG2.2$_C$ peptide was generated. This peptide, scr. SAH-OLIG2.2$_C$, was synthesized such that the overall sequence composition and staple position remained constant but the location of the natural amino acids were randomly placed or scrambled. Surprisingly, this peptide exerted the same stabilization effect on the OLIG2/DNA complex, as evaluated by EMSA (**Figure 3-4B**), suggesting that amino acid composition or overall charge, rather than the linear sequence itself,

Figure 3-3 (next page)

Evaluation of SAH-OLIG2 and -E12 peptides by electrophoretic mobility shift assays (EMSA). Purified OLIG2 from COS-7 cells was incubated with radiolabeled *Hb9* E-box oligonucleotides in the presence or absence of increasing concentrations of SAH-OLIG2.1 (**A**), -OLIG2.2 (**B**), and -E12 (**C**) peptides. Complexes and free DNA were separated by polyacrylamide gel electorphoresis. The top band represents protein-DNA complex, whereas the bottom band is free DNA probe. While neither SAH-OLIG2.1 nor SAH-E12 peptides showed any effect, several SAH-OLIG2.2 peptides appeared to increase the amount of shifted DNA complex.

(**Figure 3-3**, cont.)

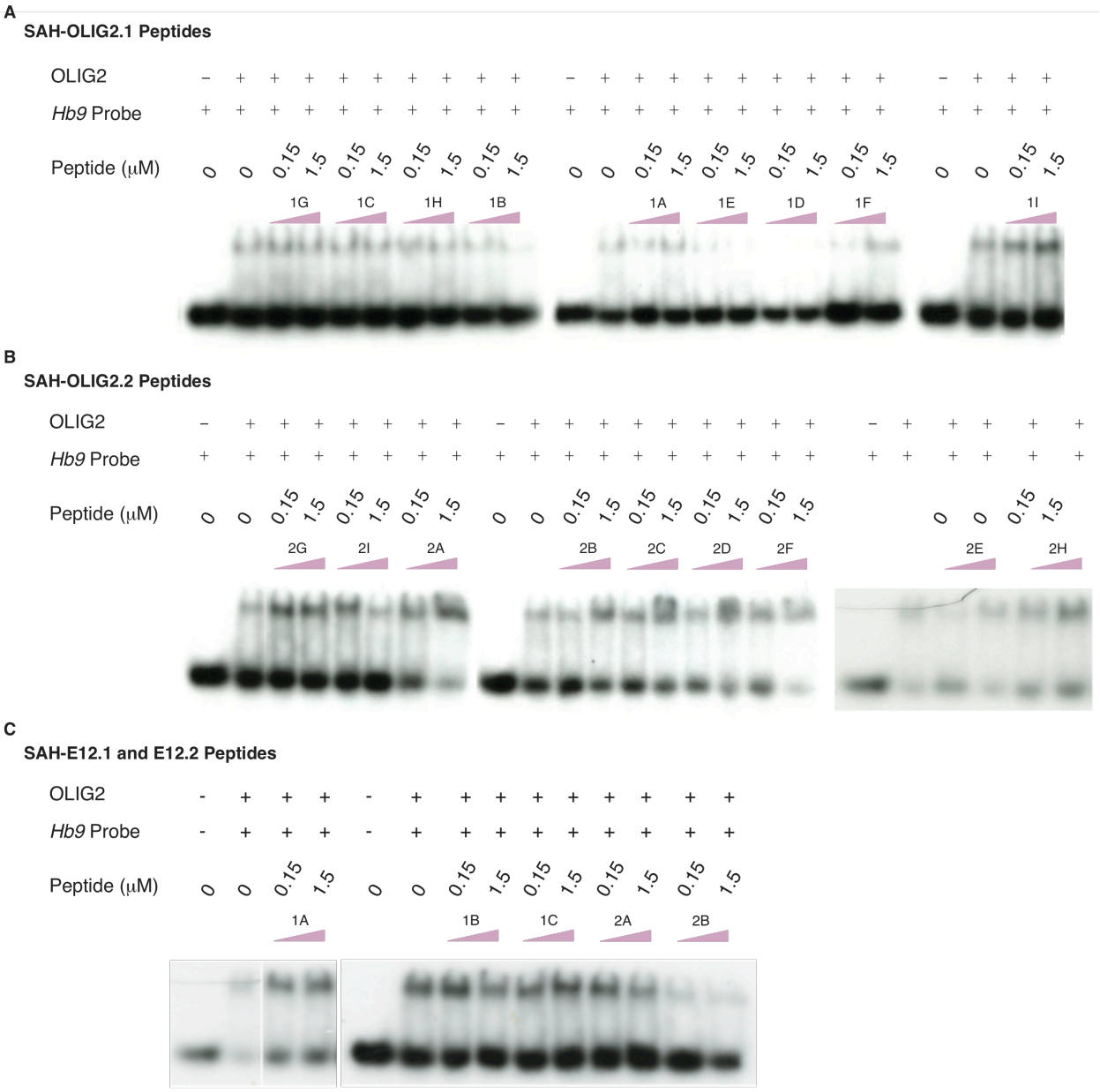

Figure 3-4

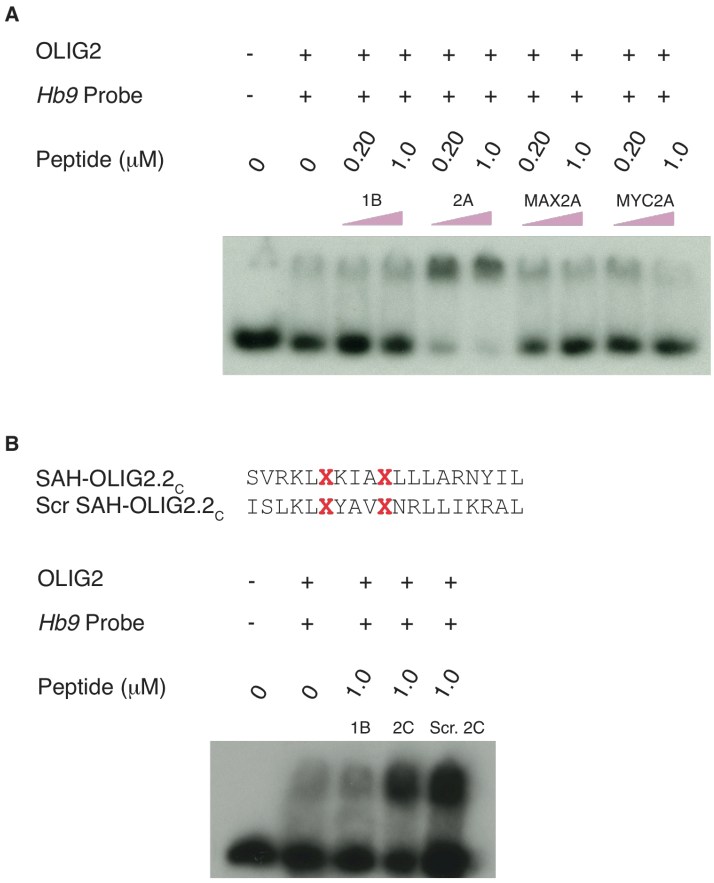

Specificity testing identifies charge, not sequence, as the driving force behind the observed SAH-OLIG2.2 activity. Purified OLIG2 from COS-7 cells was incubated with radiolabeled *Hb9* E-box oligonucleotides in the presence or absence of increasing concentrations of SAH peptides for specificity analysis. (**A**) SAH-MYC and SAH-MAX Helix 2 peptides were generated as bHLH family control peptides. While SAH-OLIG2.2$_A$ caused an increase in shifted DNA complex, neither SAH-MYC nor SAH-MAX had any effect. (**B**) A scrambled version of SAH-OLIG2.2C was generated, maintaining overall amino acid content, staple position, and charge but randomizing the linear sequence. Both SAH-OLIG2.2$_C$ and its scrambled control caused an increase in shifted DNA complex, suggesting that the observed effect was non-specific.

was the driving force for the observed phenomenon. Additional testing of unrelated stapled peptides with positive charges (+4 and +7) identified charge as a major causal factor for the increased dimerization/DNA binding activity of OLIG2 (data not shown). Thus, the observed stabilization of the OLIG2/DNA complex was a charge-driven DNA binding effect, rather than a sequence-specific stabilization of the protein/DNA complex.

Yeast two-hybrid binding assay for Olig2 subdomains

In an effort to determine the minimal binding determinants for OLIG2 dimerization, we decided to utilize a high throughput yeast two-hybrid approach to test the binding of OLIG2 subdomains to one another (**Figure 3-5A**). Subdomains of OLIG2, as well as full-length OLIG2, the close homolog OLIG1, and the homeobox domain protein NKX2.2, were cloned into yeast two-hybrid vectors containing either activating or DNA-binding domains. (**Figure 3-5B**). Each construct was evaluated against all others for their ability to grow on selective media, resulting in a 10x10 matrix of binding partner pairings. Indeed, full-length OLIG2 homodimerized with itself, and heterodimerized with full-length OLIG1. Additionally, binding occurred between full-length OLIG2 and an OLIG2ΔN construct but not a OLIG2ΔC construct, suggesting an important role for the C-terminus of OLIG2 for dimerization. However, no constructs consisting of only the bHLH domain or its subcomponents were found to dimerize with OLIG2 (**Figure 3-5C**). These data indicated that (1) truncated regions of OLIG2 express poorly in yeast, as has been observed in human cells, (2) short peptide subcomponents of the OLIG2 bHLH domain are insufficient for engaging full-length OLIG2, or (3) the weighting of the applied yeast two-hybrid system toward low false positive rates (Type I errors) and high false negative rates (Type II errors) may have prevented observation of these (potentially lower affinity) complexes.

Figure 3-5

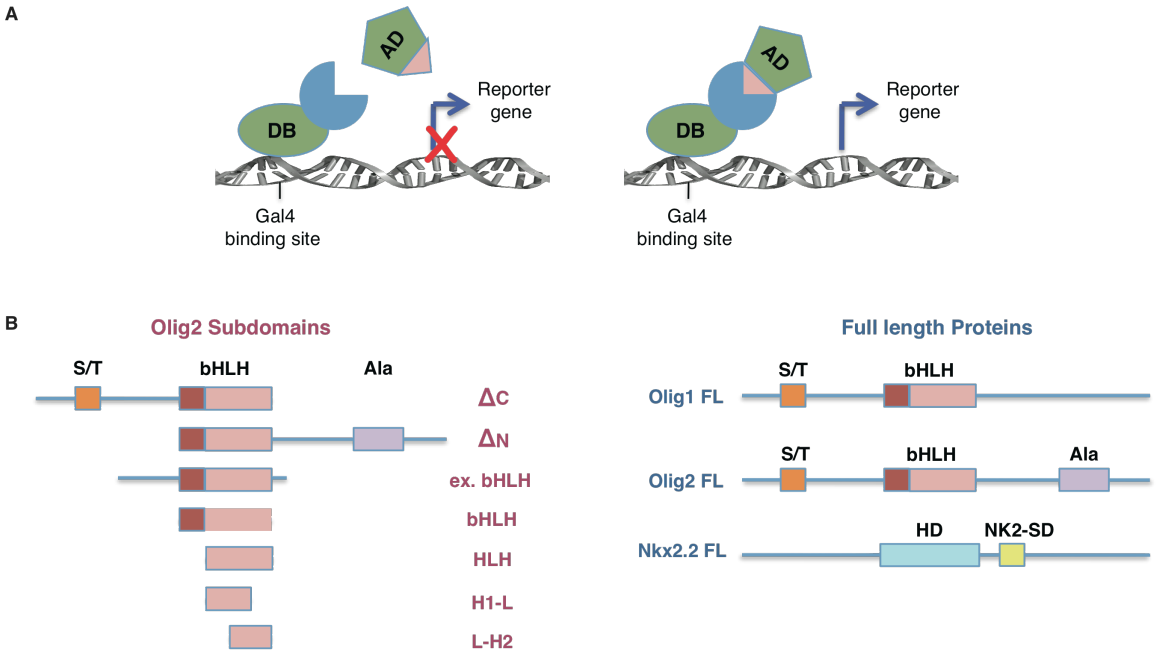

C

DB \ AD	OLIG2 FL	ΔC	ΔN	ex. bHLH	bHLH	HLH	H1-L	L-H2	OLIG1 FL	NKX2.2 FL
OLIG2 FL	++++									
ΔC										
ΔN	+++									
ex. bHLH										
bHLH										
HLH										
H1-L										
L-H2										
OLIG1 FL	+									
NKX2.2 FL										

Yeast two-hybrid analysis of full-length OLIG2 and its subdomains. (**A**) Experimental outline of yeast two-hybrid analysis. A functional transcription factor is separated into activating domains (Ads) and DNA-binding domains (DBs), and the two domains are fused to two potentially interacting species. If the species do in fact interact, the activating and DNA-binding

(**Figure 3-5**, cont.)

domains are brought in close enough proximity to activate transcription, allowing for expression of a reporter gene. (**B**) Full-length human *Olig2, Olig1*, and *Nkx2.2* cDNAs were cloned into yeast two-hybrid vectors containing ADs or DBs. Additionally, subdomains of *Olig2* of decreasing size were generated and cloned into the same yeast two-hybrid vectors. (**C**) A 10x10 matrix represents the yeast two-hybrid binding experiment of each transcription factor (full-length or subdomain) paired with all others, using both orientations of ADs and DBs. Yellow cells represent expected interactions, while +s represent observed strength of interaction in the yeast two-hybrid system, as evidenced by colony formation on selective yeast extract peptone dextrose plates. While OLIG2 homodimerization and OLIG1-OLIG2 heterodimerization were observed, dimerization of full-length OLIG2 and its subdomains was not detected.

Design, synthesis, and biophysical characterization of doubly-stapled SAH-OLIG2 peptides

Given the ambiguous results of the OLIG2 subdomain yeast two-hybrid interaction analysis, we decided to generate OLIG2 peptides that encompassed a larger portion of the bHLH dimerization domain in an effort to maximize potential sequence-specific interactions. To do so, peptides were synthesized that incorporated the C-terminal portion of the basic DNA-binding region as well as the entirety of Helix 1, the loop, and Helix 2 of OLIG2. Since these peptides were designed to mimic two separate and defined helices, with helix-breaking prolines in the intervening loop region, hydrocarbon staples were inserted into both helical regions to induce α-helicity, creating double stabilized alpha-helical (dSAH) OLIG2 peptides. Additionally, the non-natural amino acids were placed two α-helical turns apart (*i,i+7*), rather than one (*i,i+4*), in order to stabilize a longer region of the peptide. A native sequence, unstapled peptide (OLIG2 bHLH) and a scrambled version (scr. dSAH-OLIG2$_B$) were also generated as negative control peptides. To evaluate the successful induction of α-helicity, circular dichroism was performed on both the OLIG2 bHLH and dSAH-OLIG2$_B$ peptides (**Figure 3-6**). Once again, while the unstapled peptide was unstructured, dSAH-OLIG2$_B$ was over 50% α-helical, confirming the efficacy of stapling in restoring α-helicity.

Functional evaluation of dSAH-Olig2 peptides using electrophoretic mobility shift assays

Next, the dSAH-OLIG2 peptides were screened for their ability to alter the formation of an OLIG2/DNA complex by EMSA, as described above. At μM dosages, addition of the dSAH-OLIG2 peptides caused a decrease in observed OLIG2/DNA complex. However, addition of the dSAH-OLIG2 peptides to DNA alone resulted in a shifted species, suggesting that dSAH-OLIG2 may be competing with OLIG2 for binding to the DNA target (**Figure 3-7A**). To address this question, a scr. dSAH-OLIG2$_B$ was incubated with DNA alone to evaluate nonspecific DNA binding. This control peptide also bound to the DNA probe at similar doses, suggesting a

Figure 3-6

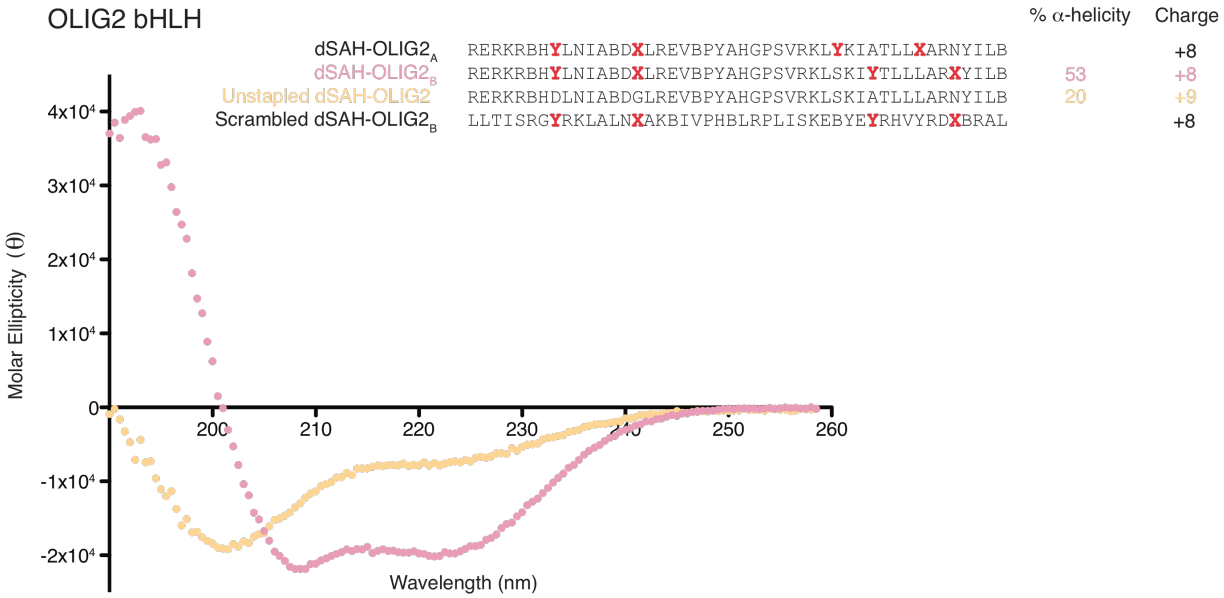

Double stapled, two helix SAH-OLIG2 peptides demonstrate enhanced α-helical character. Peptides corresponding to the C-terminal portion of the basic domain, Helix 1, the loop, and Helix 2 of OLIG2 were generated using i,i+7 staples. Stapling increased the α-helicity of the sequence by 2.5x fold, as demonstrated by circular dichroism analysis. X = S5 non-natural stapling amino acid, Y = R8 non-natural stapling amino acid, B = norleucine. nonspecific disruption of the protein/DNA complex.

Figure 3-7

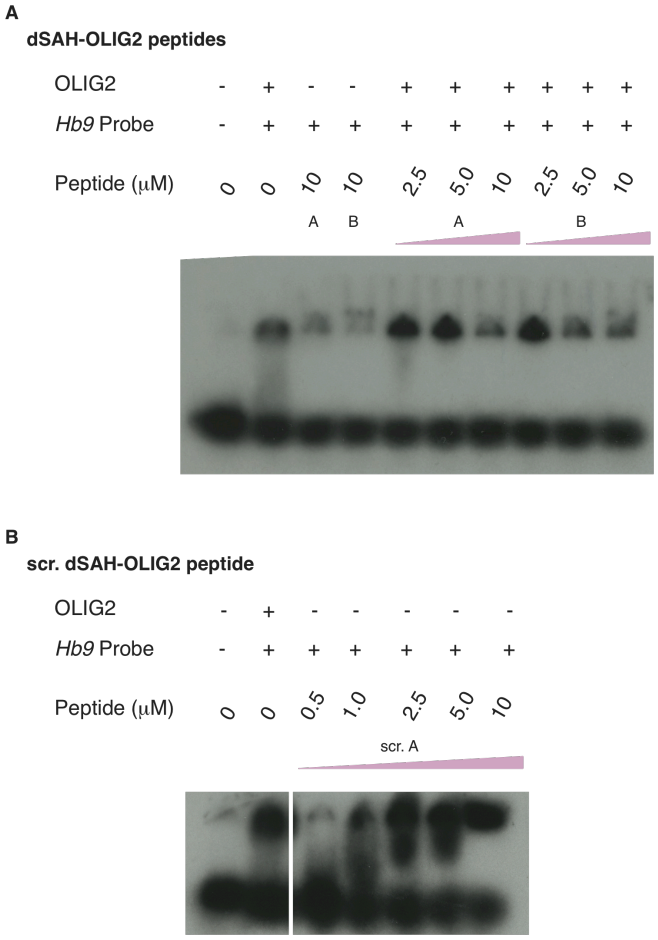

dSAH-OLIG2 peptides compete non-specifically for DNA as assessed by EMSA. (**A**) Purified OLIG2 from COS-7 cells was incubated with radiolabeled *Hb9* E-box oligonucleotides in the presence or absence of increasing concentrations of dSAH-OLIG2$_A$ and -OLIG2$_B$. Complexes and free DNA were separated by polyacrylamide gel electrophoresis. The top band represents protein-DNA complex, whereas the bottom band is free DNA probe. Both dSAH-OLIG2$_A$ and -OLIG2$_B$ appeared to decrease the levels of protein-DNA complex at μM concentrations. However, incubation of scr. dSAH-OLIG2$_B$ with radiolabeled DNA alone showed an increase in shifted complex at equivalent concentrations (**B**), suggesting that the peptide was binding to and obstructing the DNA.

nonspecific disruption of the protein/DNA complex (**Figure 3-7B**). These data suggest that neither short, singly-stapled helical peptides nor longer, doubly-stapled helical peptides of the OLIG2 bHLH domain could specifically bind and disrupt full-length OLIG2 dimerization and DNA binding.

Generation of recombinant OLIG2 protein

Previous research on *Olig2* has been carried out primarily using genetic and cellular systems, with little progress made on structural or biophysical characterization. This is in part due to the longstanding inability to generate OLIG2 in large quantities. To better accomplish our biochemical goals, we endeavored to develop a soluble construct of OLIG2 protein that could be expressed in a bacterial system. cDNA of human *Olig2* was cloned into the pGEV2 vector[32], which fuses the B1 immunoglobulin binding domain of streptococcal protein G (GB1) followed by a short linker region to the N-terminus of the OLIG2 protein. Additionally, a hexahistidine tag was added to the C-terminus of the protein to facilitate protein purification by affinity chromatography (**Figure 3-8A**).

Purification of this construct using cobalt affinity resin and size exclusion chromatography yielded milligram quantities of soluble GB1-OLIG2 protein. The identity of the protein was confirmed by both Western blot and mass spectrometry analysis (**Figure 3-8, B-D**). The recombinant protein was then evaluated by EMSA for functionality. GB1-OLIG2 successfully bound to the E-box of *MycN*, an OLIG2 transcriptional target, but not to the corresponding mutant E-box (**Figure 3-8E)**, confirming the ability of the recombinant protein to bind to target-specific DNA.

Figure 3-8 (next page)

Production and purification of functional, recombinant GB1-OLIG2. (**A**) Schematic of GB1-OLIG2-His protein expressed from pGEV2 vector in *E. coli* bacteria. The GB1 tag increases solubility of the protein, while the His tag allows for efficient affinity-based purification. Prominent OLIG2 features include the triple phosphoserine motif and the bHLH dimerization domain. (**B**) Size exclusion chromatography (SEC) of cobalt agarose-purified GB1-OLIG2-His protein shows two peaks, corresponding to the GB1-OLIG2-His monomer and dimer species. (**C**) Coomassie staining and Western blot analysis of collected SEC peaks confirmed the relative purity and identity of OLIG2. (**D**) Mass spectrometry analysis further confirmed the identity of the isolated protein as OLIG2. Tryptic sites are indicated by arrowheads, and identified peptide fragments of OLIG2 are highlighted in yellow. (**E**) GB1-OLIG2-His functionally recapitulates known OLIG2 function, as shown by DNA binding in the EMSA using *MycN* oligonucleotide probes (left). The upper band represents DNA bound to GB1-OLIG2-His protein, whereas the lower band is free DNA probe. GB1-OLIG2-His binding was documented to be sequence-specific, as protein incubation with a mutant *MycN* E-box sequence caused no DNA shift (right).

(**Figure 3-8**,cont.)

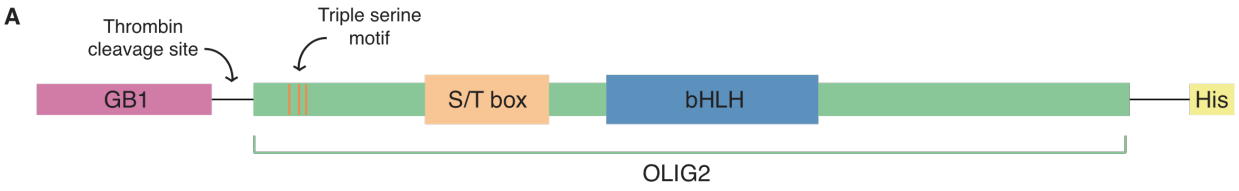

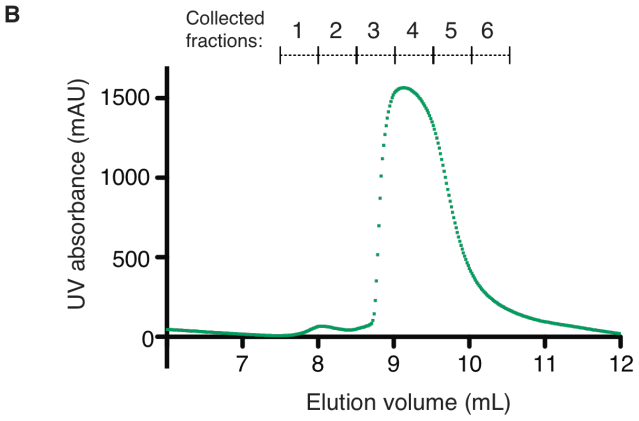

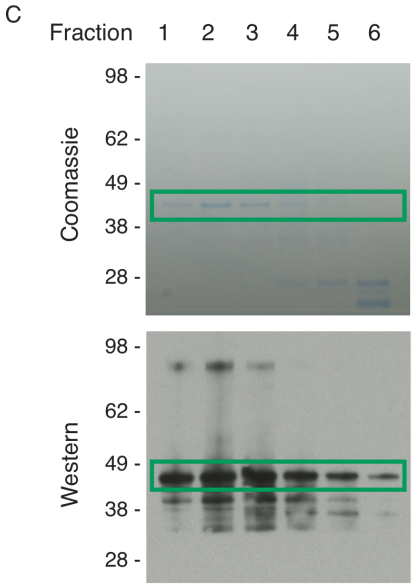

D

```
M D S D A S L V S S R P S S P E P D D L F L P A R S D G S S G S A F T G G T V S
S S T P S D C P P E L S A E L R G A M G S A G A H P G D K L G G S G F K S S S S
S T S S S T S S A A A S S T K K D K K Q M T E P E L Q Q L R L K I N S R E R K R
M H D L N I A M D G L R E V M P Y A H G P S V R K L S K I A T L L L A R N Y I L
M L T N S L E E M K R L V S E I Y G G H H A G F H P S A C G G L A H S A P L P A
A T A H P A A A A H A A H H P A V H H P I L P P A A A A A A A A A A A A V S S
A S L P G S G L P S V G S I R P P H G L L K S P S A A A A A A P L G G G G G G S G
A S G G F Q H W G G M P C P C S M C Q V P P P H H H V S A M G A G S L P R L T S
D A K
```

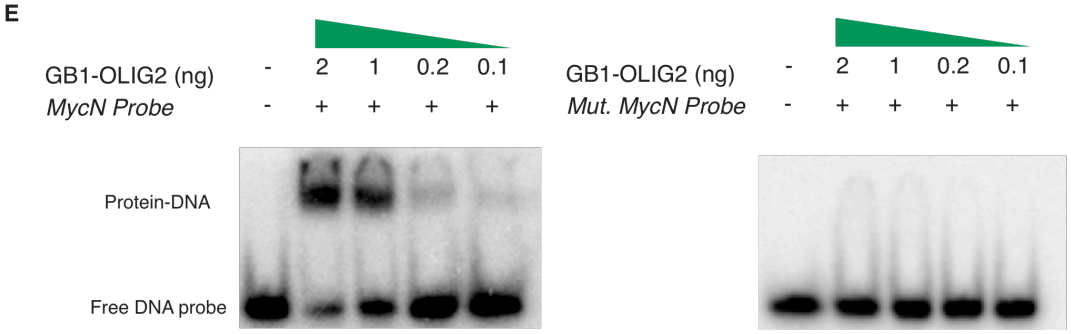

Improved EMSA assay allows for separation of DNA/peptide binding from potential protein/peptide disruption effect

Our previous EMSA experiments determined that many of our charged peptides bound to DNA at high concentrations, resulting in an apparent shift of the radioactive DNA. While we have confirmed that this DNA binding was nonspecific, we were concerned that such an effect could have obscured specific binding of our SAH-OLIG2 and -E12 peptides to OLIG2. In an effort to quench this effect, non-specific DNA (dCdG oligonucleotides) was added to the experimental design. In this assay, examination of control bands identified a non-specific DNA binding band (top) and a specific protein-DNA complex band (middle). Upon addition of excess dCdG oligonucleotides, the non-specific DNA binding largely disappeared, allowing for evaluation of specific disruption of the protein-DNA complex.

In addition to the difficulties of nonspecific DNA-peptide binding, we were also concerned about the variability of the expressed OLIG2 protein in mammalian cells. Previous experiments were performed with purified OLIG2 protein from COS-7 cells, with only 1-2 μg of purified protein obtained per preparation. Consequently, several independent purifications were required for the analysis of our full panel of stapled peptides. Thus, variability in purity and quantitation was unavoidable, potentially influencing the reproducibility of the EMSA results. Following successful purification of recombinant GB1-OLIG2 protein, we could apply a single purification batch for > 300 EMSA experiments, ensuring continuity of protein quality and quantity for the comparative experiments.

Finally, while the binding of OLIG2 to the E-box of the *Hb9* gene has been observed in p19 carcinoma cells[33], it has not been detected in neural progenitor cells (the more appropriate context for OLIG2). Work in the Stiles lab (Dana-Farber Cancer Institute) has identified a number of additional OLIG2 binding targets, including the E-box of the *MycN* gene (D. Meijer,

personal communication). As such, we began to use *MycN* E-box oligonucleotides in our EMSA system as a higher fidelity OLIG2 binding target.

With these improvements to our EMSA experimental set-up, all SAH-OLIG2, SAH-E12, and dSAH-OLIG2 peptides were retested for a specific OLIG2-DNA disruption effect (**Figure 3-9, A-E**). However, none of the peptides showed a significant disruption of the OLIG2-DNA complex at 0.15 or 1.5 micromolar peptide dosing . We have thus determined that our singly- and doubly-stapled SAH-OLIG2 and E12 peptides have, to date, not proven to be a viable, sequence-specific approach for targeted disruption of OLIG2 dimerization and DNA binding.

Discovery of putative novel interactors of OLIG2 using a whole genome yeast two-hybrid screen

Given the inherent difficulty of directly targeting transcription factors, we also decided to investigate other potential mechanisms for therapeutic intervention by searching for novel OLIG2 interaction partners. We previously generated yeast two-hybrid constructs of full-length OLIG2 and its subdomains, as well as full-length NKX2.2, with both DNA-binding and activating domain fusions (**Figure 3-10A**). These 9 constructs were screened in a pooled format against a library of yeast two-hybrid constructs of the human genome. Initial hits were then confirmed with one-on-one match-ups, generating a list of putative OLIG2 interacting proteins (**Figure 3-10B**). The list included a number of intriguing hits.

- LNX2 (Ligand of Numb 2) is a scaffolding protein that can oligomerize through its PDZ and RING domains, functionalities that regulate subcellular localization of unrelated proteins. In particular, LNX2 controls the subcelluar localization of NUMB, a membrane-associated protein that modulates neurogenesis by regulating asymmetric cell division[34].

Figure 3-9 (next page)

Evaluation of SAH-OLIG2, -E12, and dSAH-OLIG2 peptides by a refined EMSA. Purified GB1-OLIG2 cells was incubated with radiolabeled *MycN* E-box oligonucleotides and excess dCdG oligonucleotides in the presence or absence of increasing concentrations of SAH-OLIG2.1 (**A**), -OLIG2.2 (**B**), -E12 (**C**), dSAH-OLIG2 (**D**), and control SAH (**E**) peptides. Complexes and free DNA were separated by polyacrylamide gel electorphoresis. The top band represents protein-DNA complex, whereas the bottom band is free DNA probe. However, none of the peptides exhibited an effect at either 0.15 or 1.5μM doses.

(**Figure 3-9**, cont.)

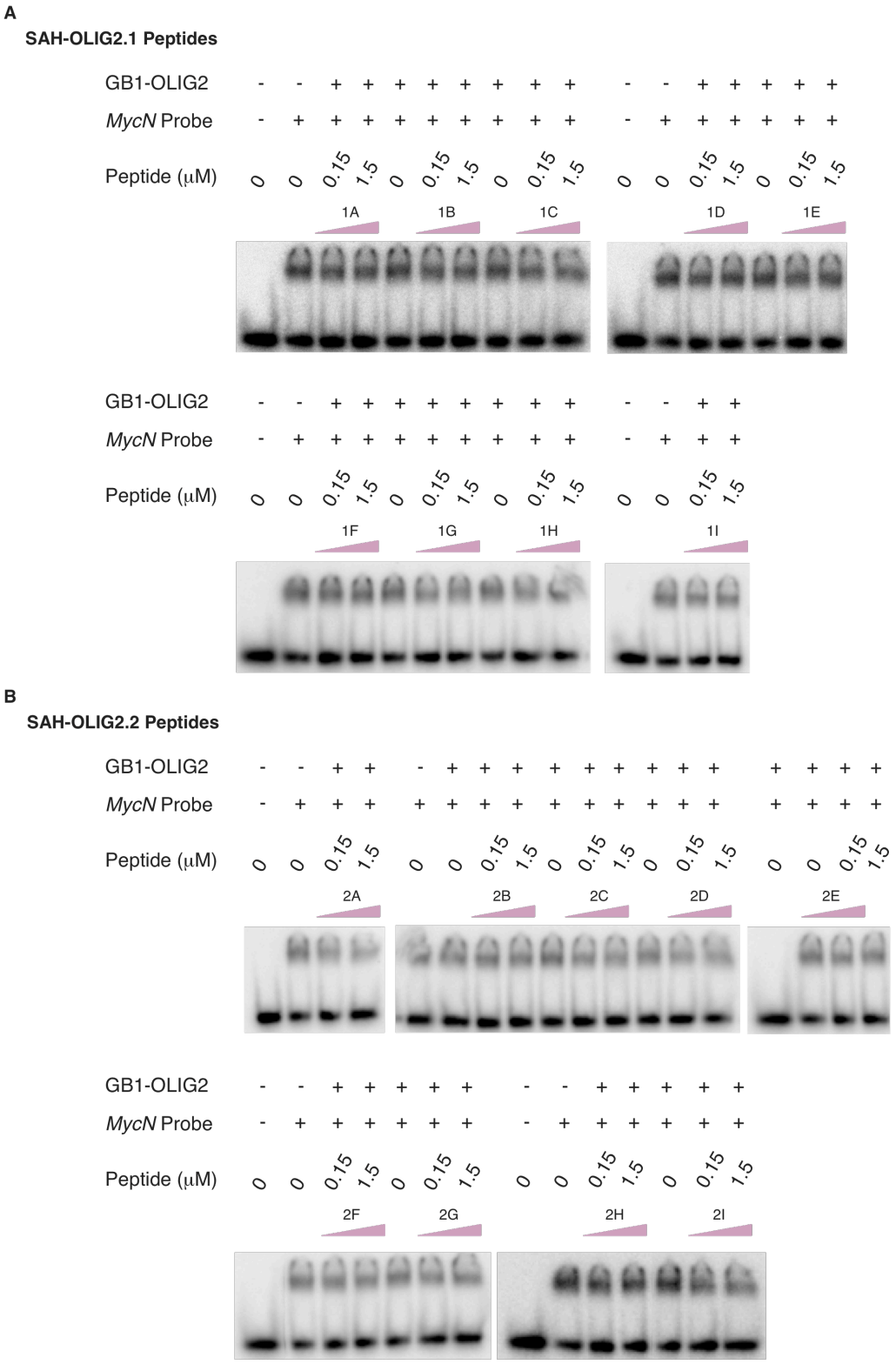

(**Figure 3-9**, cont.)

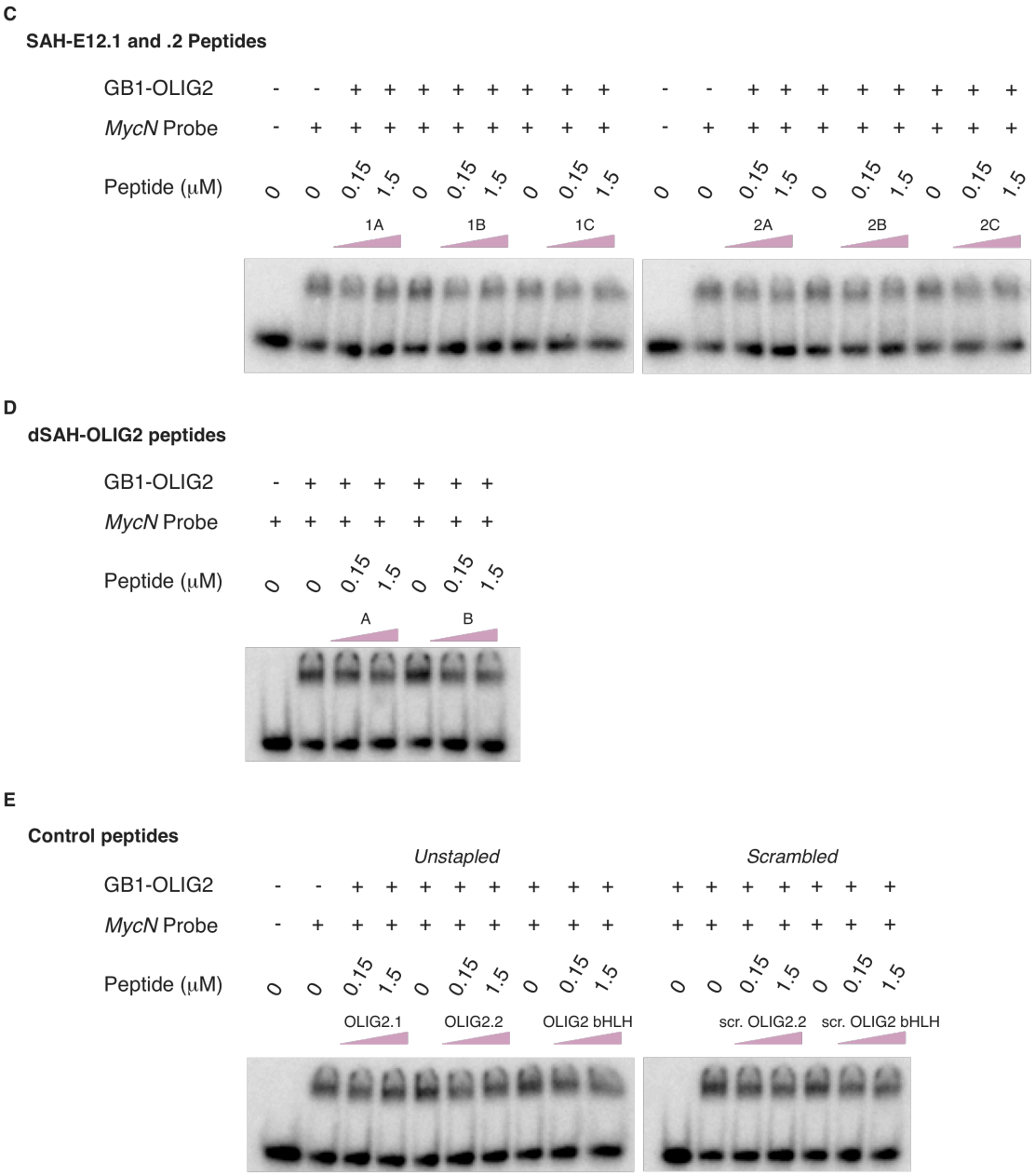

Figure 3-10

A

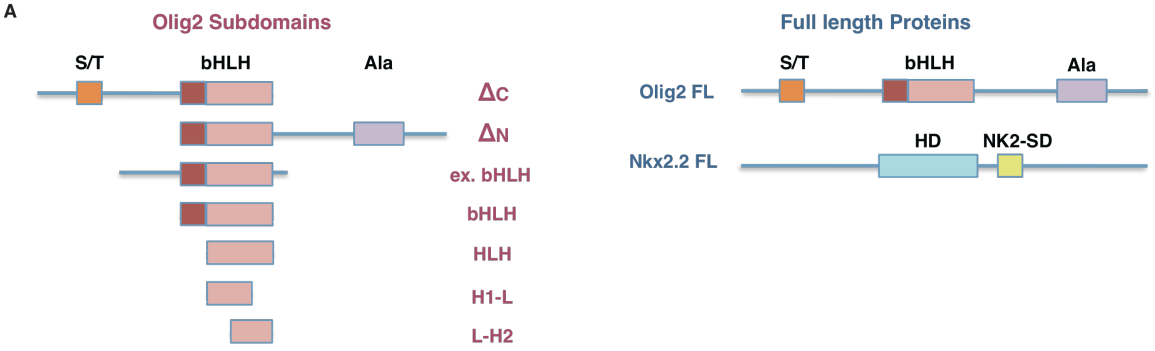

B

Fragment name	OLIG2 FL	ΔC	ΔN	ex. bHLH	bHLH	HLH	H1-L	L-H2	Nkx2.2 FL
Configuration (bait)	DB	DB	DB	DB	DB	DB	AD	AD	AD
	DVL3		BHLHE40	FAM9B	FAM9B	FAM9B	LNX2	FAM9B	BHLHE40
	OLIG3		DVL3						C1orf94
	RBMPS		LNX2						CRX
	RRN3		OLIG3						CXorf41
			RBMPS						DAB1
			RFX6						MAGED1
			RRN3						PRR20A
			TRIP6						RBPMS
									REL
									RRN3

Whole human genome yeast two-hybrid analysis of full-length OLIG2 and its subdomains identifies novel candidate OLIG2 interaction partners. (**A**) Full-length human *Olig2, Nkx2.2* cDNAs were cloned into yeast two-hybrid vectors containing ADs or DBs. Additionally, subdomains of *Olig2* of decreasing size were generated and cloned into the same yeast two-hybrid vectors. (**B**) Following pooled screening of all AD and DB *Olig2* vectors, one-on-one confirmations of all first-round hits yielded a list of putative OLIG2 interaction partners. For comparison, full-length homebox domain transcription factor NKX2.2 was also assayed in the yeast two-hybrid screen.

- DEC1 (BHLHE40) is another member of the bHLH class of transcription factors and is thought to serve as a transcriptional repressor. Its known functions range from regulating circadian rhythm[35] to promoting cartilage differentiation[36].
- DVL3 (Dishevelled 3) is an integral member of the Wnt signaling cascade, transmitting an activation signal from the Frizzled membrane receptor to the nucleus[37]. The interaction between DVL3 and Frizzled is mediated by DVL3's PDZ domain: notably, the same domain that regulates oligomerization of the LNX2 proteins.

Future work will continue the validation of these interactions in mammalian cells, including an assessment of the structural and functional significance of the putative interactions. Through this work, we have identified a novel set of proteins that may serve as targets for indirect modulation of OLIG2 and its tumorigenic activity.

Discussion

The bHLH transcription factor OLIG2 is a critical regulator of oligodendrocyte and somatic motor neuron development. With both antineural and proneural functions, OLIG2 can drive cells towards replication[33] or differentiation[38], depending on the cell type and stage of development. Aside from its developmental roles, OLIG2 is required for the formation of gliomas in both a mouse model[19] and from human brain tumor cells[20]. Thus, there is significant interest in therapeutic targeting of OLIG2. As a bHLH transcription factor, OLIG2 must dimerize to stably bind DNA promoter and enhancer elements, recruit necessary co-factors, and exert its transcriptional effects. This dimerization is driven by parallel intertwining of two adjacent α-helices. We endeavored to disrupt OLIG2 dimerization, and thereby inhibit its activity, through

the generation of stabilized α-helical peptides that mimic subcomponents of the OLIG2 dimerization domain.

A comprehensive panel of stabilized peptides modeled after Helix 1, Helix 2, and the entirety of the bHLH domain of OLIG2 was synthesized. Circular dichroism studies revealed a wide range of α-helical stabilization, confirming that in many cases, all-hydrocarbon stapling successfully restored the native conformation of the peptide sequence. Electrophoretic mobility shift assays were conducted with purified OLIG2 protein, either immunopurified from COS-7 cells or generated recombinantly in *E.coli*, in order to evaluate the ability of the SAH constructs to disrupt OLIG2 dimerization and DNA binding. Unfortunately, none of the singly- or doubly-stapled peptides significantly impaired the formation of an OLIG2/DNA complex. At this stage, without additional structural information about the OLIG2 homodimer (for which the newly produced recombinant OLIG2 protein should be helpful) or alternate strategies for potentially increasing targeting and binding affinity, short stabilized α-helical peptides have not proven to be a viable strategy for disrupting the dimerization of OLIG2 or its downstream oncogenic activities.

Previously, several groups have generated peptides consisting of Helix 1, Helix 2, or the leucine zipper of the bHLH-LZ proteins MYC and MAX to hinder formation of the pathologic dimer[6,8]. Such attempts have had limited success at dimer disruption *in vitro*, with even less success *in vivo*. While some of the challenge may reflect proteolytic instability and lack of cell penetrance (issues at least partially remedied by hydrocarbon stapling[29]), the necessity for high affinity, high specificity binding to a relatively featureless surface may ultimately represent the major obstacle. Indeed, thus far, stapled peptides have demonstrated therapeutic success when the targeted protein interaction is comprised of a helix-in-groove interface, allowing for numerous energetically favorable interactions between the stapled peptide helix and the protein target[10,29,39]. Future attempts to engage the more featureless interaction surfaces of transcription

factors may require additional chemical interventions to increase affinity. Alternatively, efforts to identify the “hot spots” for transcription factor engagement may provide a clearer roadmap for peptide design.

As an alternative approach to direct targeting of the OLIG2 dimerization domain, it may be feasible to intervene indirectly through targeting OLIG2 interaction partners – kinases, transcriptional co-regulator proteins, and perhaps others. However, only a limited number of OLIG2 interaction partners have been defined. In order to uncover new opportunities for indirect targeting of OLIG2, we undertook a yeast two-hybrid screen using full-length OLIG2 and several truncated fragments as bait. A number of interesting candidates emerged from the human genome library, including a member of the Wnt pathway and a regulator of embryonic neurogenesis, both of which merit further study of their potential interplay with OLIG2 function and the capacity to target them for therapeutic benefit.

Methods

OLIG2 purification from human cells. OLIG2-V5-HIS cDNA was transiently transfected into COS-7 cells using the pcDNA3.1 vector. Following cellular lysis, the protein was purified by immunoprecipiation with V5 antibody (Sigma) and V5 peptide (Sigma) elution, followed by immunoprecipitation with Ni-NTA beads (Qiagen) and elution in 200 mM imidazole and Buffer A (50mM Tris, pH 7.5, 150mM KCl, 5mM $MgCl_2$, 10% glycerol, 0.1% NP40, and protease inhibitors).

Recombinant OLIG2 production. GB1-OLIG2-His was expressed in *Escherichia coli* BL21 (DE3) from the pGEV2 vector[32] and induced with 1 mM isopropylthio-β-galactoside for 4 hours at 30°C. Bacterial pellets were resuspended on ice in Buffer A (50 mM Tris, pH 7.5, 150 mM KCl, 5 mM $MgCl_2$, 10% glycerol, 0.1% NP40, and protease inhibitors), lysed by microfluidization,

and centrifuged at 45,000 rpm for 45 minutes at 4°C. Cleared lysate was purified by affinity chromatography using nickel-NTA agarose beads (Qiagen), followed by washes with Buffer A containing 5, 10, and 15 mM imidazole. GB1-OLIG2-His was eluted with Buffer B (50 mM Tris, pH 7.5, 150 mM KCl, 5 mM $MgCl_2$, 250 mM imidazole), concentrated, and buffer exchanged to Buffer C (50 mM Tris, pH 7.5, 150 mM KCl, 5 mM $MgCl_2$) to remove the imidazole. GB1-OLIG2-His protein was further purified by gel filtration FPLC and ultimately stored in Buffer A. Fractions were analyzed by gel electrophoresis, followed by Western blot analysis with and Olig2 antibody (gift from the Stiles lab, DFCI).

Mass spectrometry identification of OLIG2. Recombinant GB1-OLIG2 fractions purified by FPLC were electrophoresed using a 4%-12% gradient Bis-Tris gel (Invitrogen), and then stained for protein content by Coomassie Blue. The GB1-OLIG2 band at 45kD was excised and prepared for mass spectrometry analysis as previously described[40]. Samples were subjected to LC-MS/MS in an LTQ Orbitrap XL hybrid mass spectrometer (ThermoFisher, San Jose, CA). MS/MS spectra were searched using the SEQUEST algorithm (Yates 1995) against a tryptic database of the human proteome.

Stapled peptide synthesis and characterization. Stapled peptides were synthesized, derivatized, purified to >95% homogeneity by LC/MS, quantified by amino acid analysis, and subjected to circular dichroism (Aviv Biomedical spectrophotometer) in water as previously described[41,42]. Singly stapled *i,i+4* peptides employed (S)-N-Fmoc-2-(4'-pentylenyl)alanine [S5] as both of the non-natural amino acids, whereas doubly-stapled i, i+7 peptides used (R)-N-Fmoc-2-(7'-octenyl)alanine [R8] for one of the non-natural amino acids of the staple pair and S5 for the second. SAH-$MYC2_A$: VVILXKATXYILS; SAH-$MAX2_A$: RAQILXKATXYIQY

Electrophoretic mobility shift assays. OLIG2 protein (purified as described above) was quantified by silver stain against known concentrations of BSA protein. Oligonucleotides included the *Hb9* and *MycN* E-box-containing promotors with the following DNA sequences: *Hb9*: 5' AGCTAATTTCCCAGATGGGCCAA 3' and 3' AGCTTTGGCCCATCTGGGAAATT 5'; *MycN*: 5' AGCTAGAAGACAGCTGTTGGAAG 3' and 3' AGCTCTTCCAACAGCTGTCTTCT 5'. In addition, negative control mutant sequences were also generated: *Hb9* mutant : 5' AGCTAATTTCCTAGACTGGCCAA 3' and 3' AGCTTTGGCCAGTCTAGGAAATT 5'; *MycN* mutant: 5' AGCTAGAAGATAGCCTTTGGAAG 3' and 3' AGCTCTTCCAAAGGCTATCTTCT 3'. Oligonucleotides were annealed in annealing buffer (10 mM Tris [pH7.5], 50 mM NaCl, 1 mM EDTA) using a thermocycler for 5 min at 95°C, and allowed to cool down for approximately 1 hour. The annealed probe was labeled with [α-^{32}P] 6000 Ci/mmol dCTP (PerkinElmer) using Klenow (New England Biolabs). The radioactive DNA probe was incubated with 2 ng of GB1-OLIG2 protein in binding buffer (20 mM Tris [pH7.5], 5 mM $MgCl_2$, 0.1% NP40, 0.5 mM DTT, 10% glycerol) and increasing concentrations of SAH-OLIG2 peptides for 30 min at 4°C. Protein:DNA complex was analyzed using 4% non-denaturing poly-acrylamide gel electrophoresis (PAGE) for 30 min at 4°C. After drying the gel, radioactive signal was detected using a Typhoon 9400 (GE Healthcare Life Sciences).

Yeast two-hybrid screening. Complete methods for the yeast two-hybrid screening have been described elsewhere[43]. *Olig2, Olig1, and Nkx2.2* constructs were amplified by PCR and cloned into pDONR entry vectors, followed by recombination into pDEST destination vectors containing an activating or DNA-binding domain, respectively (Gateway cloning system, Invitrogen). *Olig2* truncation fragments were as follows: FL *Olig2* (1-972), *Olig2ΔC* (1-510), *Olig2ΔN* (277-972), *Olig2* ext. bHLH (277-510), *Olig2* bHLH (325-489), *Olig2* HLH (361-489), *Olig2* H1-Loop (361-

429), *Olig2* Loop-H2 (406-489), *Olig1* (1-816), *Nkx2.2* (1-822). Completed plasmids were transformed into the yeast strains Y8800 *MAT*a and Y8930 *MAT*Aα. For primary screening, a single bait was mixed in liquid yeast extract peptone dextrose (YEPD) with a single prey (for the 10x10 screen) or with pools of approximately 200 preys, with the pools representing the entirety of the human genome[44]. Diploids were then selected in liquid YEPD lacking leucine and tryptophan. Successful interaction of the bait and prey was identified by growth on YEPD plates containing 3-amino-1,2,4-triazole (3-AT). Auto-activators were discarded following growth on YEPD plates containing cyclohexamide. True hit colonies were lysed, PCRed, and submitted for Sanger sequencing to identify the relevant AD-X and DB-Y interacting constructs. To verify the interaction, individual hits were pulled from the database, and the screen repeated in a one-on-one fashion. All stages of screening were completed using each construct fused to both AD and DB domains as bait.

Attributions

Contributions to this part of the thesis were made by Amanda L. Edwards, Dimphna H. Meijer, Federico Bernal, Amelie Dricot, Nidhi Sahni, Charles D. Stiles, and Loren D. Walensky.

F.B. and L.D.W. designed an initial panel of single helix SAH-OLIG2 peptides. A.L.E. and L.D.W. designed all subsequent SAH-OLIG2, SAH-E12, and dSAH-OLIG2 peptides. A.L.E., D.H.M., C.D.S., and L.D.W. designed all subsequent experiments. A.L.E. and F.B. synthesized all SAH-OLIG2 peptides. A.L.E. and D.H.M performed all EMSA experiments. A.L.E. performed all yeast two-hybrid experiments, aided by A.D. and N.S. from the Vidal lab (DFCI). A.L.E. generated and performed downstream experiments with GB1-OLIG2.

References

1. Darnell, J. E. Transcription factors as targets for cancer therapy. *Nat Rev Cancer* **2,** 740–749 (2002).

2. Dervan, P. B. & Edelson, B. S. Recognition of the DNA minor groove by pyrrole-imidazole polyamides. *Curr. Opin. Struct. Biol.* **13,** 284–299 (2003).

3. Beerli, R. R., Segal, D. J., Dreier, B. & Barbas, C. F. Toward controlling gene expression at will: specific regulation of the erbB-2/HER-2 promoter by using polydactyl zinc finger proteins constructed from modular building blocks. *Proc Natl Acad Sci USA* **95,** 14628–14633 (1998).

4. Follis, A. V., Hammoudeh, D. I., Wang, H., Prochownik, E. V. & Metallo, S. J. Structural Rationale for the Coupled Binding and Unfolding of the c-Myc Oncoprotein by Small Molecules. *Chemistry & Biology* **15,** 1149–1155 (2008).

5. Koehler, A. N. A complex task? Direct modulation of transcription factors with small molecules. *Current Opinion in Chemical Biology* **14,** 331–340 (2010).

6. Draeger, L. J. & Mullen, G. P. Interaction of the bHLH-zip domain of c-Myc with H1-type peptides. Characterization of helicity in the H1 peptides by NMR. *J Biol Chem* **269,** 1785–1793 (1994).

7. Ghosh, I. & Chmielewski, J. A beta-sheet peptide inhibitor of E47 dimerization and DNA binding. *Chemistry & Biology* **5,** 439–445 (1998).

8. D'Agnano, I., Valentini, A., Gatti, G., Chersi, A. & Felsani, A. Oligopeptides impairing the Myc-Max heterodimerization inhibit lung cancer cell proliferation by reducing Myc transcriptional activity. *Journal of Cellular Physiology* **210,** 72–80 (2007).

9. Bernal, F., Tyler, A. F., Korsmeyer, S. J., Walensky, L. D. & Verdine, G. L. Reactivation of the p53 tumor suppressor pathway by a stapled p53 peptide. *J Am Chem Soc* **129,** 2456–2457 (2007).

10. Moellering, R. E. *et al.* Direct inhibition of the NOTCH transcription factor complex. *Nature* **462,** 182–188 (2009).

11. Montagne, M. *et al.* The Max b-HLH-LZ can transduce into cells and inhibit c-Myc transcriptional activities. *PLoS ONE* **7,** e32172 (2012).

12. Murre, C., McCaw, P. & Baltimore, D. A new DNA binding and dimerization motif in immunoglobulin enhancer binding, daughterless, MyoD, and myc proteins. *Cell* **56,** 777–783 (1989).

13. Murre, C. *et al.* Interactions between heterologous helix-loop-helix proteins generate complexes that bind specifically to a common DNA sequence. *Cell* **58,** 537–544 (1989).

14. Lu, Q. R. *et al.* Sonic hedgehog--regulated oligodendrocyte lineage genes encoding

bHLH proteins in the mammalian central nervous system. *Neuron* **25,** 317–329 (2000).

15. Zhou, Q., Wang, S. & Anderson, D. J. Identification of a novel family of oligodendrocyte lineage-specific basic helix-loop-helix transcription factors. *Neuron* **25,** 331–343 (2000).

16. Takebayashi, H. *et al.* Dynamic expression of basic helix-loop-helix Olig family members: implication of Olig2 in neuron and oligodendrocyte differentiation and identification of a new member, Olig3. *Mechanisms of development* **99,** 143–148 (2000).

17. Rowitch, D. H., Lu, Q. R., Kessaris, N. & Richardson, W. D. An 'oligarchy' rules neural development. *Trends Neurosci* **25,** 417–422 (2002).

18. Meijer, D. H. *et al.* Separated at birth? The functional and molecular divergence of OLIG1 and OLIG2. 1–13 (2012).

19. Ligon, K. L. *et al.* Olig2-regulated lineage-restricted pathway controls replication competence in neural stem cells and malignant glioma. *Neuron* **53,** 503–517 (2007).

20. Mehta, S. *et al.* The central nervous system-restricted transcription factor Olig2 opposes p53 responses to genotoxic damage in neural progenitors and malignant glioma. *Cancer Cell* **19,** 359–371 (2011).

21. Sun, Y., Meijer, D., Alberta, J., Mehta, S. & Kane, M. Phosphorylation State of Olig2 Regulates Proliferation of Neural Progenitors. *Neuron* (2011).

22. Ligon, K. L. *et al.* The oligodendroglial lineage marker OLIG2 is universally expressed in diffuse gliomas. *J. Neuropathol. Exp. Neurol.* **63,** 499–509 (2004).

23. Bouvier, C. *et al.* Shared oligodendrocyte lineage gene expression in gliomas and oligodendrocyte progenitor cells. *J. Neurosurg.* **99,** 344–350 (2003).

24. Jackson, E. L. *et al.* PDGFR alpha-positive B cells are neural stem cells in the adult SVZ that form glioma-like growths in response to increased PDGF signaling. *Neuron* **51,** 187–199 (2006).

25. Stiles, C. D. & Rowitch, D. H. Glioma stem cells: a midterm exam. *Neuron* **58,** 832–846 (2008).

26. Benezra, R., Davis, R. L., Lockshon, D., Turner, D. L. & Weintraub, H. The protein Id: a negative regulator of helix-loop-helix DNA binding proteins. *Cell* **61,** 49–59 (1990).

27. Blackwell, H. E. & Grubbs, R. H. Highly efficient synthesis of covalently cross-linked peptide helices by ring-closing metathesis. *Angewandte Chemie International Edition* **37,** 3281–3284 (1998).

28. Schafmeister, C. E., Po, J. & Verdine, G. L. An All-Hydrocarbon Cross-Linking System for Enhancing the Helicity and Metabolic Stability of Peptides. *J Am Chem Soc* **122,** 5891–5892 (2000).

29. Walensky, L. D. *et al.* Activation of apoptosis in vivo by a hydrocarbon-stapled BH3 helix. *Science* **305,** 1466–1470 (2004).

30. Longo, A., Guanga, G. P. & Rose, R. B. Crystal structure of E47-NeuroD1/beta2 bHLH domain-DNA complex: heterodimer selectivity and DNA recognition. *Biochemistry* **47,** 218–229 (2008).

31. Forood, B., Feliciano, E. J. & Nambiar, K. P. Stabilization of alpha-helical structures in short peptides via end capping. *Proc Natl Acad Sci USA* **90,** 838–842 (1993).

32. Huth, J. R. *et al.* Design of an expression system for detecting folded protein domains and mapping macromolecular interactions by NMR. *Protein Sci* **6,** 2359–2364 (1997).

33. Lee, S., Lee, B., Ruiz, E. & Pfaff, S. Olig2 and Ngn2 function in opposition to modulate gene expression in motor neuron progenitor cells. *Genes Dev* **19,** 282 (2005).

34. Rice, D. S., Northcutt, G. M. & Kurschner, C. The Lnx family proteins function as molecular scaffolds for Numb family proteins. *Mol. Cell. Neurosci.* **18,** 525–540 (2001).

35. Honma, S. *et al.* Dec1 and Dec2 are regulators of the mammalian molecular clock. *Nature* **419,** 841–844 (2002).

36. Shen, M. *et al.* Basic helix-loop-helix protein DEC1 promotes chondrocyte differentiation at the early and terminal stages. *J Biol Chem* **277,** 50112–50120 (2002).

37. Gao, C. & Chen, Y.-G. Dishevelled: The hub of Wnt signaling. *Cell Signal* **22,** 717–727 (2010).

38. Lu, Q. R. *et al.* Common developmental requirement for Olig function indicates a motor neuron/oligodendrocyte connection. *Cell* **109,** 75–86 (2002).

39. Stewart, M. L., Fire, E., Keating, A. E. & Walensky, L. D. The MCL-1 BH3 helix is an exclusive MCL-1 inhibitor and apoptosis sensitizer. *Nat Chem Biol* **6,** 595–601 (2010).

40. Braun, C. R. *et al.* Photoreactive stapled BH3 peptides to dissect the BCL-2 family interactome. *Chemistry & Biology* **17,** 1325–1333 (2010).

41. Bird, G. H., Bernal, F., Pitter, K. & Walensky, L. D. Synthesis and biophysical characterization of stabilized alpha-helices of BCL-2 domains. *Meth Enzymol* **446,** 369–386 (2008).

42. Bird, G. H., Christian Crannell, W. & Walensky, L. D. Chemical Synthesis of Hydrocarbon-Stapled Peptides for Protein Interaction Research and Therapeutic Targeting. *Current Protocols in Chemical Biology* 99–117 (2011).

43. Dreze, M. *et al.* High-quality binary interactome mapping. *Meth Enzymol* **470,** 281–315 (2010).

44. Rual, J. *et al.* Human ORFeome version 1.1: a platform for reverse proteomics. *Genome*

Res **14,** 2128 (2004).

Chapter 4

Ongoing and Future Work

Work in Chapters 2 and 3 utilized stapled α-helical peptides to investigate and modulate known functions of the PUMA and OLIG2 proteins. However, much remains unknown about both proteins, including structural details of their protein interactions and alternative binding partners. Our ongoing work aims to use both full-length proteins and stapled peptides derived from them to explore these new frontiers in their biochemistry and cell biology.

Identification of novel binding partners of PUMA

The interplay among members of the BCL-2 family is well established as a mechanism of mitochondrial apoptosis regulation. However, additional "day jobs" and interaction partners have been identified for several BCL-2 proteins, including the regulation of calcium homeostasis[1], glucose metabolism[2,3], and mitochondrial fusion and morphogenesis[4]. From a therapeutic perspective, knowledge of these additional roles is critical in order to anticipate and monitor potential side effects of therapies targeting BCL-2 proteins as well as leverage these roles for non-apoptotic therapies. However, the potential for noncanonical protein interactions remains an understudied area of BCL-2 biology, and we therefore have undertaken a proteomics study using both full-length proteins as well as our stapled peptides in order to investigate novel PUMA interacting proteins (**Figure 4-1)**.

Full-length PUMA protein pulldowns identify a variety of novel interaction partners

As a first step in elucidating new biological roles for PUMA, vectors containing Flag- or HA-tagged versions of PUMAα were generated and transiently transfected into human embryonic kidney (HEK) 293T cells. PUMA protein and associated proteins were immunoprecipitated using Flag or HA affinity beads and separated by gel electrophoresis. Sections of each gel lane were then excised and prepared for mass spectrometry analysis. From this analysis, a list of 650 proteins was identified, 365 of which were identified with both

Figure 4-1

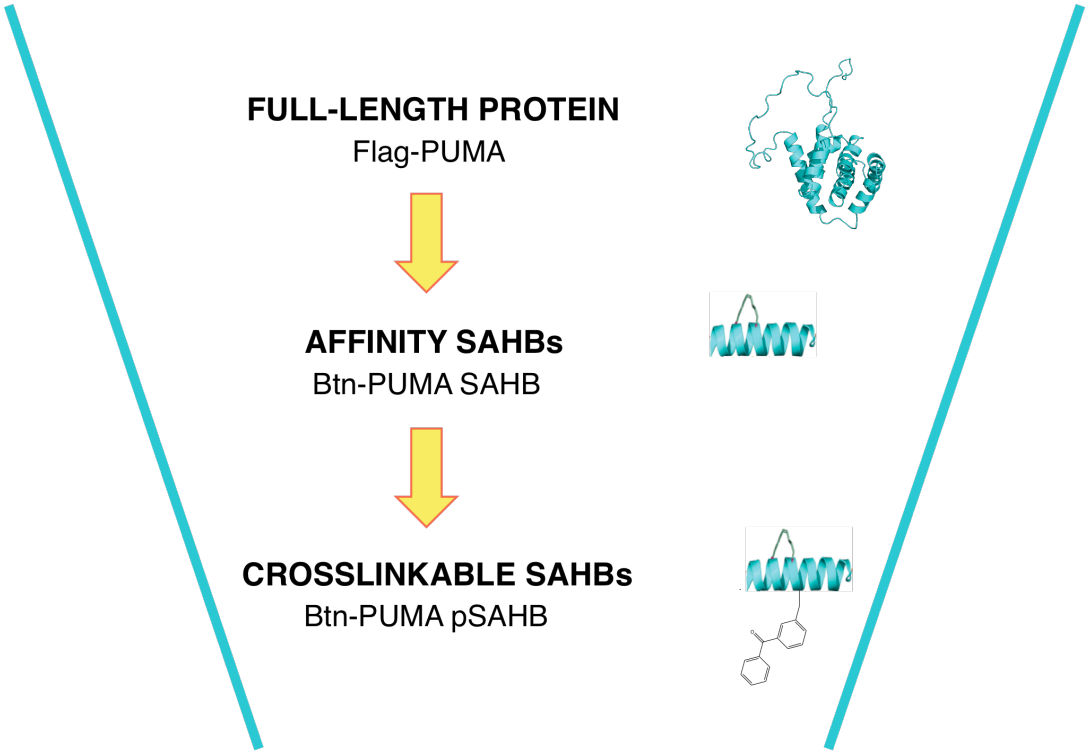

Schematic of proteomics screen to identify novel PUMA interaction partners. Our proteomics workflow began with identification of novel binding partners of the full-length PUMA protein. Hits were narrowed to those that directly bound to the PUMA BH3 domain using stapled peptides, first as affinity probes and then as covalent crosslinkers. All target identification was performed by LC/MS/MS analysis.

Flag-PUMA and HA-PUMA pulldowns. Examination of those proteins using pathway enrichment software (Ingenuity Pathway Analysis) identified several protein pathways that were statistically upregulated in the immunoprecitations, including RNA post-transcriptional modification, molecular transport, RNA trafficking, and DNA replication, recombination, and repair (**Table 4-1**).

Stapled PUMA peptides identify direct PUMA BH3-binding proteins

While the pulldown of full-length PUMA protein provided a wealth of new information regarding putative PUMA interactions, we decided to restrict our focus to those proteins that interact directly with PUMA BH3, the only known functional domain of the protein. To do so, we made use of our previously generated PUMA stapled peptides, which we have shown recapitulate known PUMA binding interactions and function. Biotinylated PUMA $SAHB_{A3}$ was incubated with U937 lymphoma cell lysates, and SAHB-protein complexes were captured with streptavidin agarose and analyzed by mass spectrometry, as above. A list of 840 proteins was identified, 235 of which were also identified in the protein pulldowns. These proteins represent those proteins that bind either directly to, or as part of a complex with, the BH3 domain of PUMA.

In order to identify those proteins from the list that directly bind to PUMA BH3, we utilized photoreactive PUMA SAHB (PUMA pSAHB) peptides containing a benzophenone residue. Benzophenone moieties covalently bind to adjacent C-H bonds upon UV irradiation, allowing for stringent washes and identification of direct binders. U937 lymphoma cell lysates were incubated with biotinylated PUMA pSAHB-2, with or without UV irradiation, and complexes were captured by incubation with streptavidin agarose. Following a series of stringent washes, the proteins were separated by electrophoresis, and sections of each gel lane excised and analyzed by mass spectrometry, which identified 610 proteins. Of these proteins, 80 overlapped with both

Table 4-1

Cellular pathway	p-value	Example interactor identified in pathway
tRNA charging	1.37×10^{-7}	SYAC: Alanyl-tRNA synthetase
Mismatch repair	3.93×10^{-6}	MSH2: DNA mismatch repair protein
RAN signaling	5.50×10^{-6}	XPO1: Exportin-1
Endocytosis signaling	1.86×10^{-4}	DYN2: Dynamin-2

Top four identified biological pathways of full-length PUMA interaction partners. Analysis was performed using Ingenuity Pathway Analysis software

Table 4-2

Cellular function	p-value	Example interactor identified in pathway
RAN signaling	1.60×10^{-8}	XPO1: Exportin-1
tRNA charging	1.68×10^{-6}	SYAC: Alanyl-tRNA synthetase
Cell cycle control of chromosomal replication	1.21×10^{-5}	MCM3: DNA replication licensing factor
THF salvage from 4,10-methenyl-THF	2.80×10^{-4}	C1TC: C-1-tetrahydrofolate synthase

Top four identified biological pathways of direct PUMA BH3 interaction partners.

Analysis performed using Ingenuity Pathway Analysis software.

the full-length PUMA protein, PUMA SAHB, and PUMA pSAHB pulldowns. Pathway enrichment analysis of these 80 genes identified several pathways of potential interest with high statistical significance, including RAN signaling (nuclear import/export), tRNA charging, and DNA mismatch repair (**Table 4-2**).

Initial validation of nuclear exportins as PUMA-interacting proteins

One of the families identified as a direct binder of the PUMA BH3 domain was the exportin protein family, which regulates the process of nuclear export. Exportins circulate between the nucleus and cytoplasm carrying cargo through the nuclear pore, aided by Ran and the GTP-GDP gradient[5]. There are a variety of exportin proteins, each having a specific subset of cargo. For instance, XPO-1 transports the majority of proteins that move out of the nucleus[6,7], while XPO-T moves tRNAs across the nuclear membrane[8,9].

To confirm the interaction between PUMA and XPO, the Flag-PUMA and PUMA pSAHB-2 pulldowns were repeated, and immunoprecipitated proteins were analyzed by Western blot. Both PUMA and PUMA pSAHB pulled down XPO5 (transports double-stranded RNA[10,11]), which was one of the early top identified hits (**Figure 4-2**). Two potential functional roles for the interaction between PUMA and the exportins can be envisioned: 1) PUMA may be exported from the nucleus as exportin cargo or 2) PUMA may regulate the export process. To evaluate the possibility that PUMA might be cargo for an exportin protein, we blotted for and confirmed that PUMA protein can also bind to XPO1, the major exporter for proteins from the nucleus (**Figure 4-3A**). In contrast, expression and immunoprecipitation of Flag-BIM did not pull down XPO1 (**Figure 4-3B**), highlighting the specificity of the PUMA interaction. These preliminary data suggest that a previously undocumented functional interaction may exist between the PUMA BH3 domain and the exportin proteins, an interaction that may be specific to PUMA among BCL-2 family members.

Figure 4-2

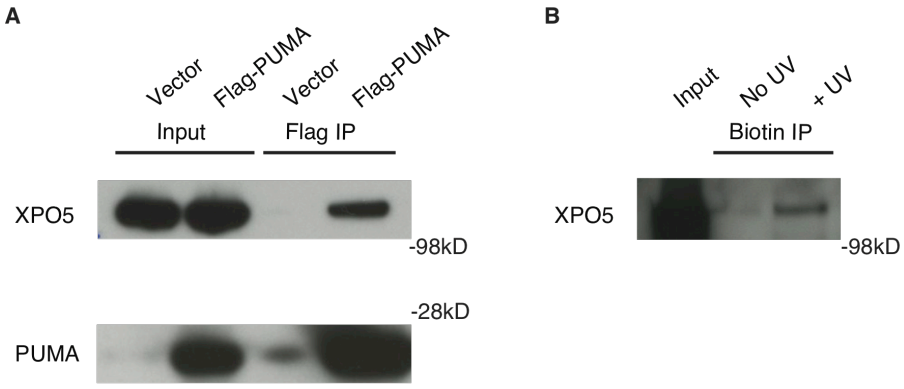

Full-length PUMA protein and biotinylated PUMA pSAHB both pull down native XPO5 from mammalian cells. (**A**) Human embryonic kidney (HEK) 293T cells were transiently transfected with vector or full-length Flag-PUMA protein. Complexes were captured with Flag affinity resin and analyzed by gel electrophoresis and Western blotting for XPO5. (**B**) Lysates from HEK 293T cells were incubated with biotinylated PUMA pSAHB-2 with and without ultraviolet light for benzophenone activation. Complexes were captured with streptavidin affinity resin and analyzed by gel electrophoresis and Western blotting for XPO5. In both cases, PUMA pulled down XPO5, confirming a PUMA-XPO5 interaction.

Figure 4-3

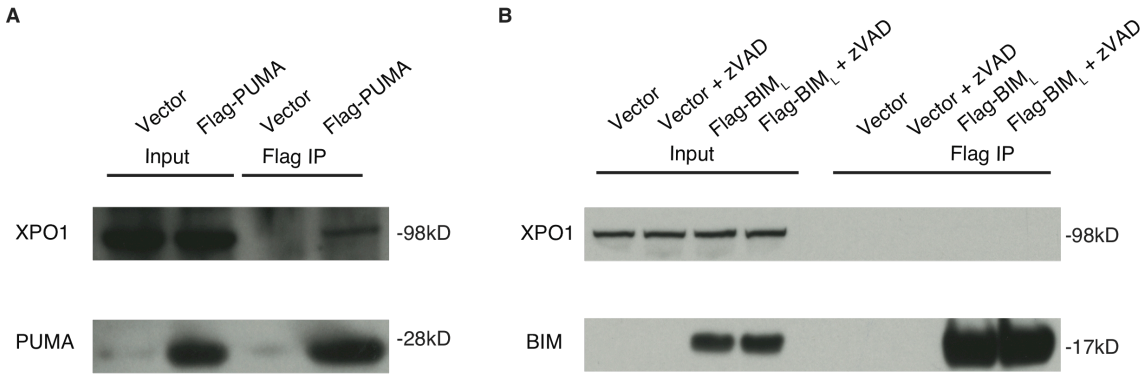

Full-length PUMA protein pulls down native XPO1, whereas BIM does not.

Human embryonic kidney (HEK) 293T cells were transiently transfected with (**A**) vector or full-length Flag-PUMA protein, or (**B**) vector or full-length Flag-BIM_L protein (with and without zVAD to prevent apoptosis). Complexes were captured with Flag affinity resin and analyzed by gel electrophoresis and Western blotting for XPO1. While PUMA successfully pulled down XPO1, BIM did not, highlighting the specificity of the PUMA-XPO1 interaction.

Future directions

In order to understand the interaction between PUMA and XPO, two areas of study will be pursued. First, structural analyses of PUMA-XPO binding using crosslinkable PUMA pSAHBs and recombinant XPO, as previously performed with PUMA pSAHBs and BCL-2 family proteins, will provide information regarding the binding interface. Such data could fuel hypotheses about the function of the interaction. Secondly, future biological studies will investigate the possibility that PUMA localization is regulated by XPO through the use of nuclear export inhibitors and subcellular fractionation or immunofluorescence imaging of PUMA. To investigate whether PUMA is regulating XPO function, changes in nuclear export will be evaluated in *Puma*$^{+/+}$ and *Puma*$^{-/-}$ mouse embryonic fibroblasts. Taken together, these experiments will enable us to investigate how PUMA and XPO interact and what functional role a PUMA-XPO interaction might have in a cellular context.

While we have piloted this proteomics platform with PUMA protein, SAHB, and pSAHB pulldowns, we are also interested in expanding this work to other BH3-only and BCL-2 family proteins. The BH3-only proteins BID and BIM, when coupled with PUMA, constitute the known direct activators of the multidomain pro-apoptotic proteins[12,13]. While BID, BIM, and PUMA serve generally similar pro-apoptotic functions within the BCL-2 family, we hypothesize that, based on their differential expression patterns during development and homeostasis, distinguishing non-traditional roles may exist. A large scale proteomics effort will allow for the identification of novel interaction partners of BID, BIM, and PUMA, as well as enable a comparison between interactors of these three direct activator BH3-only proteins. Eventually, similar proteomic studies for all members of the BCL-2 family will expand our knowledge of how this diverse group of proteins work to regulate cellular processes, including apoptosis and beyond.

Structural and interaction analyses of OLIG2

Our attempts to modulate pathogenic OLIG2 activity using stapled peptides have thus far been unsuccessful, due to difficulties in obtaining specificity in targeting the bHLH dimerization domain of OLIG2. Looking ahead, we plan to investigate several approaches for targeting OLIG2, which will include structural, biochemical, and cellular studies of OLIG2 biology.

Structural and biochemical studies using recombinant OLIG2 protein

Previous successes with stapled peptides have two things in common: a helix-in-groove binding interface, which increases the chance for specificity and potency of interaction[14-16]; and detailed structural knowledge of the targeted interaction, either through mutagenesis, NMR, or crystallographic studies[13,17]. At this stage, neither of these are the case for targeting the OLIG2 dimerization domain. The interaction of the OLIG2 bHLH domain with its homodimeric partner is not a helix-in-groove interaction, but rather a helix-on-helix handshake, making this interface unique and perhaps more difficult to target by traditional and stapled peptide approaches. Since the inherent structural aspects of OLIG2 homodimerization cannot be altered, improvements in inhibitor (or stapled peptide inhibitor) design await high resolution structural determination of the homodimer.

Current structural information about OLIG2 can be derived from two sources. Secondary structure prediction programs suggest that OLIG2 has two α-helical domains separated by a short loop region, consistent with a bHLH domain (**Figure 4-4**). Additionally, high resolution structures have been obtained of the bHLH dimerization domains of homologous bHLH proteins, including the E47/NeuroD1[18] and cMYC/MAX heterodimers[19]. While these data predict that the structure of an OLIG2 bHLH homo- or heterodimer is similar, confirmation of amino acid-level resolution can only be obtained by further structural studies of OLIG2 itself.

Figure 4-4

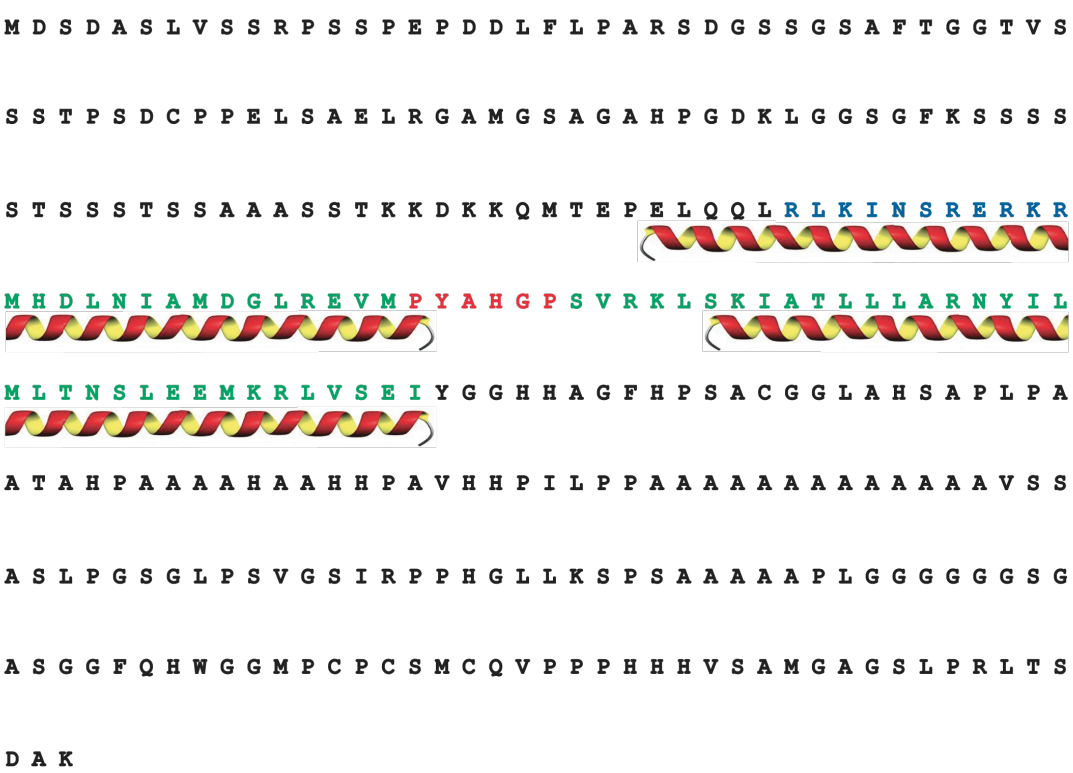

Figure 4-4: OLIG2 has a predicted helix-loop-helix domain. Secondary structure prediction program JPRED predicts two α-helices (green) in the OLIG2 structure, separated by a short loop region (red) and preceded by a string of basic residues (blue).

Previously, structural determination has proven difficult due to the inability to generate recombinant OLIG2. However, as reported in Chapter 3, we are now able to generate milligram quantities of GB1-OLIG2 protein. This construct is functional in electrophoretic mobility shift assays (EMSAs), confirming that the generated protein can bind to DNA. We propose to use this recombinant protein in two ways to further our knowledge of OLIG2 structural biology. First, systematic mutagenesis of the bHLH domain, followed by screening for loss of function in EMSAs, will allow us to identify key residues critical for OLIG2 dimerization and/or DNA binding. While similar studies are possible using mutated *Olig2* DNA constructs in a cellular environment, the use of recombinant protein and *in vitro* assays provides a more high-throughput system for evaluation. Secondly, generation of recombinant OLIG2 allows for the possibility of high-resolution whole protein (or subdomain) structural analyses by NMR or X-ray crystallography. Future efforts will emphasize high purity isolation and optimization of conditions for such biochemical and structural experiments. Definitive structural information about the OLIG2 bHLH dimerization domain should allow for more sophisticated design of prototype therapeutics for OLIG2 targeting.

Evaluation of putative interacting proteins of OLIG2 identified by yeast two-hybrid

bHLH proteins must homo- or heterodimerize with other bHLH proteins in order to carry out their transcriptional functions. Following DNA binding of promoter or enhancer elements, additional co-regulator proteins are recruited to the complex for the induction of transcriptional activation or repression[20,21]. OLIG2 is known to both homodimerize and heterodimerize with OLIG1[22], and it associates with the co-regulator protein p300[23]. However, the list of confirmed OLIG2 binding partners and co-regulator proteins remains quite short[22]. In an effort to expand our knowledge of OLIG2 interaction partners, which may serve as useful indirect targets for therapeutic intervention in OLIG2-driven cancers, we performed a full human genome yeast

two-hybrid screen for direct OLIG2 binding partners (Chapter 3). From this screen, we identified a small number of high-confidence hits as candidate OLIG2 interaction partners (**Figure 3-10,** Chapter 3).

By the nature of the yeast two-hybrid experimental system, the observed interactions were identified in a yeast cell environment and may not be representative of endogenous human protein interactions. Initial efforts have been made to validate these putative interactions in mammalian cells. Indeed, pulldown of OLIG2 from cultured mouse neurospheres successfully immunoprecipitated DVL3, a component of the Wnt signaling pathway and one of the hits from the yeast two-hybrid screen (**Figure 4-5**). Ongoing studies will continue these validation efforts using endogenous protein in order to confirm the biological relevance of the observed interactions.

Preliminary examination of the identified interaction candidates revealed that two of the proteins, DVL3 and LNX2, contain a PDZ protein interaction domain [24,25]. This similarity suggests that the PDZ domain could be important for the interaction between OLIG2 and DVL3/LNX2, as well as other unknown binding partners. This hypothesis will be tested using mutations or deletions in the PDZ domain of DVL3 and LNX2, followed by immunoprecitation with OLIG2. Further cellular and biochemical studies will be performed using such constructs, as well as strategically mutated constructs of OLIG2, to dissect the structural and biochemical nature of these interactions. Ultimately, cellular experiments will be designed to explore biological relevance, which could provide an opportunity to modulate OLIG2 indirectly by targeted disruption of these novel protein-protein interactions.

Summary

This thesis research has focused on the mechanistic dissection and therapeutic targeting of two proteins implicated in neuroectodermal pathology, PUMA and OLIG2. While the

Figure 4-5

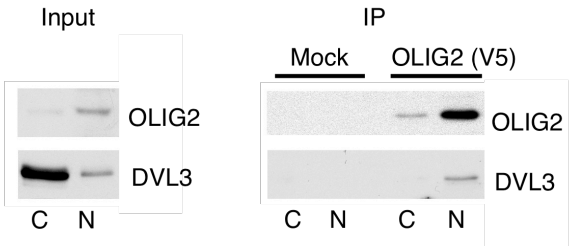

OLIG2 binds to DVL3 in mouse neurospheres. Subcellular fractionation of mouse neurospheres in culture, followed by immunoprecipitation of OLIG2, identified DVL3 as an OLIG2 interaction partner in the nuclear fraction.

primary biological interactions of both proteins are well-documented, additional interaction partners may play an important role in their biology and open new doors for therapeutic intervention. Initial work has been carried out to identify and characterize novel interaction partners for both PUMA and OLIG2 using a diverse set of experimental techniques, include mass spectrometry-based proteomics, stapled peptide-based protein capture and targeting, and yeast two-hybrid screening. Future interrogation of these interactions will include structural analyses, studies that will be aided by our successful production of recombinant OLIG2 protein.

Methods

Stapled peptide synthesis and characterization. SAHBs were synthesized, derivatized, purified to >95% homogeneity by LC/MS, quantified by amino acid analysis, and subjected to circular dichroism (Aviv Biomedical spectrophotometer) in 5 mM potassium phosphate buffer, pH 7.4, as previously described[26,27]. Biontinylated PUMA $SAHB_{A3}$: Btn-βAla-QWAREIGAQLRXBADXLNAQY; biotinylated PUMA pSAHB-1: Btn-βAla-QWARXIGAXLRRBADDUNRQYE; biotinylated PUMA pSAHB-2: Btn-βAla-QUAREIGAQLRXBADXLNAQYE. X = (S)-N-Fmoc-2-(4'-pentylenyl)alanine [S5]; U = 4-benzoylphenylalanine, B = norleucine.

***Puma/Bim* DNA constructs, cell transfection, and Flag co-immunoprecipitation.** HEK 293T cells were transiently transfected with pcDNA3 plasmid containing Flag-PUMAα or Flag-BIM_L using polyethylenimine[28] (PEI) at a 4:1 PEI:DNA ratio. Two days following transfection, cells were lysed in 1% CHAPS buffer (50 mM Tris [pH 7.5], 200 mM NaCl, 1% [w/v] CHAPS, 1 mM EDTA, 1.5 mM $MgCl_2$, complete protease inhibitor tablet [Roche]) on ice for 20 minutes. Lysates were isolated after table top centrifugation and then incubated with 30 mL of anti-Flag magnetic affinity beads (Sigma) in lysis buffer for 2 hours at room temperature. The beads were

washed with 3 x 500 mL lysis buffer, and immunoprecipitated proteins eluted by incubation with 4x FLAG peptide for 1 hour at 4°C. The immunoprecipitates were subjected to electrophoresis and analyzed by western blot or by LC/MS/MS (see below for complete methods). Antibodies: PUMA H-136 (sc-28226, Santa Cruz Biotechnology), BIM 22-40 (202000, EMD Biosciences), XPO1 H-300 (sc-5595), XPO5 H-300 (66885).

PUMA SAHB co-precipitation from cellular lysates. U937 cells were collected by centrifugation, washed twice in cold PBS, and lysed in a 1% CHAPS buffer (50 mM Tris [pH 7.5], 200 mM NaCl, 1% [w/v] CHAPS, 1 mM EDTA, 1.5 mM $MgCl_2$, complete protease inhibitor tablet [Roche]), on ice for 20 minutes. Lysates were isolated after table top centrifugation and then incubated (1.25 mg) with 50 nmol biotinylated-PUMA $SAHB_{A3}$ in lysis buffer overnight at 4°C. Biotin pull down was accomplished by incubation with high-capacity streptavidin agarose (Thermo) for 2 hours at 4°C, followed by washing the beads with 3 x 500 mL lysis buffer. Proteins were eluted with 1x LDS and precipitated using trichloroacetic acid. Pellets were washed with cold acetone, followed by trypsinization and sample clean-up as previously described[29] Samples were analyzed by LC/MS/MS (see below for complete methods).

PUMA pSAHB co-precipitation from cellular lysates. HEK 293T cells were trypsinized, collected by centrifugation, washed twice in cold PBS, and lysed in a 1% CHAPS buffer (50 mM Tris [pH 7.5], 200 mM NaCl, 1% [w/v] CHAPS, 1 mM EDTA, 1.5 mM $MgCl_2$, complete protease inhibitor tablet [Roche]), on ice for 20 minutes. Lysates were isolated after table top centrifugation, mixed with 40 nmol of biotinylated PUMA pSAHB-1 or -2, and irradiated (365 nm, Spectroline Handheld UV Lamp Model En280L, Spectronics Corp.) for 1.5 hours on ice. Biotinylated species were captured by incubation with high-capacity streptavidin agarose (Thermo) for 2 hours at 4°C. Streptavidin beads were sequentially washed at room temperature

three times each in 1% SDS in PBS, 1 M NaCl in PBS, and 10% ethanol in PBS, boiled 2 x 10 minutes in a 10% SDS solution (Promega) containing D-biotin (10 mg/ml), and the eluates electrophoresed. Samples were analyzed by Western blot or by LC/MS/MS (see below for complete methods). Antibodies: XPO5 H-300 (66885).

Protein identification by chromatography and spectrometry. Electrophoresed samples were excised and prepared for mass spectrometry analysis as previously described[29]. Samples were subjected to LC/MS/MS using an LTQ Orbitrap Discovery hybrid mass spectrometer (ThermoFisher, San Jose, CA). MS/MS spectra were searched using the SEQUEST algorithm[30] against a partially tryptic human protein database for protein identification. Reversed protein sequences were used to generate an estimate of the false discovery rate.

Subcellular fractionation. Cultured primary mouse neural progenitor cells were collected and treated with 5x packed cell volume (pcv) hypotonic buffer (10 mM HEPES [pH 7.9], 1.5 mM $MgCl_2$, 10 mM KCl), and centrifuged at 6000 rpm to collect nuclei. The supernatant was treated with 0.11x pcv 10x cytoplasmic extract buffer (0.3 M HEPES [pH 7.9], 1.4 M KCl, 0.03 M $MgCl_2$). Cell nuclei were incubated in a mild salt buffer (20 mM HEPES [pH7.9], 10% glycerol, 1.5 mM $MgCl_2$, 0.2 mM EDTA, 150 mM KCl) for 10 minutes on ice and rotated for 10 minutes at 4°C. The soluble nuclear protein fraction was collected by centrifugation at 10,000xg. All buffers were supplemented with protease inhibitors (Roche), 1mM $NaVO_4$, 5 mM NaF, 1 mM $Na_4P_2O_7$, 25 mM beta-glycerophosphate and 0.5 mM PMSF.

OLIG2 immunoprecipitation and immunoblotting. *Olig2*$^{-/-}$ null mouse neural progenitor cells were transduced with retrovirus encoding V5-tagged OLIG2 constructs. Subcellular fractions were generated as described above, and each fraction was incubated with V5 (Sigma) or Myc

(Sigma) antibodies overnight, rotating at 4°C. Antibody-bound fractions were washed four times in buffer B (50 mM Tris [pH 7.5], 100 mM KCl, 5mM $MgCl_2$, 10% glycerol, 0.1% NP40) over bio-spin columns (Biorad) and incubated with 0.5 mg/mL V5 peptide for 30 minutes at 4°C. Immunopurified fractions were collected by centrifugation at 8,000 rpm for 1 minute at 4°C and analyzed by standard SDS-PAGE followed by Western analysis. Antibodies: rabbit polyclonal OLIG2 (Stiles lab, DFCI), DVL3 (Cell Signaling Technology #3218).

Attributions

Contributions to this part of the thesis were made by Amanda L. Edwards, Dimphna H. Meijer, and Loren D. Walensky.

A.L.E. and L.D.W. designed all PUMA SAHB constructs and experiments. A.L.E. performed all PUMA experiments and mass spectrometry analysis. D.H.M. performed the OLIG2-DVL3 validation pulldowns.

References

1. He, H., Lam, M., McCormick, T. S. & Distelhorst, C. W. Maintenance of calcium homeostasis in the endoplasmic reticulum by Bcl-2. *The Journal of Cell Biology* **138,** 1219–1228 (1997).

2. Danial, N. N. *et al.* BAD and glucokinase reside in a mitochondrial complex that integrates glycolysis and apoptosis. *Nature* **424,** 952–956 (2003).

3. Danial, N. N. *et al.* Dual role of proapoptotic BAD in insulin secretion and beta cell survival. *Nat Med* **14,** 144–153 (2008).

4. Karbowski, M., Norris, K. L., Cleland, M. M., Jeong, S.-Y. & Youle, R. J. Role of Bax and Bak in mitochondrial morphogenesis. *Nature* **443,** 658–662 (2006).

5. Cook, A., Bono, F., Jinek, M. & Conti, E. Structural biology of nucleocytoplasmic transport. *Annu. Rev. Biochem.* **76,** 647–671 (2007).

6. Fukuda, M. *et al.* CRM1 is responsible for intracellular transport mediated by the nuclear

export signal. *Nature* **390,** 308–311 (1997).

7. Hutten, S. & Kehlenbach, R. H. CRM1-mediated nuclear export: to the pore and beyond. *Trends Cell Biol* **17,** 193–201 (2007).

8. Arts, G. J., Fornerod, M. & Mattaj, I. W. Identification of a nuclear export receptor for tRNA. *Curr Biol* **8,** 305–314 (1998).

9. Kutay, U., Bischoff, F. R., Kostka, S., Kraft, R. & Görlich, D. Export of importin alpha from the nucleus is mediated by a specific nuclear transport factor. *Cell* **90,** 1061–1071 (1997).

10. Yi, R., Qin, Y., Macara, I. G. & Cullen, B. R. Exportin-5 mediates the nuclear export of pre-microRNAs and short hairpin RNAs. *Genes Dev* **17,** 3011–3016 (2003).

11. Okada, C. *et al.* A high-resolution structure of the pre-microRNA nuclear export machinery. *Science* **326,** 1275–1279 (2009).

12. Walensky, L. D. *et al.* A stapled BID BH3 helix directly binds and activates BAX. *Mol Cell* **24,** 199–210 (2006).

13. Gavathiotis, E. *et al.* BAX activation is initiated at a novel interaction site. *Nature* **455,** 1076–1081 (2008).

14. Walensky, L., Kung, A., Escher, I., Malia, T. & Barbuto, S. Activation of apoptosis in vivo by a hydrocarbon-stapled BH3 helix. *Science* (2004).

15. Stewart, M. L., Fire, E., Keating, A. E. & Walensky, L. D. The MCL-1 BH3 helix is an exclusive MCL-1 inhibitor and apoptosis sensitizer. *Nat Chem Biol* **6,** 595–601 (2010).

16. Bernal, F., Tyler, A. F., Korsmeyer, S. J., Walensky, L. D. & Verdine, G. L. Reactivation of the p53 tumor suppressor pathway by a stapled p53 peptide. *J Am Chem Soc* **129,** 2456–2457 (2007).

17. Moellering, R. E. *et al.* Direct inhibition of the NOTCH transcription factor complex. *Nature* **462,** 182–188 (2009).

18. Longo, A., Guanga, G. P. & Rose, R. B. Crystal structure of E47-NeuroD1/beta2 bHLH domain-DNA complex: heterodimer selectivity and DNA recognition. *Biochemistry* **47,** 218–229 (2008).

19. Nair, S. K. & Burley, S. K. X-ray structures of Myc-Max and Mad-Max recognizing DNA. Molecular bases of regulation by proto-oncogenic transcription factors. *Cell* **112,** 193–205 (2003).

20. Torchia, J., Glass, C. & Rosenfeld, M. G. Co-activators and co-repressors in the integration of transcriptional responses. *Curr Opin Cell Biol* **10,** 373–383 (1998).

21. Lemon, B. Orchestrated response: a symphony of transcription factors for gene control. *Genes Dev* **14,** 2551–2569 (2000).

22. Meijer, D. H. *et al.* Separated at birth? The functional and molecular divergence of OLIG1 and OLIG2. 1–13 (2012). doi:10.1038/nrn3386

23. Fukuda, S., Kondo, T., Takebayashi, H. & Taga, T. Negative regulatory effect of an oligodendrocytic bHLH factor OLIG2 on the astrocytic differentiation pathway. *Cell Death Differ* **11,** 196–202 (2003).

24. Rice, D. S., Northcutt, G. M. & Kurschner, C. The Lnx family proteins function as molecular scaffolds for Numb family proteins. *Mol. Cell. Neurosci.* **18,** 525–540 (2001).

25. Gao, C. & Chen, Y.-G. Dishevelled: The hub of Wnt signaling. *Cell Signal* **22,** 717–727 (2010).

26. Bird, G. H., Christian Crannell, W. & Walensky, L. D. Chemical Synthesis of Hydrocarbon-Stapled Peptides for Protein Interaction Research and Therapeutic Targeting. *Current Protocols in Chemical Biology* 99–117 (2011).

27. Bird, G. H., Bernal, F., Pitter, K. & Walensky, L. D. Synthesis and biophysical characterization of stabilized alpha-helices of BCL-2 domains. *Meth Enzymol* **446,** 369–386 (2008).

28. Ehrhardt, C. *et al.* Polyethylenimine, a cost-effective transfection reagent. *Signal Transduction* **6,** 179–184 (2006).

29. Braun, C. R. *et al.* Photoreactive stapled BH3 peptides to dissect the BCL-2 family interactome. *Chemistry & Biology* **17,** 1325–1333 (2010).

30. Yates, J. R., Eng, J. K., McCormack, A. L. & Schieltz, D. Method to correlate tandem mass spectra of modified peptides to amino acid sequences in the protein database. *Anal Chem* **67,** 1426–1436 (1995).

Chapter 5

Conclusions

Discussion of results

Mechanistic dissection of PUMA BH3 domain's role in promoting apoptosis

The BCL-2 family of proteins regulates the ultimate decision of a cell to live or die through the intrinsic pathway of apoptosis. Interplay among these family members is a complex network of signal propagation, ligand-induced activation, inhibitory binding, and homo-oligomerization. Knowledge of these interactions has led to therapeutic modulation of apoptosis, activating neutralized pro-apoptotic proteins and inhibiting overexpressed anti-apoptotic proteins. While this may suggest that the series of biochemical steps that leads to activation (or avoidance) of mitochondrial apoptosis is fully understood, the reality is that there is still much to be learned about how these proteins operate within the family, and with other proteins, to govern cellular viability.

PUMA (p53-upregulated modulator of apoptosis) is a BH3-only pro-apoptotic protein that functions as a downstream effector of p53-driven death, following such stressors as DNA damage, irradiation, and hypoxia. In order to gain a better understanding of the mechanisms by which PUMA drives apoptosis forward, we made use of hydrocarbon-stabilized PUMA BH3 domain peptides to study PUMA-BCL-2 family interactions. PUMA SAHB directly bound to both anti- and pro-apoptotic members. While contact with the anti-apoptotic proteins was found exclusively in the canonical BH3 binding grove, PUMA SAHB engaged the pro-apoptotic protein BAX at both the α1/α6 trigger site and at the canonical BH3 pocket. Additional NMR and photocrosslinking studies suggested two sequential binding events: primary binding at the α1/α6 trigger site to allosterically release the α1/α2 loop and α9 C-terminal helix, and secondary binding in the vacated canonical binding pocket for further downstream activation. These sequential steps of activation lead to interesting questions about the potential role of a secondary binding event and the spectrum of BH3-only proteins that could execute such a step.

Notably, PUMA SAHB was found to directly activate BAX in a membrane system, suggesting a functional consequence for its direct binding interaction.

Among the BH3-only proteins, PUMA has been shown to be of particular importance in the induction of apoptosis of neural precursor cells. To evaluate the ability of PUMA SAHB to stimulate apoptosis in these cells, a cell-permeable version of PUMA SAHB was generated. Incubation of a variety of neuroblastoma cell lines with this peptide induced caspase 3/7-dependent apoptosis. Cellular targets of PUMA SAHB and full-length PUMA protein were determined to include both anti- and pro-apoptotic BCL-2 family members, implying a multimodal mechanism of apoptotic targeting by this BH3-only protein.

To date, the mechanisms by which PUMA induces apoptosis have remained controversial, with substantial experimental effort put towards a more complete understanding of PUMA's function. This work has utilized biochemical and structural approaches with stapled peptides, coupled with cellular work using full-length protein, to definitively answer this question. Like the BH3-only proteins BIM and BID, PUMA is able to directly bind and activate the proapoptotic executioner protein BAX. In addition to addressing an ongoing scientific debate, the binding determinants for BID, BIM, and PUMA at the trigger site of BAX will also facilitate ongoing projects to target proapoptotic molecules for direct activation of apoptosis.

Targeting pathogenic OLIG2 transcription using stabilized α-helical peptides

Induction of cell death in neuroblastomas with stabilized PUMA peptides is one mechanism for therapeutic intervention in diseases of neural precursor cell origin. While PUMA activity is not specific to neuronal cells, aberrant expression of the protein OLIG2 is exclusively found in gliomas and is thus a potentially ideal therapeutic target.

A member of the bHLH transcription factor family, OLIG2 is an early regulator of central nervous system development, maintaining neural precursor cells in a replication-competent

state until ultimately driving them toward differentiation. Beyond its developmental role, OLIG2 is expressed in all diffuse human gliomas and is required for glioma formation. Both of these roles stem from OLIG2's function as a transcription factor. bHLH transcription factors, including OLIG2, must dimerize through their bHLH domains to stably engage regulatory DNA sequences and recruit additional co-regulator proteins. Disruption of this dimerization could thus ablate pathogenic OLIG2-mediated transcription.

A synthesized panel of stabilized OLIG2 and E12 Helix 1, Helix 2, and bHLH peptides exhibited a spectrum of α-helical stabilization, ranging from 23-100% α-helicity in solution. Unfortunately, analysis of all SAH-OLIG2 and -E12 peptides by electrophoretic mobility shift assay did not identify a construct capable of specifically disrupting an OLIG2 homodimer/DNA complex. Several of the peptides exhibited nonspecific binding to the DNA, in large part due to the high positive charge of many of the sequences. However, this effect was partially abrogated by the addition of excess nonspecific DNA to the EMSA system. Taken together, these data suggest that our current library of stapled peptides corresponding to the dimerization domain of bHLH proteins is unable to specifically and potently disrupt the obligate dimerization for OLIG2 transcriptional activity.

Since, thus far, we have been unable to target OLIG2 directly, we decided to search for OLIG2 interaction proteins that might serve as indirect targets using a yeast two-hybrid approach. Whole genome screening with full-length and truncated OLIG2 constructs resulted in a limited list of high-confidence candidate OLIG2 interaction partners, including DVL3 and LNX2. Future work will investigate the roles of such interactions in OLIG2 biology and whether they are amenable to therapeutic targeting.

In the course of these studies, it became apparent that the generation of a recombinant form of OLIG2 would greatly facilitate biochemical and structural studies of this key pathogenic protein. Previous efforts at producing recombinant OLIG2 faced solubility and purification

challenges. As an extension of this thesis research, we have now successfully generated and purified milligram quantities of GB1-tagged OLIG2 in *E.coli*. This protein product was functional in an EMSA assay using a verified OLIG2 target DNA sequence. We anticipate that this recombinant protein will prove valuable for OLIG2 structural determination and small molecule screens.

While our efforts to therapeutically target OLIG2 using stapled peptides have yet to yield a prototype tool reagent, our ongoing work to further elucidate OLIG2 structural biology and binding partners will hopefully produce new leads for future targeting. If we are able to learn how to target the bHLH dimerization domain of OLIG2, using stapled peptides or derivatives of such peptides, this will potentially provide new opportunities to target the range of high-profile bHLH transcription factor targets, including proteins such as MYC and MAX.

Considerations

Structured peptide versus whole protein biology

In both major projects that comprise this thesis, chemically-stabilized peptides were generated to mimic an essential structured domain of the target protein. A primary consideration in executing such studies is whether or not the peptide mimetic will accurately represent the binding specificity and function of the full-length protein. PUMA SAHB was determined to bind to the full array of recombinant anti-apoptotic proteins, in accordance with published data for PUMA protein. In addition, when immunoprecipitated from cellular lysates, both PUMA SAHB and PUMA protein bound to the native anti-apoptotic proteins MCL-1 and BCL-2 as well as the pro-apoptotic protein BAX. These experiments indicate that PUMA SAHB, a structurally accurate version of the bioactive domain of the PUMA protein, is capable of correctly targeting native PUMA interactors for functional analyses. In contrast, SAH-OLIG2 peptides were unable to bind and disrupt OLIG2 homodimers *in vitro*, suggesting that such peptides are either

incapable of simulating bHLH function or that the “hot spots” for dimer disruption, and the peptidic means for targeting them, have not been adequately determined.

The structural distinctions between these two classes of protein-protein interactions - helix-in-groove vs. intertwined helices - are critical when considering how to best design and apply structured peptides for biological studies and therapeutic targeting. In the case of PUMA interactions, PUMA SAHBS were effective surrogates for the native full-length protein, recapitulating its pro-apoptotic functions and simulating its key interaction domain for trapping known binding partners and identifying candidate novel interactors (as suggested in Chapter 4). However, the current iteration of SAH-OLIG2 peptides failed to substitute for the OLIG2 bHLH domain or full-length OLIG2. In both cases, careful consideration must be given to potential drawbacks of using a short peptide to represent the protein as a whole, including loss of regulatory post-translational modifications, localization sequences, and differential splice variants. Nevertheless, stapled α-helical peptides have proven to be powerful mechanistic tools and prototype therapeutics in dissecting a variety of therapeutically relevant helix-in-groove protein interactions.

Future generations of stapled peptides

Peptides designed to mimic native α-helices have been a work-in-progress for decades, with hydrocarbon stapling successfully transforming unfolded peptides into proteolytically stable, α-helical peptides. However, much remains to be learned and accomplished. As detailed above, PUMA SAHB was able to potently bind to BCL-2 family member targets, while α-helical SAH-OLIG2 peptides failed to bind and disrupt full-length OLIG2 dimers, despite significant excess of the SAH-OLIG2 peptides and the ability of truncated protein fragments of the bHLH domain of other bHLH transcription factors to dimerize with one another. This dichotomy is consistent with known differences in the binding interfaces of these two interactions. BH3 α-helices bind into

hydrophobic binding grooves, which may themselves provide favorable energetics for high affinity ligand engagement. However, the α-helices of the bHLH domain of OLIG2 crisscross upon one another, limiting the number of potential high affinity contacts. It is therefore likely that additional constraints and contact points from the rest of the protein are necessary to support the dimerization interaction, providing the optimal context for bHLH domain dimerization. Although stapled peptides have yet to simulate this interaction, new opportunities for OLIG2 structural determination may provide the blueprint for optimizing the stapled peptide designs.

To potentially broaden the utility of stapled peptides for engaging diverse protein surfaces, new design considerations are envisioned. For example, to increase the affinity for interaction surfaces adjacent to DNA, such as in targeting bHLH domains, joining two targeting molecules, a stapled peptide to engage the α-helical interaction surface and a polyamide group to specifically target the adjacent DNA sequence, may represent an optimal design. Alternatively, a peptide-nucleic acid hybrid may achieve the desired targeting properties. To match the diverse topographic landscape of protein-protein interactions, new generations of stapled peptides with discrete chemical and structural enhancements may serve to expand this promising new chemical toolbox for protein interaction discovery and therapeutic targeting.